PERMEABILITY AND GLYCOCALYX MEDIATED SHEAR STRESS RESPONSE OF ENDOTHELIUM IN HYPERGLYCEMIA

by

SANDRA V. LOPEZ

A dissertation submitted to the Graduate Faculty in Engineering in partial fulfillment of the requirements for the degree of Doctor of Philosophy, The City University of New York

2010

This manuscript has been read and accepted for the Graduate Faculty in Engineering in satisfaction of the dissertation requirement for the degree of Doctor of Philosophy.

John M. Tarbell

Date	Chair of Examining Committee

Mumtaz Kassir

Date	Executive Officer

David Antonetti
Luis Cardoso
Bingmei Fu
Steven B. Nicoll
John M. Tarbell

Supervisory Committee

THE CITY UNIVERSITY OF NEW YORK

Abstract

PERMEABILITY AND GLYCOCALYX MEDIATED SHEAR STRESS RESPONSE OF ENDOTHELIUM IN HYPERGLYCEMIA

by: Sandra V. Lopez

Advisers: Dr. John M. Tarbell and Dr. David Antonetti.

Diabetic retinopathy (DR) is the most common microvascular complication of diabetes mellitus. Increased permeability of the capillaries comprising the inner blood retinal barrier (iBRB) is one of the characteristics of the disease. Therefore, understanding of the transport properties of the iBRB is an essential step towards elucidating means to control vascular permeability in persons with DR.

We have developed an *in-vitro* model of the iBRB by culturing monolayers of bovine retinal endothelial cells (BREC) onto polyester porous inserts. We quantified the diffusive and the apparent permeability of (TAMRA, 70-kDa Dextran and LDL), as well as the hydraulic conductivity (Lp). Based on the results, we developed a 3-pore transport model to estimate the routes taken by the different molecules and water to cross the endothelium.

Culturing the cells in a high glucose (HG) environment for six days did not alter any of the measurements mentioned above, consistent with intact cell-cell junctions, as shown by immunostaining and protein and gene expression. However, incubation with vascular endothelial growth factor (VEGF) increased permeability and hydraulic conductivity under both normal and HG environments. The results support the existence of an indirect pathway by which iBRB permeability is increased through the established up-regulation of retinal VEGF in response to hyperglycemia.

In addition, an in-vitro model of aortic endothelium was developed by culturing bovine aortic endothelial cells (BAEC) onto polyester porous inserts. We studied how the shear induced Lp response, known to be mediated by increases in NO, is changed by enzymatically cleaving specific components of the glycocalyx (GCX). Both cleaving the heparan sulfate component and culturing the monolayers in HG, significantly attenuated the shear stress mediated Lp response while maintaining the baseline Lp unaltered. Consistently, HG incubation diminished the heparan sulfate component of the GCX as shown by immunostaining. Western blots showed that eNOS activation was significantly lower in monolayers exposed to physiological levels of shear stress that were incubated in HG media compared to monolayers incubated in normal glucose media. These results support the hypothesis that early GCX modifications in response to hyperglycemia can induce endothelial dysfunction that may accelerate atherosclerosis development.

Acknowledgements

I would like to express my gratitude to my mentors Dr. John Tarbell and Dr. David Antonetti for their guidance and support during the duration of these studies. I would also like to thank Ellen B. Wolpert, Limary Cancel, Zhong-Dong Shi, Danielle Berardi, Alexis Pierides, Ronny Amaya, Henry Qazi, Eno Ebong, Maria Nikmanesh, Rocio Palomino, Rishi Mathura, Xinying Ji, Giya Abraham, Guanglei Li, Veronica Dudu, Jeff Garanich, Manolis Pahakis and Michael Dancu for their friendship, collaboration and teachings. I am also most grateful to the members of the committee and the faculty and staff members of the department of Biomedical Engineering at the City College of New York.

I also would like to thank my dear family for their unconditional support. Thanks to my parents Oliverio Lopez, and Elizabeth Quintero for their dedication throughout my life. Thanks to my sisters Catalina Lopez, and Vivian Lopez who always inspire me and guide me to be a better person. To my uncle Pedro Quintero and my aunt Mery Quintero, because my accomplishments are theirs. To all my friends in New York for making me feel at home in this city and to my beloved husband Albeiro Ordonez for all he has been to me.

TABLE OF CONTENTS

LIST OF ILLUSTRATIONS

LIST OF TABLES

CHAPTER 1

Introduction

Diabetes mellitus has been recognized as a world-wide epidemic. According to a 2007 report from the National Diabetics Information Clearinghouse, 7.8 percent of the US population has diabetes (23.6 million people). The process responsible for type 1 diabetes is destruction of insulin-secreting pancreatic islet cells, which is manifested by a mononuclear infiltrate and beta-cell lysis in the islets. The process underlying type 2 diabetes is insulin resistance. Both type 1 and type 2 diabetes result in abnormal elevation of blood glucose levels. Getting older, gaining weight and becoming more sedentary are factors that lead to diabetes in patients with a tendency to insulin resistance.

Vascular complications due to elevated blood glucose levels continue to be a major health burden in the world. Diabetic retinopathy (DR), one of the most frequent complications of diabetes and the principal cause of blindness among working age people, affects the microvasculature. Many diabetic patients are referred to the ophthalmologist only when visual deterioration has already started [1]. There are substantial economic expenditures [2, 3] as well as decreased health related quality of life for patients with DR [4]. Nearly all patients with type 1 diabetes and 60% of patients with type 2 diabetes have retinopathy [5].

Elevated glucose levels are believed to be the cause of different vascular complications, among them, loss of microvascular barrier integrity [6-8], increased systemic vascular permeability [9, 10] and abnormal endothelial response [11]. Several mechanisms have been proposed to account for changes in the vasculature due to diabetes but a decisive one has not been established yet [12]. These changes are manifested in both micro and macro vasculature.

In tissues of the central nervous system, including the brain and the retina, strict control is needed to separate the sensitive tissues from the systemic circulation. The blood retinal barrier and blood brain barrier help to maintain specific conditions for neural tissue homeostasis, among them: ion concentration, amino acid, sugar and water transport and permeability [13]. These barriers also prevent the neural tissue from being exposed to circulating antibodies and immune cells. In the retina, the barrier is comprised of endothelial cells, extracellular matrix and pericytes; however the major barrier to microvascular leakage is thought to be the continuous endothelial monolayer found at the luminal surface of the microvasculature. Therefore understanding the transport properties of the endothelial monolayer and how they are altered during an elevated glucose environment is of great importance.

It is well established that during DR there is increased capillary permeability [14], plasma leakage and increased vascular endothelial growth factor (VEGF) contents followed by proliferation of blood vessels [15]. Studies of transport across the retinal endothelium, however, are very limited since small capillaries are not easy to manipulate. In order to

overcome this limitation, we used an in-vitro model of the retinal endothelium based on seeding Bovine Retinal Endothelial Cells (BREC) onto porous polyester filters to elucidate the effects of elevated glucose levels on the transport of solutes and water. The results of this study should help us understand the mechanism by which hyperglycemia alters retinal endothelial transport properties.

In the main vascular branches, an elevated level of glucose and other risk factors can lead to different pathologies. Nitric oxide (NO), a fundamental signaling molecule in the vasculature, accomplishes homeostasis through diverse biological processes such as vasodilation, anticoagulation, suppression of leukocyte adhesion, smooth muscle cell proliferation, and enhancing antioxidant capacity. The interest in this molecule and its role in diabetes has increased in the recent years. Several studies have suggested that during diabetes, an impaired NO production or availability leads to endothelial dysfunction and progression to atherosclerosis [16-18]

Shear stress moderates endothelial NO production through the mechanosensing action of the glycocalyx (GCX) [19, 20] and there is evidence to support the idea that hyperglycemia interferes with either the synthesis or the shedding of at least two glycosaminoglycans (GAG) components of the GCX [21, 22]. Previously in our laboratory we have observed that shear stress increases endothelial hydraulic conductivity and that this effect can be attenuated with an eNOS inhibitor [23]. In the present study we will examine how the shear-induced Lp response is modified when certain GAGs are enzymatically cleaved from the GCX. We will also look for differences in the shear-

induced Lp response when monolayers are cultured in high glucose. In order to accomplish this, we will develop an in-vitro model of the aorta by seeding Bovine aortic endothelial cells (BAEC) onto polyester filters.

The specific aims for this research are:

1. To determine the effect of hyperglycemia on the transport of solutes and water across the retinal endothelium. To do this we will measure the transport of fluorescently tagged molecules and water across our in-vitro model, which will consist of BREC monolayers grown under normal and elevated glucose conditions. In addition we will use immunostaining of the tight junction protein ZO-1 and the adherens junction protein VE-Cadherin for monolayers grown under normal and elevated glucose conditions. We will also determine the effect of hyperglycemia on apoptotic rates, using the TUNEL assay for monolayers grown in normal and elevated glucose conditions.

2. To determine the role of VEGF in elevated permeability across the retinal endothelium. To do this, we will incubate endothelial cell monolayers with the growth factor and measure water and solute transport for monolayers grown under normal and elevated glucose conditions.

3. To determine the effect of hyperglycemia on the shear-induced transport of water across the arterial endothelium. We will develop an in-vitro model using BAEC plated onto porous polyester inserts. We will consider the differences in shear-

induced Lp response when various GCX components are cleaved, and when cells are grown in normal and high glucose. Additionally we will use immunostaining to visualize the major glycosaminoglycan component of the GCX for monolayers grown under normal and elevated glucose conditions, and quantify the activation (phosphorylation) of eNOS by shear stress in normal and high glucose.

CHAPTER 2

Background

2.1 The Endothelium

The structure and anatomy of blood vessels change according to their location in the circulatory system. Arteries have three layers, the intima, the media and the adventitia (Figure 1). The intima is composed of endothelial cells (EC) that lie on a basement membrane that they secrete and is in contact with an extracellular matrix (EM) with mesenchymal undifferentiated cells immersed in it. The media is composed mostly of smooth muscle cells which control contraction and relaxation of the blood vessel. The adventitia or outermost layer is composed of FB, some SMC and extracellular matrix components [24].

In contrast, capillaries are basically formed by the endothelium, a monolayer of EC that can be surrounded by other types of cells (Figure 1). For instance, in the retina, the endothelium is in contact with pericytes and Muller glial cells [25] while in the brain it is in contact with pericytes and astrocytes [26].

Studies on the endothelium have shown that this unicellular organ covers the inner surface of the blood vessels, lymphatic vessels and cardiac cavities and plays a major role

in the operation of the cardiovascular system. Initially the endothelium was thought to be an inert and inactive layer, but in the recent decades it has been found that its function is crucial in synthesis, storage, signaling and release of special molecules that have an effect on the normal functioning of different organs [27]. It constitutes an active layer that is crucial in water, gas and solute exchange [28]. The endothelium is a transport barrier between the circulating blood and the tissues that must be protected and nourished [29].

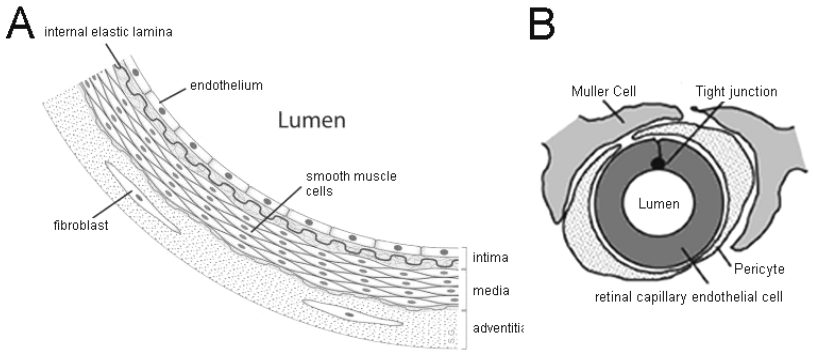

Fig. 1. Cross section of vessel walls. Panel A shows a schematic representation of the cross section of an artery wall, which is composed of three main layers, the intima, the media and the adventitia. The endothelium is localized towards the lumen side and is in close contact with the circulating blood. Panel B shows a schematic representation of the cross section of a retinal capillary, which is composed of an endothelial cell surrounded by pericytes and Muller cells. Adapted from Wikipedia and Abukawa et al. [25]

Due to its location, the endothelium is susceptible to chemical, physical and immunological signals. These signals may be translated into gene activation and protein expression, that can have an effect on the vascular wall and the intracellular population [30, 31]. If the stimulus on the endothelium is not normal, the intima may thicken

(neointima) or a pseudotumoral lesion (atheroma) may form [32]. Atherosclerosis and hypertension are regulated by the endothelium because this organ controls the extracellular matrix composition, lipid accumulation and the smooth muscle cell behavior in the vascular wall. Because the subendothelial EM is a thrombogenic surface that favors platelet adhesion and coagulation, the injury or dysfunction of the endothelium can lead to vessel occlusion [16, 31].

EC are attached one to the other by complex junctions that provide a strong and selective barrier for transport. Figure 2 depicts the three main zones or junctions at the cleft between endothelial cells i.e. Zonula Occludens (ZO) or tight junction (TJ), Adherens Junctions (AJ) and Gap Junctions (GJ). The first two play a role in cell-cell attachment and permeability and therefore are relevant to this study. The last one is significant for cell-cell communication [33, 34].

The features of the endothelium that are relevant for the transport of molecules from the lumen to the interstitial space, include not only TJ and AJ but also breaks in the TJ, leaky junctions, the glycocalyx, vesicles and aquaporins. A further explanation of these components will be given in the following subsections.

2.1.1 Tight junctions and breaks in the tight junctions

TJ limit the paracellular flux of hydrophilic molecules and together with adherens junctions form a seal between adjacent endothelial cells. TJ are located at the apical side of the endothelium, closest to the lumen.

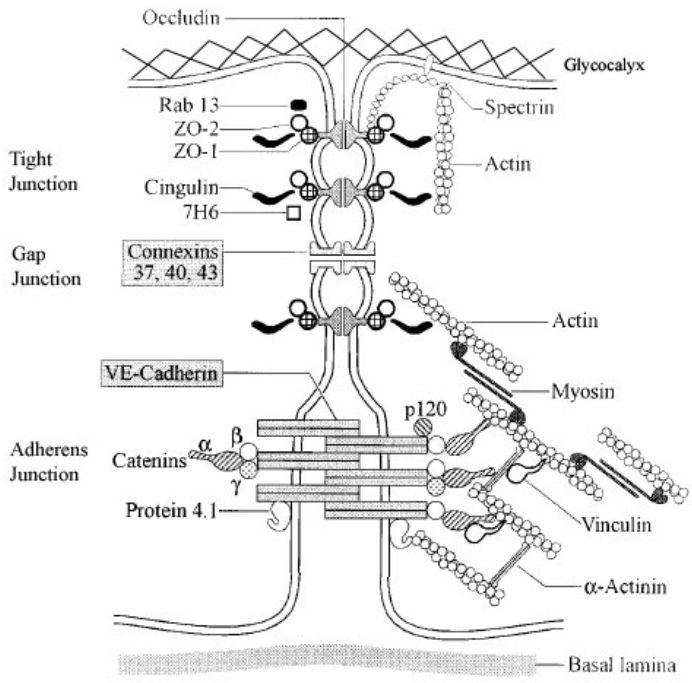

Fig. 2. Schematic of the cleft between endothelial cells, its junctions and the association with filaments of the cytosol. TJ are located at the apical side of the cleft and AJ are located closer to the basal side. The glycocalyx, shown as a coating on the cell membrane extends into the cleft and serves as a sieve for macromolecules. Adapted from Michel et al. [35]

The integrity of the TJ is partly governed by three families of proteins; occludin [36], the claudins [37] and the junctional adhesion molecules (JAMs), all of which bind to ZO-1, a 220 kDa cytoplasmic protein strongly involved in TJ structure and regulation. Occludin's carboxy-terminal binds to zonula occludens (ZO-1, ZO-2, and ZO-3) which in turn bind to the actin cytoskeleton, [38-40]. Claudins have two intracellular loops that bind to ZO-1, ZO-2 and ZO-3 also via their carboxy-terminals [34, 41], and JAMs have a

single transmembrane domain which binds intracellularly to ZO-1 among other proteins [42]. ZO-1 therefore is a molecule that acts as a central organizer of the TJ complex. Apart from this protein, it has been shown that occludin is critical to maintain endothelial barrier and regulation of paracellular transport in large vessel endothelium in the retina [43].

Due to the presence of TJ, the plasma membranes of the two neighboring cells are in close proximity. However, ultrastructural studies have found that these membranes are not fused together and that there is still a small gap between them. This gap has been measured to be 4 nm in rat heart capillaries [33] and 2.3 nm in mesenteric capillaries of the frog [44], where another feature of the intercellular cleft was observed, a widening of the gap to about 20 nm with an average length of 150 nm. These regions where the TJ is wider have been termed breaks in the TJ.

2.1.2 Adherens junctions

The adherens are anchoring junctions between cells and connect their actin cytoskeleton to the plasma membrane. VE-Cadherin also known as cadherin-5, is the main transmembrane protein in the AJ. It is connected to the actin cytoskeleton through accessory proteins, the catenins (α-, β-, γ-catenins) and mediates homophilic cell-cell adhesion in a calcium dependent manner [45]. The structural stability of AJ is provided by the cytoplasmic interactions with the catenins [46], which also play a role in paracellular permeability. In fact, despite their basal location, they influence the apical TJ permeability barrier through α-catenins which also bind to ZO-1 [47]. VE-Cadherin is

necessary for vessel formation in vivo [48]. In the retina, other cadherin proteins, such as N-cadherin (cadherin-2) are expressed at contact zones between capillary pericytes and endothelial cells [48].

2.1.3 Leaky junctions

Leaky junction is the term used to characterize bigger spaces in the endothelium, through which macromolecules can pass. The main sources of leaky junctions are Y-junctions, the place where three endothelial cells intersect, and cells in a mitotic or apoptotic state. Y-junctions, also called tricellular regions, have been previously studied in guinea pig pulmonary capillaries analyzed by freeze fracture, where it was found that their average width was 27.4 nm, their average length was 1.1 microns and they completely crossed the cleft region [49]. In corneal endothelium, Y- junctions have shown discontinuities in specific tight junction proteins, such as ZO-1 [50].

Cells undergoing mitosis or apoptosis have been suggested to provide among the most important pathways for macromolecules the size of LDL (23nm) to go across from the luminal to the abluminal side of the endothelium [51]. The presence of transient leaky junctions was evident in rat thoracic aorta, where the average width for mitotic leaky junctions was 487 nm and ranged from 80 to 1330 nm while for dying or dead cells (cells containing cytoplasmic immunoglobulin G) the width ranged from 15 nm to 1000 [52]. Apoptosis can be caused by an upregulation of tumor necrosis factor-alpha (TNF-α), a factor whose expression is increased in diabetic rats [53], and is related to significant loss

of retinal endothelial microvascular cells. The transport of macromolecules through leaky junctions is supported by the finding that apoptosis and intraretinal oxidized LDL were present in diabetic patients and increased with the severity of DR [54, 55].

2.1.4 Vesicles and transporters

Channels, transporters and general or specific vesicle transport are essential for controlled metabolic activity in the delicate retinal neural tissue [56-59]. In the case of receptor-mediated endocytosis, the cell internalizes molecules by the inward budding of plasma membrane vesicles, called clathrin coated vesicles, which contain specific receptors for the molecule being internalized.

Vesicles can also originate as caveolae, which are small (50- 100 nm) invaginations of the plasma membrane in the shape of caves that are mostly present in endothelial cells and adipocytes. Figure 3 shows a diagram of these organelles and their relative localization. The internalization of caveolae and the movement to the basal side of the endothelium is signaled by caveolin-1, the most important structural protein for the formation of caveolae. Caveolin-1 is also involved in the process of vesicle fusion, delivery and exocytosis [60]. The presence of vesicles has been observed in rat endothelial retinal cells where they are mostly localized on the luminal side, continuous with the cell surface [61, 62] and in retinal endothelium of monkeys [63]. However, in both animals, the number of caveolae and vesicles seemed to be low compared to non barrier endothelium.

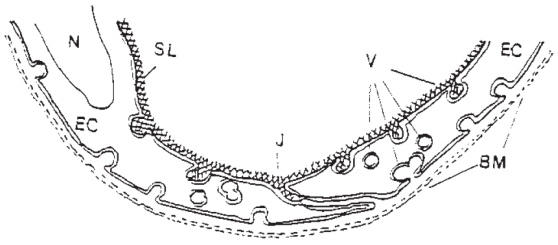

Fig. 3. Schematic of a continuous endothelium. N= nucleus, EC=endothelial cell, SL= luminal surface coat or glycocalyx, J=junction, V=caveolae or vesicles, BM=basement membrane. From Michel [64].

2.1.5 Glycocalyx

Even though the GCX was visualized some 40 years ago for the first time by Luft [65] using electron microscopy, there are still many unknowns related to its composition and function. The endothelial glycocalyx is a network of membrane-bound proteoglycans and glycoproteins, covering the endothelium at the luminal side (Figure 4). Within this network, soluble molecules, of endothelial or plasma origin are incorporated, therefore the GCX should not be viewed as a static layer but as a dynamic interaction layer between the circulating blood and the endothelium. Enzymatic degradation of any of its constituents affects GCX properties, which emphasizes the importance of the synergistic interaction of its constituents as a whole [66]. Recent studies indicate that in the arteries, GCX thickness increases with vascular diameter and can range from 0.5 μm in capillaries to 3 μm in small arteries [29] and 4.5 μm in carotid arteries [67].

Other descriptions of the GCX are found in previous studies [19, 68, 69]. Due to its

polyanionic constituents, the GCX displays a net negative charge. The GCX is important in the barrier function of the endothelium because it not only covers the cell membrane but also extents into the cleft between cells forming a sieve for macromolecules [29]. It has been shown also that it plays a role in water transport, mechanotransduction and NO production [70].

Proteoglycans (PG) are the most abundant components of the GCX, they are classified according to their link to the membrane and composition. Of them, Syndecans (4 types) connect to the membrane via membrane-spanning domains, Glypicans (6 types) connect via glycosylphosphatidylinositol anchors. Other less abundant PG include mimecan, perlecan and biglycan. One core protein can bind different types of glycosaminoglycan (GAG) chains. The proportion of the various chains is determined by different circumstances and stimuli [71]. There are five different types of GAG chains, Heparan Sulfate (HS), Chondroitin Sulfate (CS), Dermatan Sulfate (DS), Keratan Sulfate (KS) and Hyaluronan or Hyaluronic acid (HA). GAG are linear disaccharide polymers with variable lengths that are modified by sulfation and/or (de)acetylation. The disaccharides are each composed of a uronic acid and a hexosamine; classification of the glycosaminoglycans depends on which uronic acid or hexosamine is incorporated and on the pattern of sulfation. The presence of heparan sulfate and chondroitin sulfate is reported to have a typical ratio of 4:1 for the vascular endothelium [72].

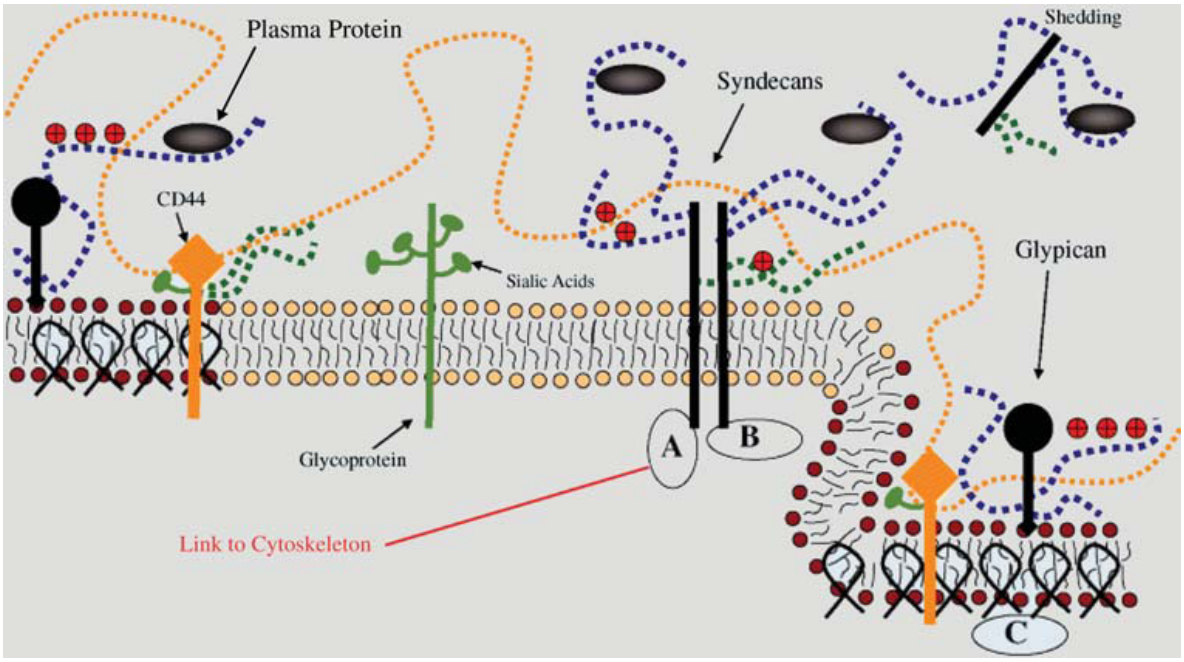

Fig. 4. Schematic of endothelial glycocalyx. The luminal domain of the GCX is stabilized because of the dynamic interaction of core proteins proteoglycans and glycoproteins with soluble molecules of both endothelial and blood origin. Glypicans, along with their heparan sulfate (HS) chains (blue dotted lines) localize at the caveolae regions (C). Syndecans contain both HS and chondroitin sulfate (CS - green dots). The intracellular domain of the Syndecans is linked to the cytoskeleton and it is associated with intracellular signaling effectors (A) (B). Hyaluronic acid (yellow chain) binds to CD44. Transmembrane CD44 can also bind to HS, CS or oligosaccharides and is localized in caveolae. Plasma proteins (grey), along with cations and cationic amino acids (red circles) associate with glycosaminoglycans. Figure from [73].

Small modifications in the GAG chains can have great functional consequences, since they contain specific binding sites for plasma derived proteins. In fact, modifications vary in time and in response to different physiological and pathological stimuli [74-76]. For instance oxidized low density lipoprotein (ox-LDL) infusion can remove GCX components and increase platelet-vessel wall interactions [77]. Heparinase, ox-LDL and TNFα vessel infusion can induce leukocyte adhesion [78]. Any alteration in the sulfation patterns or synthesis of GAG is expected to have a consequence on vascular permeability,

protein binding activity and mechanosensing.

Glycoproteins, the other major GCX component, are characterized by having short and branched carbohydrate side chains. They comprise molecules such as endothelial cell adhesion molecules (CAM) and components of the fibrinolysis and coagulation system. The three families of CAM in the endothelial GCX are; the selectin family, the integrin family and the immunoglobulin family. There are three kinds of selectins, E-selectin, P-selectin and L-selectin, but only the first two are found in the endothelium and are involved in leukocyte interactions [79].

Integrins are heterodimeric glycoproteins, with a cytoplasmic tail and a transmembrane domain. Integrins are found on many cell types, including endothelial cells, leukocytes, and platelets. Endothelial cell integrins are involved in interactions with platelets, and binding with laminin, fibronectin and collagen, all relevant during angiogenesis [80].

The immunoglobulin family of glycoproteins has a transmembrane domain with a cytoplasmic tail and immunoglobin like domains that project towards the luminal side. The most common are vascular cell adhesion molecule 1 (VCAM-1), intercellular adhesion molecules 1 and 2 (ICAM-1 and -2) and platelet/endothelial cell adhesion molecule 1 (PECAM-1).

Other components of the glycocalyx include soluble components derived either from the endothelium or from the circulating blood, such as albumin and orosomucoid. They play

a role in maintaining the charge and selectivity of the endothelial barrier [81]. Interactions between membrane-bound proteoglycans, soluble proteins, and soluble proteoglycans create a cross-linked mesh and provide stability to the luminal GCX.

2.1.6 Aquaporins

The aquaporins (AQPs) are integral membrane proteins whose main function is to transport water across cell membranes driven by an osmotic or hydraulic gradient [82]. AQP1 was discovered by chance by Nobel prize winner Peter Agre [83] while experimenting with erythrocytes. Agre and his team observed a recurrent 28 kDa protein whose function was unknown and was given the name of chip 28. The same protein was later confirmed to be present in renal proximal tubules as well as in other tissues with high membrane water permeability. AQPs form tetramers in the cell membrane, with each monomere acting as a water channel [84]. The selectivity of AQPs is so high that even protons are repelled.

The presence of AQP1 in luminal and abluminal membranes of capillary endothelium suggests that there is a role for this protein in water transport between the vascular space and the interstitium [85]. Moreover AQP1 expression in capillary endothelium can be modulated by stimuli in vivo, for example, in rat pulmonary capillary, corticosteroids can cause up to a 10 fold increase [86]. The distribution of AQPs predicts a role in physiology and disease; AQP1 mediates proximal tubule fluid reabsorption, secretion of cerebrospinal fluid and lung water homeostasis. AQP2 mediates collecting duct water

permeability. AQP3 in the basolateral membrane of the collecting duct provides an exit pathway for reabsorbed water. AQP4 is abundant in brain and probably participates in regulation of brain edema. AQP5 mediates fluid secretion in salivary and lacrimal glands and is abundant in alveolar epithelium of the lung [87].

AQP-1 is abundant in most continuous endothelia (but not in fenestrated endothelia) and in a number of transporting epithelia, most importantly in the proximal tubules and the descending limb of Henle's loop, and a number of other absorptive or secretory epithelia [82]. Even though transcellular transport of water has been postulated in endothelial cells, it has been overlooked because of its low contribution to total hydraulic conductivity [88, 89]. However, it has been estimated that up to one half of the water flow can be redirected towards these pathways during glucose induced osmosis [90].

AQP1 or AQP4 have been shown to be absent from the retinal endothelium [91-93]. In the retinal endothelium, the presence of AQPs is expected to be low because normally there are no large osmotic gradients across the barrier as in the case of the kidney.

2.1.7 Summary of transport pathways across the Endothelium

As suggested by the characteristics of the endothelium described in the previous section, the transport of molecules and fluids across the inner BRB may occur through two basic pathways, i.e. transcellular (through endothelial cells) and paracellular (between endothelial cells).

The transport of solutes and fluid across the endothelium has been studied for several years and extensively reviewed [35]. Figure 5 depicts four possible routes for macromolecular transport.

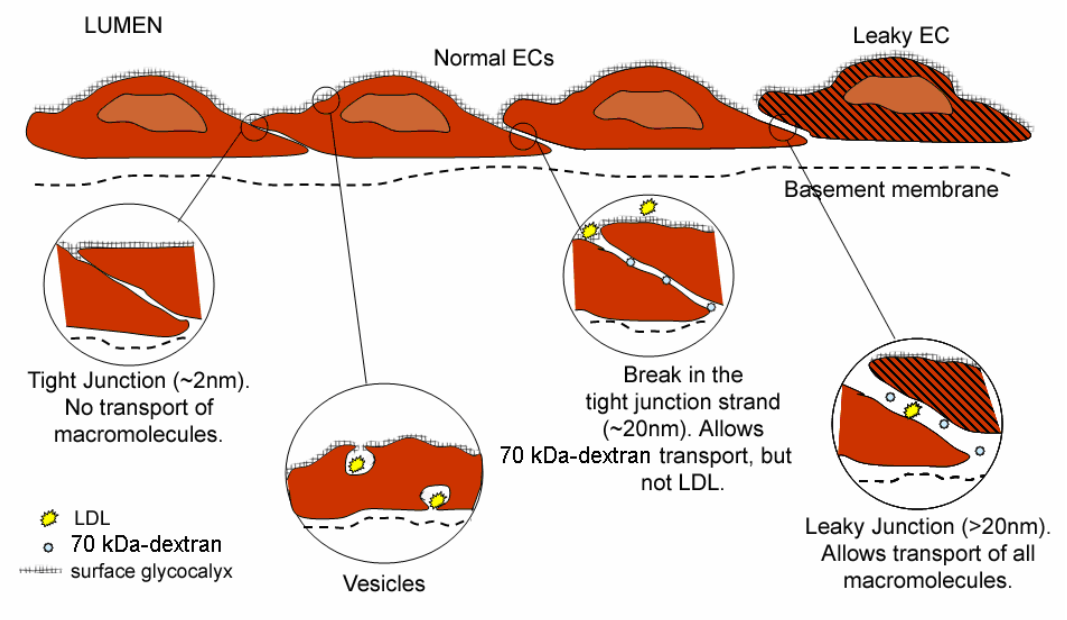

Fig. 5. Transport pathways across the endothelium for the molecules used in this study. TJ at the apical side of the endothelium represent the biggest barrier for paracellular molecular transport. Vesicles transcellularly transport LDL. Breaks in the TJ allow for the paracellular transport of 70-kDa Dextran but not LDL. Leaky junctions allow for paracellar transport of LDL and 70-kDa Dextran. Water is convectivelly transported through the breaks in the TJ and the leaky junctions, but not through TJ because of its high hydraulic resistance. Figure by Limary Cancel adapted from [73].

The transport pathways include; transport inside vesicles, transport through TJ, transport through the breaks in the TJ, and transport across leaky junctions.

In the present study (chapter 3) we have used BREC monolayers and observed the

transport of three solutes and water across them. These solutes and their respective diameter are; 5-(and-6)-carboxytetramethylrhodamine (5(6)-TAMRA) (TAMRA) (~ 1.3 nm), 70-kDa Dextran (~ 5 nm) and DiI-LDL (~ 22 nm). We cultured the monolayers in a normal and high glucose environment and looked for differences in transport. Based on the permeability measurements we analyzed a pore model to determine the routes of transport for water, LDL and 70-kDa Dextran. We anticipate that 70-kDa Dextran will be transported by the breaks in the TJ and the leaky junctions, LDL by vesicles and leaky junctions and water by the breaks in the TJ and the leaky junctions and aquaporins, but not by TJ because of high hydraulic resistance due to the narrow pathway.

2.2 Diabetis and retinopathy

Figure 6 shows the main characteristics of diabetic retinopathy (DR). The disease is basically divided into two stages according to its progression. The first stage also called non-proliferative diabetic retinopathy (NPDR) is characterized by mild nonproliferative abnormalities, among them increased vessel permeability, breakdown of the BRB [94], basement membrane thickening [95], microaneurisms (which develop as a result of excessive vascular dilation), intraretinal hemorrhages, yellowish exudates, vascular closure and swelling of the macula. The second stage also called proliferative diabetic retinopathy (PDR) is characterized by the development of new blood vessels on the retina and posterior surface of the vitreous, proliferation of fibrous tissue, vitreous hemorrhage and eventually detachment of the retina. Macular edema, characterized by retinal leakage from blood vessels, can develop at all stages of retinopathy.

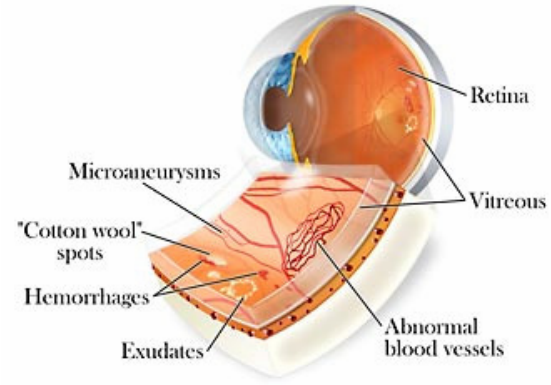

Fig. 6. Characteristic features of DR. Breakdown of the blood retinal barrier manifested by exudates, hemorrhages and subsequent formation of abnormal vessels on the retina and posterior surface of the vitreous, proliferation of fibrous tissue, vitreous hemorrhage and eventually detachment of the retina. Image from www.netheryeye.com

The two major precursors of DR are hyperglycemia and hypertension, with hyperlipidemia as a possible third major risk factor [96]. Vision loss due to DR may emerge from several mechanisms including macular edema and capillary nonperfusion. New blood vessels and contraction of the new fibrous tissue can lead to tractional retinal detachment [97], causing severe and often irreversible vision loss. In addition, the newly formed vessels, which do not have the same characteristics as healthy ones, may hemorrhage at the retina and vitreous. All of the above complications in DR typically lead to blindness and any agent that can help slow down this process is of value.

2.2.1 Nourishing of the retina

Figure 7 is a micrograph showing the three main layers of the eye, the outer most is the sclera (S), followed by the choroids (C) and the retina (R). The retina is a sensory tissue that contains photoreceptors to capture light rays and convert them into electrical impulses. These impulses travel along the optic nerve to the brain where they are converted into images.

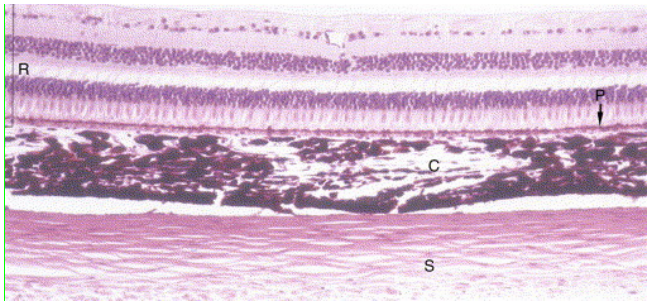

Fig. 7. Microphotograph showing the three main layers of the wall of the eye (haematoxylin and eosin staining). The outermost layer is the sclera S followed by the choroids C which is separated by the Bruch's membrane from the retina R. Reprinted from Wheater's Functional Histology in Hornof et al. [98]

Figure 8 shows schematics of the structure of the retina. This complex organ is composed of several different layers, the outer portion of which is nourished by the choriocapillaris via the outer blood retinal barrier and the remaining inner portion is nourished by retinal capillaries which are surrounded by pericytes [99] and Müller glial cells [100], while arterioles and veins are surrounded by Smooth Muscle Cells (SMC).

The Choroids receives the greatest blood flow (65-85%) [101] and is vital to maintain photoreceptors. The remaining 15-35% flows to the retina through the central retinal artery from the optic nerve. The central retinal artery has 4 main branches in the human retina that supply three layers of capillary networks. i.e. the radial peripapillary capillaries (RPCs) and an inner and an outer layer of capillaries. The precapillary venules drain into venules and through the corresponding venous system to the central retinal vein.

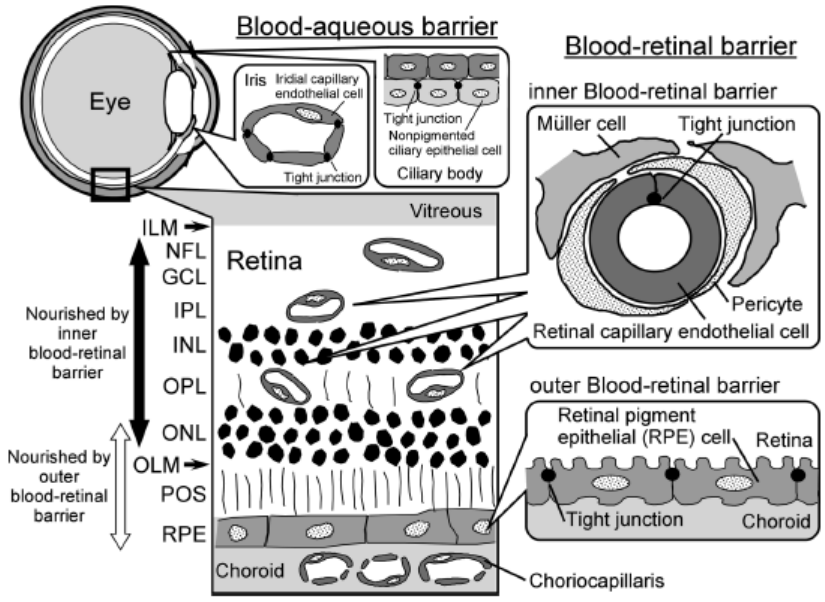

Fig. 8. Schematic of the histological structure of the retina. The layers consist of RPE, retinal pigment epithelium; POS, photoreceptor outer segments; OLM, outer limiting membrane; ONL, outer nuclear layer; OPL, outer plexiform layer; INL, inner nuclear layer; IPL, inner plexiform layer; GCL, ganglion cell layer; NFL, nerve fiber layer; ILM, inner limiting membrane. Adapted from Abukawa et al. [25]

2.2.2 Blood Retinal Barrier

Homeostasis of the retina, which is a delicate and highly differentiated tissue, is

maintained by the blood retinal barrier (BRB). The concept of BRB was first introduced by Schnaudigel in 1913 following the work by Ehrlich and Goldman who discovered the blood-brain barrier (BBB). The blood vessels of the retina form a strong barrier composed of complex tight junctions (TJ) between endothelial cells in the inner retina (inner BRB) and pigment epithelial cells in the outer retina (outer BRB) [102]. For the purpose of this study we are going to focus our attention on the inner BRB, since there is evidence that this one, rather than the outer BRB is the primary site of vascular leakage resulting in edema, macular degeneration and blindness [14].

2.2.3 Previous studies on effects of Hyperglycemia on the Endothelium of the Retina

The effect of hyperglycemia on the retinal vasculature has been studied in human subjects, in animal and in in-vitro models [94, 103, 104]. Over the last decades, these systems have allowed investigators to observe the characteristic features of DR and the effects of an elevated glucose environment on the blood vessels. However, the mechanisms by which hyperglycemia leads to DR are not yet determined. Clinical studies have used eyes extracted from deceased patients to determine which serum protein levels, especially those related to cell proliferation and cell migration, are significantly different when healthy tissue is compared to tissue presenting signs of DR at various stages [105-107].

Animal models have been mammals (mice, rats, dogs) in which diabetes had been induced by intravenous injection of streptozotocin (STZ) or by chronic elevation of blood

galactose. These animal models have been useful to monitor the progression of abnormalities in the retinal blood vessels, however due to complex systemic interactions; it has been difficult to elucidate whether DR follows from local disorders within the retina or to a metabolic response to systemic abnormalities such as hyperglycemia.

Diabetic dogs in poor glycemic control showed clear signs of retinopathy 30 months after the disease was induced, followed by an accelerated worsening during the next 30 months [108]. Diabetic rats have shown increased permeability to 66k-Da albumin after 3 months of STZ injection [104].

In-vitro models have been used to characterize retinal cells [43] or to look for interactions with factors such as vascular endothelial growth factor VEGF [23, 109] or with an elevated glucose environment [110, 111]. The responses of the endothelium to hyperglycemia have been studied with the aid of cell cultures, where mainly bovine, porcine and human retinal endothelial cells have been used.

Pathways related to hyperglycemia have been summarized before [15], and include activation of protein kinase C (PKC) [112], which has been suggested to increase endothelial albumin permeability and decrease blood flow [113-115], oxidative stress, and activation of advanced glycation end products (AGE) and their receptors. Decrease of blood flow to the retina could cause local hypoxia, which induces VEGF causing hyperpermeability and microaneurisms [116].

Oxidative stress may affect endothelial permeability by degrading the GCX [117] and therefore promoting leukocyte adherence after GCX injury[118]. AGE are highly reactive and significantly induce VEGF expression in retinal endothelial cells in vitro[119].

A compromised internal BRB, which is an early feature of DR, has been related to pericyte and or endothelial cell loss [120], but because proliferative changes eventually occur, subtle early changes in the endothelium have been difficult to define. In this sense, in-vitro models have proven to be a useful tool for investigation.

In-vitro models have indicated that high glucose concentration plays a direct role in vascular leakage. Monolayers of bovine aortic endothelial cells (BAEC) cultured in 20mM glucose for four days showed an increase in diffusive permeability to albumin of 76.2% ± 13.8% and 74.0% ± 14.2% to 70-kDa Dextran. Incubation with an aldose reductase inhibitor was able to block the increased albumin permeability but not the 70-kDa dextran one [121]. An increased vascular permeability to albumin but not to a 10-kDa Dextran was observed in rats after three months of STZ induced diabetes [104].

It seems that the response of the cells to high glucose depends on the culture methods and the molecules used to measure permeability. For instance BREC seeded on microcarriers failed to show an increase in sodium fluorescein (0.45 nm radius) and cyanocobalamin (8.5 nm radius) permeability during the first 21 days of incubation in 25 mM glucose media [110], but showed a significant increased permeability to (125)I-labeled proteins

(HRP, BSA and IgG) in as early as one day, when the cells were seeded onto porous inserts and incubated in 30mM glucose [122].

An increase in endothelial permeability related to the modification of TJ proteins has been supported by the finding that altered occludin content and distribution as well as albumin extravasation was found in STZ induced diabetic rats [104, 123]. Phosphorylation or reduced content of occludin by PKC and some of its isoforms have been shown to cause diminished barrier tightness in retinal endothelial cells [109]. Decreased expression and relocalization of ZO-1 has been observed in rat glomerular epithelial cells exposed to high glucose [124], but not in BREC monolayers [125].

Integrity of the endothelial barrier does not depend solely on cell-cell contacts; anchoring to the underlying matrix plays a role as well [126]. Focal adhesions stabilize non-migrating EC into the surroundings of the vascular wall. These complex structures consist of transmembrane integrins and intracellular adapter proteins like paxillin, vinculin, talin and zyxin, attaching the whole structure to the actin cytoskeleton. In this regard, 48 hours of high glucose induced changes in the morphology of cultured rat heart endothelial cells by reorganization of F-actin and focal adhesion proteins FAK and paxillin [127]. Integrin proteins may play a role in vascular diabetes complications as well [128]. Integrin-linked kinase (ILK) the 59-kDa protein involved in cell migration, cell proliferation, cell-adhesion and signal transduction was upregulated after 4, 8 and 12 weeks of STZ induced diabetes in rats [129].

2.2.4 VEGF upregulation in diabetic retinopathy.

Recent studies in patients with DR have shown that early stages of the disease are marked by an upregulation of VEGF, which occurs even before morphological abnormalities are observed [130-133]. There is evidence showing that BREC release VEGF into their culture media and that this characteristic is attributed only to endothelial cells cultured from the retina and brain, suggesting a specific role in neural tissue [134]. In addition to its autocrine activity on BREC, VEGF can act on these cells by a paracrine pathway since it is also released in a bioactive form by retinal pericytes [135, 136].

VEGF binds to at least two transmembrane tyrosine kinase receptors on endothelial cells, named Flt-1 (VEGF receptor-1) and Flk-1/KDR (VEGF receptor-2) [137, 138]. Among other types of cells, these receptors have been found in retinal and brain cells [139]. After VEGF binding, a cascade of events leads to increased intracellular calcium and activation of protein kinase B (Akt) and PKC [140, 141] which in turn activate endothelial nitric oxide synthase (eNOS), leading to increased nitric oxide (NO) release, which is associated with vasodilation and increased vascular permeability [138, 142-145].

VEGF is 50,000 times more potent than histamine in causing microvascular permeability [146].

With respect to tight junction alterations, VEGF was shown to cause a significant reduction in ZO-1 and occludin content in porcine retinal endothelial cell (PREC) and

BREC [104, 147]. Consistently, VEGF caused a 100% increase in the diffusive transport of 70-kDa Dextran after PREC were incubated for 24 hours with the cytokine [147]. In rat models, the intraocular injections of VEGF has caused a change in the phosphorylation state of ZO-1 and occludin [148], as well as extensive retinal leukocyte stasis (leukostasis) [149]. In the past, VEGF activation of PKC has been partially attributed to cause occludin phosphorylation and regulation of 70-kDa Dextran permeability in retinal endothelium [23, 109].

In vivo experiments have looked at intact blood vessels in rat and frog mesentery, were upon perfusion with VEGF, a transient rapid increase in hydraulic conductivity has been observed and a return to normal levels has been reached after 2 hours [150].

Not only VEGF [151], but also TNF-alpha [152] and histamine [153] which are established barrier disruptors, have been shown to increase tyrosine phosphorylation of one or more proteins within adheren junctions.

VEGF can alter the integrin expression profiles of BREC and probably influence interactions of endothelial cells with extracellular matrix thus affecting neovascularization [154]. Inhibitors of VEGF-induced permeability increases include vasoinhibins and PKC inhibitors. Vasoinhibins inhibit VEGF-induced NOS activation by eNOS dephosphorylation and thereby eNOS inactivation via protein phosphatase 2A (PP2A) [155]. Inhibiting the beta-isoform of PKC has been shown to reduce 95% of the 3-fold increase in permeability caused by VEGF induced PKC membrane translocation

[116].

In chapter 3, we systematically examine the BREC permeability barrier in vitro under both diffusive and convective (pressurized) conditions in normal and high glucose environments. We also consider how elevated glucose might affect endothelial cell permeability in response to VEGF.

2.3 Diabetes and atherosclerosis

Atherosclerosis is the leading cause of illness and death in the United States and most other developed countries. Atherosclerosis can affect the medium-sized and large arteries of the heart, kidneys, brain, other vital organs, and legs. It is the most common type of arteriosclerosis, a general term that includes several diseases in which the wall of an artery becomes thicker and less elastic. Atherosclerosis develops in a complex manner, but the primary event seems to be subtle and repeated injury to the artery‘s wall through various mechanisms (Figure 9).

The injured endothelium sends chemical signals or components of the underlying wall are exposed such that certain types of white blood cells (monocytes and T cells) attach to the artery [31]. Low density lipoprotein LDL can be easily transported across the endothelium but becomes trapped by the extracellular matrix ECM [156]. Once LDL binds to the ECM, lipid oxidation may start [157] and oxidized LDL promotes the endothelial release of monocyte chemoatractants [156] therefore recruiting monocytes to

the subendothelial space. Monocytes and their high oxidative capacity oxidize LDL even more, to the point where the molecule becomes toxic for both ECs and SMCs [158] and is no longer recognized by the LDL receptors but engulfed by macrophages that then transform into foam cells which trigger growth and migration of SMCs into the arterial intima [159]. These foam cells accumulate and form atheromas, also called plaques. Plaques are covered with a fibrous cap and with time also calcium deposits; they may narrow or block an artery, reducing or stopping blood flow. Other plaques do not block the artery completely but may split open, triggering a blood clot that suddenly blocks the artery.

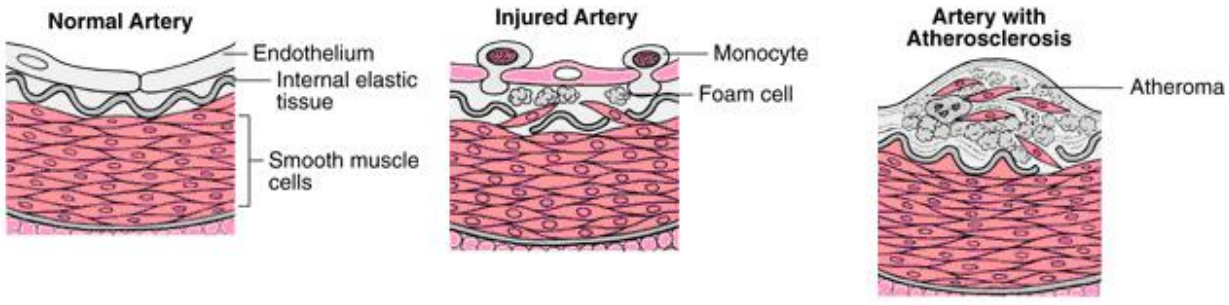

Fig. 9. Arterial plaque formation. The injured vessel wall sends chemical signals and cause certain types of white blood cells (monocytes and T cells) to attach to the wall of the artery. Once in place, they transform into foam cells which engulf cholesterol and fatty materials and trigger migration and growth of SMC into the media of the artery wall. These foam cells accumulate and form atheromas also called plaques Edited from ADAM.

Diabetes accelerates the events described. Some people with type 1 diabetes and most people with type 2 diabetes tend to develop atherosclerosis in large arteries. These people

also tend to develop atherosclerosis at an earlier age and more extensively than do people who do not have diabetes [160]. The risk of developing atherosclerosis is 2 to 6 times higher for people with diabetes, particularly women. People who have diabetes have the same risk of death as someone who has had a prior heart attack. Diabetics should keep other risk factors like high cholesterol levels and high blood pressure under careful control [161].

2.3.1 Endothelial dysfunction

A healthy endothelium can maintain homeostasis of the vascular beds through the release of various paracrine factors. The endothelium can control leukocyte adhesion, platelet reactivity, capillary permeability, SMC regulation and blot clotting [162].

Nitric oxide (NO) one of the paracrine factors, is produced by endothelial cells from L-arginine in the presence of cofactors, the most common of them being tetrahydrobiopterin (BH4) [163]. NO is an anti-atherogenic molecule, because it can relax smooth muscle cells, inhibit platelet aggregation and adhesion, smooth muscle cell proliferation, prevents leukocyte adhesion and reduces plasma fibrinogen levels [164, 165]. Reduced bioavailability of NO therefore enhances thrombotic events.

Insulin is a vasodilator and stimulates endothelial NO production, however in obese insulin-resistant or in type 2 diabetic subjects insulin is unable to modulate endothelial dependent vasodilation. Therefore although insulin levels are elevated in these subjects,

its action is reduced, leading to endothelial dysfunction [162].

Prostacyclin (PGI2) is synthesized mainly by vascular endothelial cells and it is a potent vasodilator and inhibitor of platelet aggregation. The expression of prostacyclin stimulating factor (PSF), assessed by immunostaining in SMCs of human coronary arteries is markedly reduced in diabetic subjects, suggesting that the decreased PGI2 production shown by diabetics is likely to be the result of decreased PSF [166, 167]

Thromboxane A2 a vasoconstricting agent is synthesized by both platelets and vessel wall tissues, therefore increased platelet activation in diabetics contributes to the thrombotic complications in macrovascular disease. Human aortic endothelial cells exposed to high glucose have shown increased media levels of thromboxane A2 compared to normoglycemic controls [168].

In non injured vessels, bradykinin causes relaxation of the vascular SMCs through the release of NO by the endothelium, but when the integrity of the endothelium is compromised, bradykinin acts directly on SMCs causing vasoconstriction and fibrosis [169]. Bradykinin also activates mitogen-activated protein kinases (MAPKs) that lead to an increase in ECM proteins such as collagen I and fibronectin. The B2-kinin receptors (that bind to bradykinin) on vascular SMCs have been shown to be upregulated in the vessel wall of diabetic animals, suggesting that diabetes could lead to vascular fibrosis and contribute to arteriosclerosis [170].

Endothelial cells synthesize leukocyte-specific adhesion molecules and circulating monocytes display receptors for these cell adhesion molecules. Increased levels of soluble cell adhesion molecules have been found in plasma of type 1 and type 2 diabetic patients. In addition, a positive correlation between plasma concentration of VCAM-1 and intima and media thickness of carotid arteries was observed in type 2 diabetic patients [171]. Some lipoproteins like advanced glycation end product –LDL (AGE-LDL) once bound to macrophage receptors induce the release of tumor necrosis factor (TNF), Interlukin (IL)-1, platelet derived growth factor (PDGF), and immunoglobulin growth factor-1, and these agents in turn promote the expression of adhesion molecules [172].

Diabetes appears to enhance foam cell lesion formation in experimental animals and in humans [160]. Foam cell formation may be related in diabetes to the presence of increased levels of modified lipoprotein and oxidized LDL that then is engulfed by macrophages. LDL clearance is primarily LDL-receptor mediated but glycated LDL is poorly recognized by the LDL receptor on fibroblasts and it is preferentially recognized by another receptor pathway present in macrophages [173].

2.3.2 Shear stress, mechanosensing and diabetes

Shear stress caused by the circulating blood as it travels along the vessels has been shown to be protective against atherosclerosis. However, regions in the vasculature where the flow is not laminar or is low or is turbulent or reverses, tend to be atheroprone [174].

Early observations have shown that in diabetic patients, atherosclerosis occurs earlier, is more severe and its distribution is more diffuse than in non diabetic patients [175], suggesting that there may be something different in the flow sensing mechanism in different areas of the vasculature. The production of NO by endothelial cells under shear stress stimulation is in part mediated by the mechanosensing action of the GCX and its different components [68]. The GCX has lately gained attention for its role in vascular homeostasis through its dominant role in mechanotransduction [20].

In people without diabetes, elevated blood flow (shear stress) triggers the enzyme extracellular signal-regulated kinase 5 (ERK-5). This in turn phosphorylates eNOS leading to more NO production that dilates blood vessels so blood can flow easily where needed. Shear stress also activates Kruppel-like factor 2 (KLF-2) which inhibit pro-inflammatory immune cells to adhere to diseased portions of the blood vessels. Both factors represent anti-inflammatory and vascular tone regulatory mechanisms maintaining normal endothelial function. Previous studies have suggested that overproduction of AGEs and hydrogen peroxide (H_2O_2) in diabetics interfere with ERK-5 by facilitating the attachment to it of a small ubiquitin-related modifier (SUMO), a protein tag used for cells to fine tune their control over proteins, therefore impairing the production of the atheroprotective NO [176].

Integrin mediated shear stress gene activation and the upstream molecule PECAM-1 (which transmits mechanical force directly), VE-cadherin and VEGF receptor 2 (which activates phosphatidylinositol-3-OH kinase) have also been proposed as a

mechanosensory complex, since PECAM-1-knockout mice do not activate NF-kappaB and downstream inflammatory genes in regions of disturbed flow [177].

Flow-mediated dilation, caused by upregulated NO release, has been suggested as an important pointer to endothelial function in clinical studies of diabetes mellitus and vascular disease [178]. Cross-sectional studies show reduced endothelium-dependent vasodilation in coronary and peripheral arteries of patients with Type 1 [179] and Type 2 diabetes mellitus [180].

In addition it has been shown that the GCX with its protruding proteoglycans and glycoproteins together with their GAG side chains act like a sensor of the shear stress caused by the circulating blood. The enzymatic cleavage of different GCX components has been shown to alter endothelial NO production. Shedding of over 40% of the HS and HA can significantly attenuate NO release in response to shear stress [68]. Optimal NO levels prevent leukocyte adhesion and maintains the endothelium in a quiescent, anti-inflammatory state [178]. Shedding of the GCX also exposes cell membrane adhesion molecules, such as vascular cell adhesion molecule-1 (VCAM-1) and intercellular adhesion molecule-1 (ICAM-1), which are required for the adhesion of leukocytes to the endothelial surface [181].

The effect of high glucose on the glycocalyx has been only recently studied. For instance, it has been demonstrated that acute (2 hours) hyperglycemia can diminish the GCX thickness in human subjects [182]. In addition, in-vitro high glucose incubation of

endothelial cells for a longer period (2 to 4 weeks) caused a rapid decrease in the ability of the GCX to sieve 70-kDa dextran but not 40-kDa dextran suggesting that hyperglycemia mainly affects the hyaluronan component of the GCX [183]. Other in-vitro models have shown that in the presence of high glucose there is a significant shedding of the HS and the HA components into the culture media [21], and reduced levels of HS caused by hyperglycemia have been related to impaired alignment of endothelial cells exposed to shear levels of 12 dyn/cm^2 [22].

The present study focuses on the hyperglycemia induced changes on the GCX and its possible consequences in impaired vasoreactivity. This is accomplished in two parts; first we show that selective degradation of the GCX with enzymes inhibits shear-induced increase in endothelial hydraulic conductivity (Lp) that are known to be mediated by shear-induced NO production (chapter 4). Then we show that elevated glucose suppresses the shear-induced increase in endothelial Lp, reduces the heparan sulfate component of the GCX and suppresses the phosphorylation of eNOS (chapter 5).

CHAPTER 3

A Three Pore Model Describes Transport Properties of Bovine Retinal Endothelial Cells Under Normal and Elevated Glucose

3.1 Introduction

Diabetic Retinopathy (DR) is the leading cause of blindness among working age adults [184], but the mechanisms by which diabetes leads to retinal microvascular complications is still not completely understood. The initial stage of DR is marked by an elevated permeability of the blood vessels of the retina [14] and subsequent plasma leakage to the interstitial space. Elevated glucose is believed to contribute to various vascular dysfunctions [9, 10], among them, loss of microvascular barrier integrity [7, 8]. However, an increase of VEGF that occurs even before morphological abnormalities are observed, has been described in patients with DR [130, 133]. The relative contribution of the direct effect of glucose compared with changes in cytokine expression on the iBRB remains under investigation.

Expression and organization of a well-developed TJ complex in the inner retinal capillaries contributes to the formation of the iBRB. Immunohistochemical staining for albumin performed in patients at different stages of DR has shown that these vessels are

the primary site of vascular leakage resulting in retinal edema [14]. However, while changes in lipids, albumin and fluorescein accumulation in the retina are routinely observed as an indication of altered endothelial permeability in patients with diabetic retinopathy, little has been done to characterize the various routes of transport that may affect vascular permeability. Transport of molecules across the vascular endothelium may occur by transcellular pathways including specific transporters or by paracellular transport, which includes transport across the junctional complex, across a broken junctional complex, or across a large gap caused by cell death or cell division [185].

The two principal mechanisms driving paracellular transport of molecules and fluid across the endothelium are: diffusion; or movement from regions of higher concentration to regions of lower concentration, and convection; a mechanism of transport that results from the bulk motion of fluid typically driven by a pressure gradient. Molecular motion may differ from local fluid motion because the solute molecules are also diffusing simultaneously [186]. Thus, oncotic pressure and hydrostatic pressure drive both fluid and solute transport but the availability of various routes of transport controls the rate of flux across the endothelium.

Information specific to the transport pathways of the iBRB is essential to understand vascular permeability in DR; however, this information is difficult to obtain using in-vivo models. Previous in-vitro results suggested that hyperglycemia may increase BREC diffusive permeability to small solutes [110, 111], but more recent data on human retinal endothelial cells (HREC) have suggested that up regulation of several cytokines may

cause endothelial dysfunction and not hyperglycemia per se[187]. Moreover, experiments using human retinal pigment epithelial cells (HRPEC) demonstrated that hyperglycemia reduced the diffusive flux of both 40 and 70-kDa dextran and no changes in TJs were observed. In animal studies, increased permeability is normally observed anywhere from one to six months after streptozotocin induced hyperglycemia [104], but this may be secondary to an increase in cytokines such as VEGF.

In the present study, we have examined an *in vitro* model system of retinal endothelial cells to quantify fluid and solute transport after both elevated glucose and VEGF treatments. Results from this analysis allowed the development of a three-pore model, namely: transcellular transport through vesicles, broken tight junctions, and large pores also termed leaky junctions. A determination of the fractional transport through each pore for various size solutes was calculated. Hyperglycemia was shown to have no effect on water or solute transport across the endothelium whereas VEGF increased permeability under both low and high glucose concentration. The data suggest that 6 days of high glucose has little direct effect on endothelial permeability and suggests that hyperglycemia in diabetes may alter permeability indirectly through cytokine production.

3.2 Materials and methods

3.2.1 Chemicals

Bovine serum albumin (BSA, 30% solution), trypsin, penicillin-streptomycin solution, sodium bicarbonate, fibronectin, fetal bovine serum (FBS), L-glutamine and D-glucose

were obtained from Sigma (St. Louis, MO). MCDB-131 (phenol red free), L-cysteine and L-methionine were obtained from US Biological (Swampscott, MA). An antibiotic-antimycotic mixture was obtained from GibcoBRL (Rockville, MD) and Heparin and Dubelcco's PBS (1x without Ca2+ and Mg2+) from Fisher Scientific (Houston, TX). MCDB-131 complete (with phenol red, serum and a cocktail of growth factors) was obtained from VEC technologies (Rensselaer, NY).Transwell polyester inserts (0.4 μm pore size, 12 mm diameter) were obtained from Corning Costar (Acton, MA). VE-cadherin polyclonal primary antibody was obtained from Cayman Chemical (Ann Arbor, MI). ZO-1 primary antibody was obtained from Zymed (San Francisco, CA). Claudin-5 primary antibody was obtained from Invitrogen (Carlsbad, CA). The fluorescent solutes carboxytetramethylrhodamine (TAMRA) and 70-kDa TRITC-dextran were obtained from Molecular Probes (Carlsbad, CA) and Dil-LDL from Biomedical Technologies (Stoughton, MA). The TUNEL assay kit was obtained from Roche (Indianapolis, IN), the Western blot kit, Bradford assay and Immun-Blot PVDF membrane from Bio-Rad (Hercules, CA). The Phospho-eNOS (Ser1177) and β-actin antibody were obtained from Cell Signaling (Beverly, MA), and the VEGF from R&D systems (Minneapolis, MN).

3.2.2 Cell Culture

Primary BREC were harvested from bovine eyes as described by Antonetti et al.[188] then the frozen vials were thawed as needed and grown on fibronectin coated (2μg/cm^2) T-75 flasks with MCDB-131 (US Biological) medium prepared as indicated by the vendor by addition of L-glutamine, L-cysteine, L-methionin and heparin and

supplemented with 10% FBS, 10 ng/mL EGF, 0.2 mg/mL Endo grow and antibiotic/antimycotic at 37°C and 5% CO_2. For transport experiments, Transwell inserts were seeded at a density of $6.0X10^4$ cells/cm^2. BREC were treated with 100 nM hydrocortisone to enhance monolayer formation and barrier properties. The normal glucose (NG) level of the culture media was 5 mM and the high glucose (HG) level of 25mM was reached by addition of D-glucose. The monolayers were cultured for 4 to 6 days (until they reached confluency). Transport experiments were carried out using phenol red free MCDB-131 with 1%BSA, penicillin-streptomycin solution and no other supplements. These experiments lasted no more than 4 hours. Cells were used between passages 3 and 8. For experiments where cells were treated with VEGF and 70-kDa dextran permeability was measured, high glucose was 10 mM.

3.2.3 Measurement of water and solute flux

The simultaneous measurement of water and solute flux was performed with an apparatus described previously [189, 190]. Briefly, the BREC seeded Transwell filters were placed inside each of eight chambers that were sealed so that they formed a luminal (top) and an abluminal (bottom) compartment. All of the chambers were connected to a reservoir that could be lowered 10 cm with respect to the media level in the luminal compartment thereby imposing a hydrostatic pressure differential to drive fluid flow across each monolayer. In two of the chambers, this fluid flow moved a bubble that was previously inserted in a borosilicate glass tube that connected the chamber to the reservoir to allow measurement of water flow. The movement of the bubble was tracked using a

spectrophotometer and the software Bt-Millenia both from C&L instruments. The displacement versus time data was used to calculate the water flow per unit area across the monolayer (Figure 10).

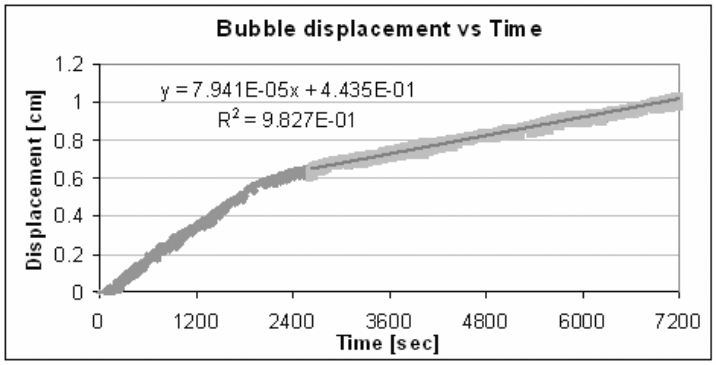

Fig. 10. Bubble displacement [cm] versus time [s]. As water moves from the luminal to the abluminal side of the chamber, the displacement of a bubble inserted in the borosilicate glass tube is measured. The water flux at equilibrium is then calculated from the slope in that range, according to equation 1.

At steady state, the slope of the curve was constant and could be obtained by applying a linear fit to the data. The water flow per unit area was calculated with the following relationship:

$$J_V = \frac{\Delta d}{\Delta t} \times \frac{F}{A} \tag{1}$$

Where $\Delta d/\Delta t$ is the slope of the linear fit of the displacement vs time curve, F is a volumetric factor for the glass tube (volume per unit length) and A is the cross sectional area of the filter.

To measure solute transport across the BREC monolayer, three fluorescently tagged

molecules with different sizes were used (Table 1). Each tagged molecule was initially added to the luminal compartment in separate experiments and was allowed to pass through the BREC monolayer to the abluminal compartment.

Molecule	**Stokes Diameter**	**Molecular Weight**	**Luminal Concentration**
TAMRA	1.3 nm	460 Da	300ng/mL
Dextran	11 nm	70 kDa	1μM
DiI-LDL	22 nm	2,000 kDa	10μg/mL

Table 1. Fluorescent molecules used to characterize solute transport properties of BREC monolayers. The Stokes diameter, molecular weight and concentration used at the luminal side of the insert are listed.

During the first hour of the experiment the abluminal reservoir was allowed to equilibrate with the height of the media in the luminal compartment to eliminate fluid flow. Then, a 10-cm H_2O hydrostatic pressure differential was applied and maintained for two hours to drive convective flow across the monolayer. Finally, convective flow was stopped by eliminating the pressure differential and the fluorescent molecule was allowed to cross the monolayer by diffusion for a period of one hour. Fluorescence in the abluminal compartment was acquired as a function of time, using the FluorMeasure software from C&L instruments. The fluorescence counts generated were converted to units of

concentration using a calibration curve. The slope of the concentration versus time curve ($\Delta C_a/\Delta t$) was used to calculate the permeability to the florescent molecule using the following equation:

$$Pe/o = \frac{(\Delta C_a/\Delta t)\times V_a}{C_l \times A} \quad (2)$$

where *Pe/o* is either the apparent permeability, *Pe*, which is calculated from the slope in the time interval where there is a convective component, or *Po*, which is calculated using the slope during the time interval when only diffusion is taking place (Figure 11). V_a is the volume of the abluminal compartment, C_l is the solute concentration on the luminal side and A is the area of the monolayer. The concentration on the luminal side is very high compared to the abluminal side and is assumed to be constant during the course of the experiment. Prior to the experiments, the monolayers were rinsed twice with phenol red free MCDB-131 media supplemented with 1%BSA. During the experiments, the media was maintained at 37^{o}C and equilibrated with 5%CO_2-95% balance air to regulate the pH at 7.4.

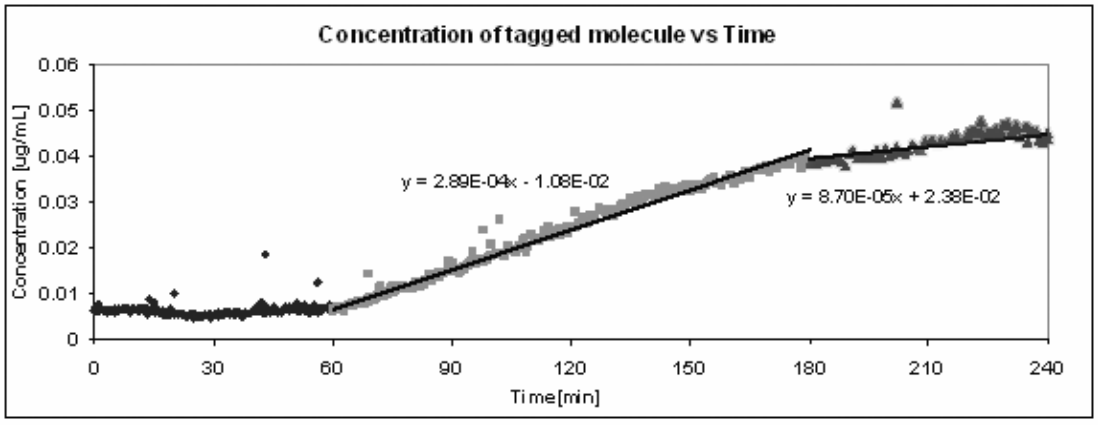

Fig. 11. Concentration of tagged molecule in the abluminal compartment as a function of time. In this case a typical DiI-LDL concentration vs time curve is shown. The apparatus is calibrated to convert units of fluorescent counts into units of concentration for each tagged molecule. During the first 60 minutes the system is left to equilibrate, after which a 10 cm H_2O hydrostatic pressure is applied for two hours and Pe is calculated using the slope of that interval and equation (2). The pressure then is removed and the diffusive permeability Po is calculated from the new slope of that interval.

3.2.4 Pore model

The endothelium has been modeled as a membrane with pores or pathways of different sizes that impose sieving restrictions to the molecules being transported but do not interact with each other. The model used herein to describe transport across BREC monolayers has been used before to describe transport across BAEC monolayers [190]. For a single pathway and solute, the apparent permeability *Pe* results from diffusive and convective contributions as described by the relation below [191]:

$$Pe = Po\ Z + Jv(1- \sigma) \tag{3}$$

The Z term is given by:

$$Z = \frac{N_{pe}}{e^{N_{pe}} - 1} \tag{4}$$

where N_{pe} is the Péclet Number defined as:

$$N_{pe} = \frac{Jv(1-\sigma)}{Po} \tag{5}$$

and, Jv is the water flux across the pathway, Po is the diffusive permeability, and σ is the reflection coefficient of the solute, which lies between 0 and 1.

The three pathways used to model the endothelium are: pathway 1-transcellular/vesicle, pathway 2-breaks in the TJ and pathway 3-large pore leaky junction. The model assumes that water is transported only through pathways 2 and 3 because the hydraulic resistance of the very narrow TJ effectively blocks water flow [192] and vesicles are not believed to conduct significant water [190]. Therefore, the total water flow Jv across the endothelium is the sum of the water flow across pathways 2 and 3:

$$Jv = Jv_2 + Jv_3 \quad (6)$$

It seems reasonable to assume that due to its size (2-4 nm) [33, 44], the TJ pathway excludes 70-kDa dextran and LDL. Also, due to its size, LDL is unlikely to go through pathway 2, breaks in the TJ. Assuming that LDL transport occurs through pathways 1 and 3, (vesicles and leaky junctions) [190] and that σ_3, the reflection coefficient for LDL in pathway 3 is equal to zero, since leaky junction dimensions are much greater than LDL diameter [52], then Eq. 3 for this molecule reduces to Eq. 7. It is worth mentioning that there is no convection through pathway1-vesicles, since there is assumed to be no water flux.

$$Pe_{LDL} = Po_{1LDL} + Po_{3LDL}\, Z_{3LDL} + Jv_3 \quad (7)$$

$$Po_{LDL} = Po_{1LDL} + Po_{3LDL} \quad (7a)$$

However, since N_{pe} is large (Z tends to zero) for LDL, the total permeability to LDL tends to be equal to the water flow through the leaky junctions (Jv_3) which tends to be much larger than the diffusive transport through vesicles (Po_{1LDL}). The LDL transport through pathway 1 has been estimated to be less than 10% [190].

Similarly, if 70-kDa dextran is assumed to be transported through pathways 2 and 3 only, since previous experiments in BAEC [193] and our own results in BREC show that there is no vesicle contribution to the transport of this molecule, and if $\sigma_{3DEX} = 0$ (dextran is much smaller than the large pore leaky junction) and σ_{2DEX} is different than zero, then Eq. 3 for 70-kDa dextran can be written as:

$$Pe_{DEX} = Po_{2DEX} Z_{2DEX} + Jv_2(1-\sigma_{2DEX}) + Po_{3DEX} Z_{3DEX} + Jv_3 \quad (8)$$

$$Po_{DEX} = Po_{2DEX} + Po_{3DEX} \quad (8a)$$

To solve the system of equations (6)-(8), it is first recognized that equations 6 and 7 can be solved for the two unknowns Jv_2 and Jv_3. The other variables in the equations are measured experimentally. For instance, by fixing the monolayers to block vesicular transport one can determine the values for $Po_{3LDL;}$ subsequently Po_{1LDL} can be determined from equation 7a.

Then, with those values for Jv_2 and Jv_3, equation 8 is solved together with equation 8a for Po_{2DEX} and $Po_{3DEX.}$ The solution to these equations will exist only for a certain range of σ_{2DEX} between 0 and 1.

3.2.5 Junction protein Immunostaining

To visualize the TJ protein ZO-1 and the adherens junction protein VE-cadherin, BREC

on filters were fixed with 1% paraformaldehyde for 10 minutes, washed with PBS, permeabilized with 0.2% Triton X-100 in PBS for 10 minutes and then blocked with 10% BSA and 0.1% Triton X-100 in PBS (blocking solution) for one hour. After washing with PBS, either rabbit anti-ZO-1 or VE-cadherin polyclonal primary antibody was diluted in blocking solution (1.25 μg/ml) and added to the filter. The next day the cells were washed five times with PBS and incubated for one hour with Alexa Fluor® 488 donkey anti-rabbit secondary antibody (Invitrogen) diluted in blocking solution (4μg/ml). Once again the cells were washed four times with PBS and placed under a Nikon Eclipse TE2000-E inverted microscope for observation. Two random fields were chosen per filter and fluorescent images were captured using a Photometrics Cascade 650 camera (Roper Scientific). Images were acquired via the MetaVue 6.2r2 imaging software (Universal Imaging). The same fixation was used for immunostaining or to block vesicular transport and determine the contribution of active transport to total transport for LDL and dextran.

3.2.6 Determination of Apoptotic cells

A terminal deoxynucleotidyl transferase dUTP nick end labeling (TUNEL) assay protocol was followed to determine the percentage of apoptotic cells. The monolayers were fixed in 4% paraformaldehyde for 1hr at room temperature, rinsed with PBS, incubated with 50 μL blocking solution (0.1% Triton X-100 in 0.1% sodium citrate) for 10 minutes at room temperature and rinsed again with PBS. The TUNEL reaction mixture was prepared and added to each filter (50 μL). The filters then were incubated in

the dark for one hour at 37˚C, rinsed three times with PBS and taken to the Nikon Eclipse TE2000-E microscope for observation.

3.2.7 Incubation with VEGF

In some experiments, the monolayers were incubated for either two or four hours with 100 ng/mL VEGF in culture media and then harvested for Western blotting. In a separate set of experiments, BREC monolayers were incubated with VEGF for four hours prior to determining water and solute flux.

3.2.8 Western Blotting

BREC were grown in MCDB-131 complete (VEC technologies) and the monolayers where scraped from the filters in the presence of RIPA lysis buffer (NaCl 0.6M, NP-40 4%, Tris 0.2M, Brij 35 0.4% EDTA 4mM) supplemented with a protease and phosphatase inhibitor cocktail, Na_3VO_4 and PMSF. Protein concentration was determined with the BioRad Bradford protein assay kit (Hercules, CA). Western blot was carried out by standard techniques, loading 20 μg of protein into the gel wells and incubating over night with the appropriate antibodies to phospho-eNOS (Serine 1177), or Claudin-5 and regulatory protein β-actin, followed by reaction with matched secondary anti-rabbit antibody. The blots were scanned with the Universal Hood II (BioRad) and visualized with the software Quantity One version 4.5 (BioRad).

3.2.9 PCR Analyisis

PCR was carried out using the Cells-to-cDNA™ II Kit from Applied Biosystems (Ambion, Austin TX). After RNA was converted to cDNA, the products were incubated with Taq master mix (New England Biolabs), and PCR primers. The PCR program was: 95ºC for 5 min, 30 cycles of 94ºC , 52ºC and 72ºC for 30 s for each step, followed by a final extension of 72ºC for 10 min. The primer sequences (Integrated DNA, Coralville IO) for the target genes were: claudin-5, forward: ACCGGCGACTATGACAAGAA and reverse: AGGGTCATCATCTCTGCACC (with 227bp of PCR product) and for the internal standard GAPDH were: forward AGGGTCATCATCTCTGCACC and reverse CCATCCACAGTCTTCTGGGT (with a 218bp of PCR product). The PCR products generated were determined by 2.5% agarose gel (Invitrogen) electrophoresis in the presence of ethidium bromide, scanned with the Universal Hood II (BioRad) and analyzed using image software(Quantity One, Biorad).

3.2.10 Statistical analysis

Water flux and solute permeability are presented as mean ± SE. Statistical difference was assessed by using the unpaired Student's t-test with $P < 0.05$ considered significant.

3.3 Results

3.3.1 Water flow and solute permeability

Table 2 summarizes the water flow and permeability data for LDL, 70-kDa dextran and TAMRA for BREC monolayers incubated with 5mM or normal glucose (NG) and 25 mM or high glucose (HG) for 6 days. Jv/A represents the water flow per unit area, P_o represents the permeability under diffusive conditions, whereas P_e represents the steady state apparent permeability.

A typical bubble displacement versus time curve is shown in figure 10, where the slope of the linear range has been used to calculate the water flux values at steady state using equation 1 (Methods). The water flux across BREC monolayers for both NG and HG showed a typical transient decrease that has been observed before *in vitro* and *in vivo* and has been termed the sealing effect or adaptive response [44, 193, 194]. Lp values for NG and HG were 1.93 and 2.74×10^{-7} cm/s cmH_2O, respectively, representing an increase of 40% in HG. However the difference was not statistically significant.

3.3.2 LDL Permeability

Upon application of a 10-cmH_2O hydrostatic pressure differential, the concentration vs time curve for LDL showed a sharp increase in slope (Figure 11), suggesting that the flux of this macromolecule is coupled to water flow by a solvent drag mechanism.

Molecule	**n**	**Jv/A x 10^{-6} [cm/s]**	**P_o x 10^{-6} [cm/s]**	**P_e x 10^{-6} [cm/s]**	**Mean P_e / P_o**
Water	12	**NG** 1.93 ±0.34 **HG** 2.74 ±0.35 p-value: 0.11			
LDL	12		**NG** 0.20 ± 0.07 **HG** 0.23 ±0.05 p-value:0.42	**NG** 1.39 ±0.33 **HG** 1.43 ±0.63 p-value:0.78	6.95 6.22
70-kDa Dextran	8		**NG** 1.24 ±0.21 **HG** 1.85 ±0.25 p-value:0.23	**NG** 2.43 ±0.45 **HG** 2.81 ±0.49 p-value:0.59	1.70 1.52
TAMRA	6		**NG** 9.64 ±0.33 **HG** 9.02 ±0.67 p-value:0.66	**NG** 11.4 ±0.35 **HG** 10.5 ±0.76 p-value:0.25	1.18 1.16

Table 2. Water flow per unit area (Jv/A) and solute permeability to LDL, 70-kDa dextran and TAMRA of BREC monolayers incubated with normal (NG) and high glucose levels (HG). The high glucose level corresponds to 25mM. After the monolayers reached confluency (4 to 6 days), they were placed in the transport apparatus to determine water flux (Jv/A) as well as solute permeability.

This behavior has been observed before in BAEC monolayers [190] and in intact hamster venules [195]. The pronounced effect of solvent drag can be seen in the mean ratio of the apparent (P_e) to the diffusive (P_o) permeability, which was 6.95 for NG and 6.22 for HG.

3.2.3 70-kDa dextran permeability

The increased transport associated with elevated water pressure, which had been observed previously [193], indicates that the flux of 70-kDa dextran is coupled to water flow as well. The solvent drag effect was highest at the moment of application of the hydrostatic pressure, and then decreased as sealing occurred. Again, permeability values for NG and HG were not significantly different. The mean ratio of the apparent to the diffusive permeability calculated at the steady state region was 1.7 for NG and 1.52 for HG.

3.2.4 TAMRA permeability

Upon application of a 10-cmH_2O hydrostatic pressure differential, the concentration vs time curve for this molecule did not show the sharp increase seen with the two larger molecules. The convective component did not have a significant contribution to transport; therefore TAMRA is readily transported by diffusion across BREC monolayers. The ratio of the apparent to the diffusive permeability was 1.18 for NG and 1.16 for HG. The permeability values obtained for NG vs HG were not significantly different.

3.2.5 Cell fixation experiments

Table 3 shows the diffusive permeability for control (P_o) and fixed ($P_{o,fixed}$) monolayers, as well as the ratio of the two permeabilities, calculated from the mean values.

Molecule	n	$P_o * 10^{-6}$ [cm/s]	$P_{o,\ fixed} * 10^{-6}$ [cm/s]	p-value for significance	Mean P_o / P_o fixed
LDL	6	0.29 ±0.03	0.09 ±0.03	0.002	3
70-kDa Dextran	6	1.24 ±0.23	1.52 ±0.32	0.62	0.81

Table 3. Effect of fixation on transport of LDL and 70-kDa dextran. Fixation of the cells with 1% paraformaldehyde significantly decreased the transport of LDL but not of 70-kDa dextran.

Upon fixation, the diffusive permeability for LDL was significantly reduced to one third of its original value (p=0.002), whereas the diffusive permeability for dextran was not significantly different (p=0.62). These results suggest that BREC present a significant vesicle contribution for LDL transport but not for 70-kDa dextran. These results are used in the three pore analysis to assign a value to the LDL vesicle transport.

3.2.6 Three-pore model analysis

The results for the three pore model are shown in table 4. For this analysis it was assumed that the endothelium can be modeled as a membrane containing 3 pores that do not interact with each other. The interaction between pores in heteroporous membranes which has been observed to be relevant for low filtration rates in the presence of a

significant osmotic gradient[88], has been neglected since we have used 1% BSA-MEM media for both the luminal and abluminal compartments, therefore the osmotic gradient across the monolayer is basically zero. The retinal TJ gap, which has been described as the place where the membranes touch, has not been included as a pore. The 3 pores are;1-transcellular/vesicle, 2-breaks in the TJ and 3- large pore leaky junctions.

Component	**Pathway 1: vesicles**	**Pathway 2: Breaks in the TJ**	**Pathway 3: Leaky Junctions**	**Total**
Water		34.75%	65.25%	100%
LDL	9.42%		90.58%	100%
Dextran		19.93%	80.07%	100%

Table 4. Molecules and pathways analyzed with a three-pore model. The model was constructed based on the assumptions and equations established in the methods section. The percentage of solute and water being transported through each pathway were estimated from the solutions to equations 6-8, using the experimental permeability values. The percentages shown correspond to $\sigma_{2DEX}=0.55$.

We have not included a water only channel (aquaporin), like in previous 2 and 3-pore models [90] used to model peritoneal dialysis because it has been observed that aquaporin presence is low or non existent in retinal endothelium [91] and as stated before there are no large osmotic gradients across the endothelial cells. The experimental values obtained for NG were used to develop this model since no significant difference was observed under HG conditions. A comparison of solute transport under normal and fixation conditions (Table 3) demonstrated that LDL, but not dextran, is transported

transcellularly, and the model was constructed following this observation. Also, given the sizes of the molecules, it was assumed that LDL, dextran and water are transported through the large pore leaky junctions, but only dextran and water are transported through breaks in the TJ that have been estimated to open to the width of the adherent junction (20 nm) [44]. Finally, it was also assumed that the reflection coefficient at the large pore leaky junctions was zero for both dextran and LDL but the reflection coefficient at the breaks in the TJ for dextran was a value between 0 and 1. Only a limited range of this coefficient yielded real solutions when applied to the transport equations. For NG the equations had real solutions for σ_{2DEX} ranging from 0.4 to 0.55, this range is in good agreement with the range obtained for BAEC monolayers that had been grown in NG [190, 193].

The solution to the model shows that the large pore leaky junction is a dominant transport pathway for both 70-kDa dextran and LDL while water tends to be more evenly distributed through the breaks in the TJ and the large pore leaky junctions. Vesicle transport accounts for less than 11% of the LDL transport. Therefore, these results suggest that alterations in pathways 2 and 3 would significantly impact solute and water transport.

It is generally believed that the reflection coefficient for the breaks in the tight junction, $\sigma_{2,}$ is determined by the fiber matrix (glycocalyx) that fills the apical aspect of this pore. With the σ_{2DEX} values obtained, between 0.4 and 0.55, and the following equations, it is possible to estimate the glycocalyx fractional fiber volume V_f by modeling the

glycocalyx as a fiber matrix [186], where the reflection coefficient σ is given by:

$$\sigma = (1 - \varphi)^2 \tag{9}$$

For a random fiber arrangement, φ, the partition coefficient, is given by:

$$\varphi = \exp[-(1-\varepsilon)(2a / r_f + a^2 / r_f{}^2)] \tag{10}$$

where (1-ε) is the fractional fiber volume, a is the radius of the solute, and r_f is the fiber radius.

For an ordered fiber arrangement, the partition coefficient is given by:

$$\varphi = 1 - V_f(1 + a / r_f)^2 \tag{11}$$

where V_f represents the fractional fiber volume. The results are shown in table 5. Using 5.5 nm for the Stoke's radius of dextran and 0.6 nm for the fiber radius [186], equation 10 predicts a volume fraction (1-ε) that ranges from 0.98 to 1.32% for a random fiber arrangement and equation 11 predicts a volume fraction V_f that ranges from 0.61 to 0.72% for an ordered fiber arrangement under NG treatment. (1-ε) ranges from 1.54 to 1.96%. These predicted fiber volume fractions are in good agreement with values estimated for capillaries (less than 5%) [35].

σ_{2DEX}	% Pore 2	φ	(1-ε)	Vf
0.4	32%	0.37	0.0098	0.0061
0.5	22.20%	0.29	0.0120	0.0068
0.55	19.93%	0.26	0.0132	0.0072

Table 5. Fractional fiber volume for different dextran reflection coefficients through pathway 2. The partition coefficient φ is calculated for a random or an ordered fiber arrangement. (1-ε) represents the fractional fiber volume when the random arrangement is used, and Vf represents the fractional fiber volume when the ordered arrangement is used. Using 5.5 nm for the solute radius and 0.6 nm for the fibers, equations 10 and 11 predict volume fraction values that are in good agreement with values estimated for capillaries [35].

3.2.7 Junction proteins under High Glucose

Organization of the tight junction requires ZO family members and ZO-1 organization is an excellent marker of tight junction formation while the transmembrane protein VE-Cadherin is a marker of adherens junction organization. Representative pictures for ZO-1 and VE-Cadherin immunostaining are shown in figure 12. Qualitatively, no differences in the intensity or continuity of these junctional proteins were observed between the normal and high glucose monolayers.

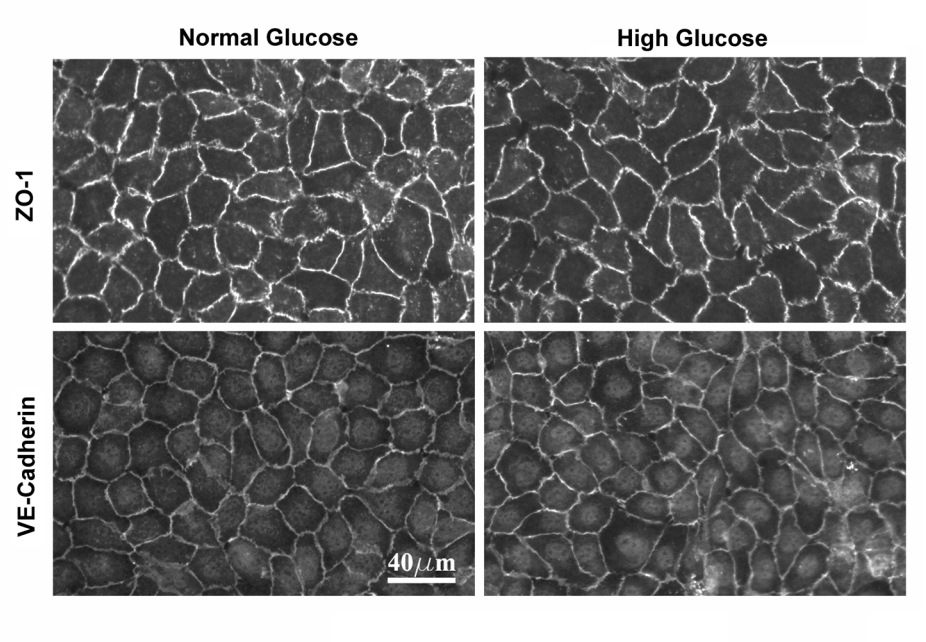

Figure 12. Representative micrographs of the TJ protein ZO-1 and the adherent junction protein VE-Cadherin. Upon exposure to HG (25 mM) for 6 days, there was no significant change in the intensity or continuity of either ZO-1 or VE-Cadherin proteins compared to NG controls.

The transmembrane tight junction protein claudin-5 is expressed in endothelial cells and required for formation of the blood-brain barrier [196] and is also present in the retina [197]. Western blotting and RTPCR analysis demonstrate that neither Claudin-5 protein nor gene expression were significantly different when cells were cultured in HG compared to NG (Figure 13). Image analysis shows a 13% ± 0.45 decrease in protein expression and an 11% ± 0.34 increase in gene expression but neither was statistically significant.

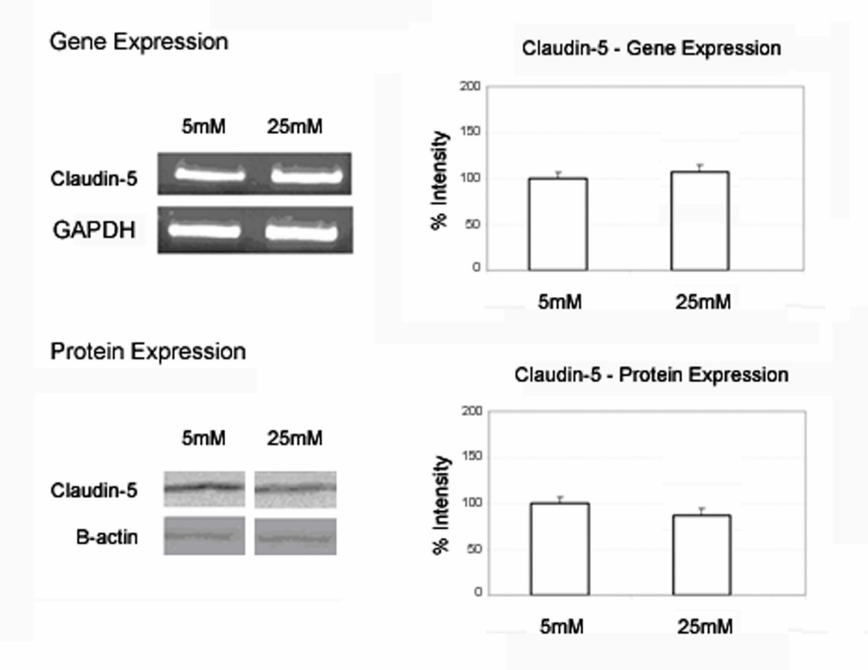

Fig. 13. Western Blots and PCR showing the expression of the TJ protein Claudin-5 for monolayers incubated for 6 days in either NG (5mM) or HG (25 mM). After analyzing the images with the software image J, we observed that the claudin-5 protein expression of monolayers in HG decreased by 13% ± 0.45 compared to NG (n=3 p=0.059) whereas the gene expression increased by 11% ± 0.34, both changes not significant (n=3 p=0.057)

3.2.8 Apoptotic Cells

Representative pictures of the TUNEL assay staining are presented in figure 14.

Cells were cultured with 25 mM glucose media for 6 days and compared to control cells. After analyzing 6 random fields, the percentage of apoptotic cells were 2.1±0.56% and 2.9±0.46% for NG and HG, respectively. Again, this change was not statistically significant (p=0.62).

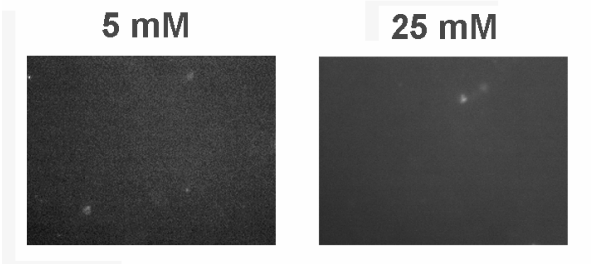

Fig. 14. TUNEL assay for apoptotic cells. Staining for cells grown in both NG and HG (25mM) glucose are shown. The mean percentage of stained cells was slightly elevated in the cells grown in high glucose. The values were 2.1±0.56% and 2.9±0.46% for normal and high glucose respectively, however they were not significantly different (p=0.62, n=6).

3.2.9 Effect of VEGF on 70-kDa dextran Apparent Permeability and Water Flux Across BREC Monolayers\

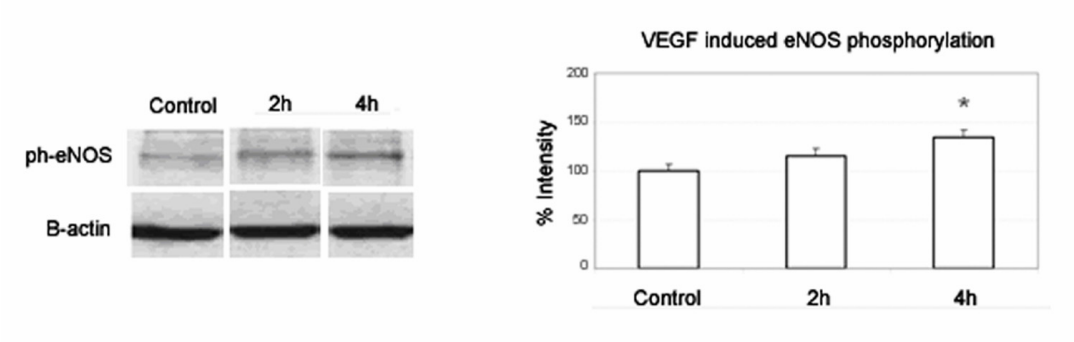

Fig. 15. Western blot for phospho-eNOS. After the BREC monolayers were incubated with VEGF (100ng/mL) for two and four hours, a western blot was performed to observe changes in the phosphorylation of eNOS. It is evident that the phosphorylation increases with the time of incubation. The dark lower band corresponds to β-actin, which was used as a control Four hours of incubation increased ph-eNOS levels by 33 ±0.34% (p=0.03).

It has been shown previously that BREC monolayers respond to VEGF with an elevated Jv/A that is attenuated by an e-NOS inhibitor [23]; therefore, BREC monolayers were incubated with 100ng/mL VEGF to determine the relative amount of phosphorylated e-

NOS compared to control monolayers.

We observed that the expression of phosphorylated eNOS increased with time and was significantly different from controls, 4 hours after initial incubation (Figure 15). Therefore, the effect of VEGF on BREC monolayer permeability was measured 4 hours after addition of VEGF in both NG (5mM) and HG (10mM) environments.

	n	Without VEGF	With VEGF (100ng/mL)	Ratio With/ Without	p-value
Jv/A x 10^{-6} [cm/s]	4	**NG** 2.42 ±0.69 **HG** 3.56 ±0.56 p-value: 0.25	**NG** 4.27 ±0.57 **HG** 5.23 ±0.60 p-value: 0.37	1.76 1.47	0.0062 0.0067
70-kDa Dextran P_e x 10^{-6} [cm/s]	4	**NG** 2.04 ±0.46 **HG** 2.31 ±0.22 p-value: 0.64	**NG** 3.03 ±0.52 **HG** 4.15 ±0.28 p-value: 0.10	1.48 1.79	0.017 0.007

Table 6. Effect of VEGF on BREC permeability. Jv/A and 70-kDa dextran apparent permeability Pe were determined for monolayers cultured for 6 days in either NG or HG (10 mM) Half of the monolayers were incubated with 100 ng/mL VEGF for 4 hours prior to the measurement of Jv/A and Pe. VEGF significantly increased Lp and Pe in both NG and HG monolayers.

The results of our measurements are shown in table 6. Comparing NG without VEGF and NG with VEGF, there was a significant increase in water flux ($p=0.0062$). Comparing HG without VEGF and HG with VEGF, again a significant increase in water flux ($p=0.0067$) was observed.

Similarly, there was a significant increase in 70-kDa dextran permeability when the cells grown in NG were incubated with VEGF ($p=0.017$), and there was a significant increase when the cells grown in HG were incubated with VEGF ($p=0.0071$). Even though there was a tendency for glucose to sensitize the monolayer to VEGF, there was no significant difference between the NG and HG monolayers incubated with VEGF ($p=0.1$).

3.4 Discussion

In this study, an *in-vitro* model of the iBRB was used to accurately assess water and solute flux across the endothelium simultaneously. A 3-pore model was developed to describe the diffusive and convective flux of small, intermediate and large molecules and to determine their routes of transport. To our knowledge, no other study addresses the transport of molecules over a broad range of sizes across BREC monolayers under convective conditions and estimates the distribution of molecular transport through the principal endothelial pathways. Therefore this set of data is an important characterization of BREC monolayers *in-vitro* and provides a novel understanding of the various routes of transport across the blood-retinal barrier.

The results shown here for retinal endothelial cells reflect similarities to those previously reported for aortic endothelium but also demonstrate important differences. Results for LDL apparent permeability (Table 2) are very similar to those previously found for BAEC monolayers where Pe was measured to be 1.31E-6 ±0.36. However, water flux was measured to be 5.39E-6 ±0.7 cm/s in BAEC [190]; whereas, BREC water flux is about half the value in BAEC. This may be due to the specialized junctional complex in BREC that form the iBRB. Indeed, the mean water flux through the large pore leaky junction for BREC monolayers was 1.26 E-6 cm/s which is very similar to the value for BAEC monolayers of 1.20E-6 [190]; however, water flux through the break in the TJ is much lower for BREC than for BAEC, 6.17E-7 compared to 4.19 E-6 respectively. The similarity in LDL apparent permeability can be explained by the similarity in water flux through the large pore leaky junctions, while the difference in total water flux can be explained by reduced water transport through junctional breaks.

The predictions of our 3-pore model, summarized in Table 4, also indicate that the large pore leaky junctions are a dominant pathway for water, 70-kDa dextran and LDL transport. The estimated LDL transport is consistent with a previous *in vitro* model for BAEC monolayers [190] and observations that regions with increased uptake of albumin predicted regions of enhanced LDL uptake [32]. The low percentage of LDL transported in vesicles is also consistent with observations by Wiklund, [198] who used methylated LDL to block its recognition by the LDL receptor in rabbit aortas.

The effect of high glucose on solute and water permeability for the three solutes used,

showed that overall, 6 days of culture in high glucose did not significantly alter the diffusive permeability, Po, or the apparent permeability, Pe, of TAMRA, 70-kDa dextran or LDL. The water flux across the monolayers did not statistically significantly change with high glucose either, although a 40% increase was observed (See Table 2). Further, upon application of a hydrostatic pressure a significant increase in Pe was observed for 70kDa dextran and, in particular, LDL, indicating that convective flux contributed to the overall transport of the larger solutes although no effect of high glucose was observed. Monolayers cultured in high glucose for 6 days did not significantly change the distribution or intensity of TJ protein ZO-1 or the AJ protein VE-Cadherin and did not demonstrate a change in expression of claudin 5. These observations are consistent with previous high-field electron micrographs of BREC monolayers grown for 30 days in high glucose, which revealed no significant cell damage or change in the intercellular junctions [122]. Further, Shivers [199]demonstrated that the edge and groove of the TJ revealed no alteration in freeze fracture images of brain capillary endothelium of hyperglycemic lizards and Vorbrodt et al, [200] were also unable to detect any changes in the ZO-1 content of brain microvessels in diabetic rats using a quantitative immunogold procedure. While decreased expression and relocalization of ZO-1 has been observed in rat glomerular epithelial cells exposed to high glucose [124], no changes were observed in BREC monolayers [125]. Taken together these data suggest that BREC permeability and junctional complex do not change in response to 25mM glucose treatment for 6 days.

A number of studies have observed increased apoptosis or altered permeability of endothelium with high glucose. For instance 7 to 9 days of high glucose treatment

decreased monolayer electrical resistance by 20% and increased diffusive transport of C-inulin 5% (Stokes diameter 3 nm) across BREC monolayers [111]. However, the same cells cultured onto microcarriers did not show any increase in sodium fluorescein (Stokes diameter 0.9nm) and cyanocobalamin (Stokes diameter 1.3 nm) permeability during the first 21 days of incubation in 25 mM glucose [110]. Differences in cell type, duration or degree of hyperglycemia may account for the observed differences of the effect of hyperglycemia on permeability.

Alternatively, glucose may not have a direct effect on endothelial permeability. Busik et al, demonstrated that human retinal endothelial cells survival or inflammatory activation were not affected by 4 days of high glucose, but in contrast, exposure of these cells to proinflammatory cytokines IL-1 or TNF-alpha increased mitochondrial superoxide production, ERK and JNK phosphorylation, tyrosine phosphorylation, NFκB activation, and caspase activation, suggesting that hyperglycemia may have little direct effect on vascular endothelium but rather may indirectly induce the release of cytokines and growth factors[187]. Moreover, human retinal pigment epithelial cells exposed to 25mM glucose for 21 days showed significantly higher trans epithelial electrical resistance (TER) and lower 40 or 70kDa dextran diffusion, while occludin and ZO-1 mRNA levels remained constant and claudin-1 levels increased[201]. The ability of VEGF to induce BREC permeability but lack of effect of 25 mM glucose on any permeability measured or apoptosis suggests that, at least within the duration of glucose challenge in these experiments, endothelial permeability is not altered by hyperglycemia directly but rather in response to local cytokines or growth factors. *In-vitro* exposure to high glucose has

been shown to rapidly increase VEGF expression in various cell types and tissues [202] which may account for the elevated VEGF in the retina of humans and animals with diabetes [203], [204]. VEGF mRNA levels in human vascular smooth muscle cells have been observed to increase after just 3 hours of incubation with high glucose and VEGF peptide production increases after 24 hours [205]. Finally, our group has recently found that hyperglycemia increases expression of VEGF in retinal Müller cells in vitro and in vivo through translational control (Manuscript under review Diabetes, 2010).

Previous studies with BREC monolayers demonstrated that VEGF (100 ng/ml) increases hydraulic conductivity dependent on NO synthase [23]. VEGF increases hydraulic conductivity as well as diffusive and apparent permeability of BREC monolayers to 70-kDa dextran (Table 6) associated with increased eNOS phosphorylation and this change in permeability was significantly attenuated with the nitric oxide synthase inhibitor, NG-monomethyl-L-arginine. In addition to the requirement for NO production, it has been demonstrated that VEGF alters phosphorylation and ubiquitination of occludin necessary for VEGF induced increase in permeability [109, 206] and alterations in ZO-1 [148] may also impact paracellular permeability. These studies clearly demonstrate that VEGF increases the breaks in the junction increasing both water flux and large solutes that are carried through these pores by convective flux. Interestingly, small molecules such as TAMRA were shown to be unaffected by convective forces.

Taken together, these data demonstrates that short term (6-day) hyperglycemia does not alter iBRB endothelial permeability and suggests that a direct effect of hyperglycemia on the endothelial cells transport barrier is not the cause of increased permeability in the

early stages of DR. Hyperglycemia may indirectly effect vascular permeability through up-regulation of VEGF or other cytokines that alter the junctional complexes or increase large pore formation through endothelial cell division or cell death.

CHAPTER 4

The endothelial glycocalyx mediates shear-induced changes in hydraulic conductivity

4.1 Introduction

Fluid shear stress-mediated regulation of endothelial hydraulic conductivity (Lp) was first demonstrated in vitro by Sill et al [189]using bovine aortic endothelial cell (BAEC) monolayers cultured on porous, polycarbonate substrates. They observed a 3.76 fold increase in Lp after three hours of exposure to steady shear stress of 20 dyne/cm^2 that could be readily reversed by exposure to dibutyrl cyclic adenosine monophosphate (db-cAMP), demonstrating that the shear-induced increase was not due to endothelial denudation. A subsequent study using the same BAEC model showed that the Lp response to steady shear stress is mediated by shear-induced nitric oxide (NO) since the shear response of Lp could be completely blocked by pre-incubation of the BAEC monolayer with a nitric oxide synthase (NOS) inhibitor [207]. Bovine retinal microvascular endothelial cells (BRECs) in vitro also displayed a marked increase in Lp in response to 20 dyne/cm^2 shear stress that could be completely blocked by a NOS inhibitor [23]

Similar phenomena have been observed in vivo. Lever et al [208] found that the Lp of rabbit carotid arteries in an ex vivo flow loop increased significantly after 20 min of exposure to a step change in shear stress of about 1 dyne/cm^2. Williams et al [209] measured Lp after step changes in shear stress in arterioles, capillaries and venules of the frog mesentery using the modified Landis technique. The response of the vessels was graded across the capillary bed, with arteriolar capillaries demonstrating no response, true capillaries a moderate response, and venular capillaries a strong response (fivefold increase) to a step change in shear stress. Most recently Kim et al [194] observed that changes in Lp were positively correlated with the magnitude of acute changes in shear stress in autoperfused microvessels in rat mesenteric tissue. The effect was greater in capillaries compared to terminal arterioles and could be eliminated by superfusion with a NOS inhibitor.

As indicated above, several studies, both in vitro and in vivo, have shown that the shear-induced increase in endothelial Lp is stimulated by shear-induced NO. It appears that shear-induced NO from endothelial cells is a mechanotransduction event that is mediated by the cell surface glycocalyx (GCX). Proteoglycans are major constituents of the GCX that are comprised of core proteins having either a trans-membrane linkage (syndecans) or a membrane linkage (glypicans) with extra-cellular domains that are covalently linked to glycosaminoglycans (GAGs), the most prominent of which are heparan sulfate (HS), chondroitin sulfate (CS) and hyaluronic acid (HA). The structure of the GCX is reviewed in much greater detail in Tarbell and Pahakis [19] and Weinbaum et al [70]. A study in canine femoral arteries showed that selective depletion of HA with

the enzyme hyaluronidase blocked flow-induced NO production [210] while an in vitro study in BAECs observed that depletion of HS with heparinase had the same effect [211]. A more extensive recent investigation in BAECs confirmed that depletion of HA and HS blocked shear-induced NO production, but similar depletion of CS (with chondroitinase) had no effect [68].

In the present study the hypothesis that the GCX is the mechanotransduction element that mediates shear-induced increases in endothelial Lp was investigated. The same BAEC monolayer preparation employed previously to study shear-effects on Lp by Chang et al [207] and the same GCX-degrading enzymes employed by Pahakis et al [68] in their investigation of shear-induced NO production were used. The influence of the GCX degrading enzymes on the baseline Lp values of BAEC monolayers was examined. Consistent with their effects on NO production, it was observed that heparinase and hyaluronidase block shear-induced increases in Lp, but surprisingly chondroitinase also inhibits shear-induced increases in Lp.

4.2 Materials and Methods

4.2.1 Chemicals

The following chemicals were obtained from Sigma-Aldrich Chemical Company (St. Louis, MO): bovine serum albumin (BSA-30% solution), Minimum Essential Medium

Eagle (MEM), phenol red-free MEM (PF), penicillin-streptomycin solution, L-glutamine, trypsin-EDTA solution, HEPES, sodium bicarbonate, heparin (sodium salt, grade I-A, 181 USP units/mg), fibronectin, heparinum heparinase III , P. vulgaris chondroitinase ABC, S. hyalurolyticus hyaluronidase, pronase E from streptomyces griseus, and (6R)-5,6,7,8-Tetrahydrobiopterin (BH4). Fetal bovine serum (FBS) was purchased from Hyclone Laboratories (Logan, UT). Transwell polyester filters (24.5-mm diameter, 0.4-μm pore size) were purchased from Costar (Cambridge, MA).

4.2.1 BAEC culture and insert preparation

BAECs were purchased from VEC Technologies (Rensselaer, NY) and grown in T-75 flasks with 10% FBS-MEM. The flasks were kept at 37°C in 5% CO_2. Upon reaching confluency (3-4 days) the cells were split for continuing maintenance of the cell line. The model for the endothelium was developed by plating BAECs at a density of 1.20 x 10^5 cells/cm^2 on Transwell polyester filters with 0.4 μm pores that were previously coated with fibronectin. The filters were incubated in 5% CO_2 at 37°C with 10%FBS-MEM. The shear-permeability experiments were run 6-8 days after plating, once the cells reached total confluency but were free from overgrowth. Cells were used from passages 5 to 8.

4.2.2 Enzyme treatments

Prior to the water flux measurement, the monolayers were incubated for two hours with

one of the following Enzymes; F. heparinum heparinase III (15 mU/mL), P. vulgaris chondroitinase ABC (12 mU/mL), or S. hyalurolyticus hyaluronidase (1.5 U/mL). All of these enzyme concentrations are in Sigma units and the time of incubation is in agreement with our previous study of shear-induced NO production [68]. The enzymes were used to degrade heparan sulfate, chondroitin sulfate and hyaluronic acid, respectively. In addition, a set of monolayers was incubated for one minute prior to the Lp measurements with the non-specific protease, pronase E (0.1 mg/ml). This is the same dose and the same time of exposure employed by Adamson [44] and Williams [209]. It should be noted that all of the shear experiments used media that was enriched with BH4 (60μM), a cofactor for eNOS activity [212, 213] that was used in a previous study by our lab on the role of the glycocalyx in shear-induced NO [68].

4.2.3 Determination of Water Flux across the Endothelium

The measurement of water flow across the endothelial monolayer was performed with an apparatus developed in our lab [189] that was kept inside a Plexiglas box and maintained at 37°C. The seeded filters were placed inside a chamber to form a luminal (top) compartment and an abluminal (bottom) compartment separated only by the BAEC monolayer. The abluminal compartment was connected to a reservoir via Tygon and borosilicate glass tubing. The vertical displacement of the reservoir with respect to the liquid covering the cells, allowed for the application of a hydrostatic pressure differential across the monolayer. When a 10 cmH_2O differential pressure was applied, the

volumetric flow rate (Jv) was measured by tracking the position of a bubble that was inserted into the calibrated borosilicate glass tube. The hydraulic conductivity (Lp) was calculated from the relationship: Lp= (Jv/A)/ΔP, where A is the BAEC monolayer area and ΔP is the pressure differential across the monolayer. After 60 minutes of applied pressure differential to drive water flux, a baseline Lp was established, and then a defined shear stress was applied to the endothelial monolayer using a rotating disk separated by a distance h (500 μm) from the monolayer surface. The rotating disk generated a fluid shear stress distribution on the monolayer surface defined by: $\tau = \mu \times \omega \times r/h$, where μ is the viscosity of the media, ω is the rotational speed, and r is the radial distance from the center of the disk. The parameters were adjusted in order to achieve a maximum steady shear stress of 20 dyn/cm^2 at the edge of the disk, and this is the value that is reported in the tables and figures. The average shear stress over the entire filter area is 2/3 of the maximum. During the entire experiment, the luminal compartment and the reservoir were supplied with gas (5% CO_2-95% balanced air) to maintain the experimental media at the physiological pH of 7.4. The experimental media for all of the Lp measurements was MEM supplemented with 1% BSA. The Lp values were recorded for four hours.

Two experiments were always run side-by-side. One endothelial monolayer was untreated, while the companion monolayer was treated with enzyme. These pairs of monolayers were always plated together from the same flask and grown the same number of days in the same media. This procedure allowed us to minimize effects associated with cell variability. In presenting the results, there was a separate set of controls for each enzyme.

4.2.4 Nitric Oxide determination

This specific Nitric oxide determination was performed by former student Manolis Pahakis. The measurements were taken under static and shear conditions by exactly the same methods described in Pahakis et al [68] using the fluorometric assay described by Misko et al. [214] with accuracy down to 10 nmol/L to detect nitrite, the major stable metabolite of nitric oxide. Cumulative concentrations are reported that account for sample dilutions and evaporation.

4.2.5 Statistical Analysis

Lp values are presented as means ± SE. Tests for statistical significance were conducted using the 2 way ANOVA function (time and treatment) from Minitab software, and a post hoc analysis using the Tukey method with $P < 0.05$ considered significant.

4.3 Results

Table 7 displays the baseline values for Lp 60 min after the application of a 10 cm H_2O pressure differential.

	Baseline Lp [cm/s/cm H_2O]	SE
Control (n=4) Heparinase III (n=4)	$2.51x10^{-7}$ $3.15x10^{-7}$	$2.83x10^{-8}$ $4.36x10^{-8}$
Control (n=5) Hyaluronidase (n=5)	$4.26x10^{-7}$ $8.39x10^{-7}$	$2.67x10^{-8}$ $9.48x10^{-8}$
Control (n=16) Chondroitinase (n=14)	$4.81x10^{-7}$ $8.92x10^{-7}$	$4.56x10^{-8}$ $6.12x10^{-8}$
Control (n=4) Pronase (n=5)	$4.74x10^{-7}$ $9.05x10^{-7}$	$8.670x10^{-8}$ $11.8x10^{-8}$

Table 7. Average baseline Lp and Standard Error (SE) for the different enzymatic treatments. Hyaluronidase, Chondroitinase and Pronase significantly increased the hydraulic conductivity compared to controls ($p < 0.05$). Heparinase III did not alter baseline hydraulic conductivity significantly ($p=0.25$).

The control values of the baseline Lp are within the normal ranges that have been reported for BAECs in previous studies [190, 193, 207] and are within a factor of two of values reported for in vivo studies in frog mesenteric capillaries [215, 216]. The heparinase III treatment increased the baseline Lp by 25% (not significant), whereas the hyaluronidase treatment led to a 97% increase; the chondroitinase treatment led to a 81% increase and the pronase treatment led to a 91% increase (all significant).

Figure 16 shows the shear stress responses of Lp for each of the selective enzyme treatments for GAG components compared to the companion control responses without

treatment.

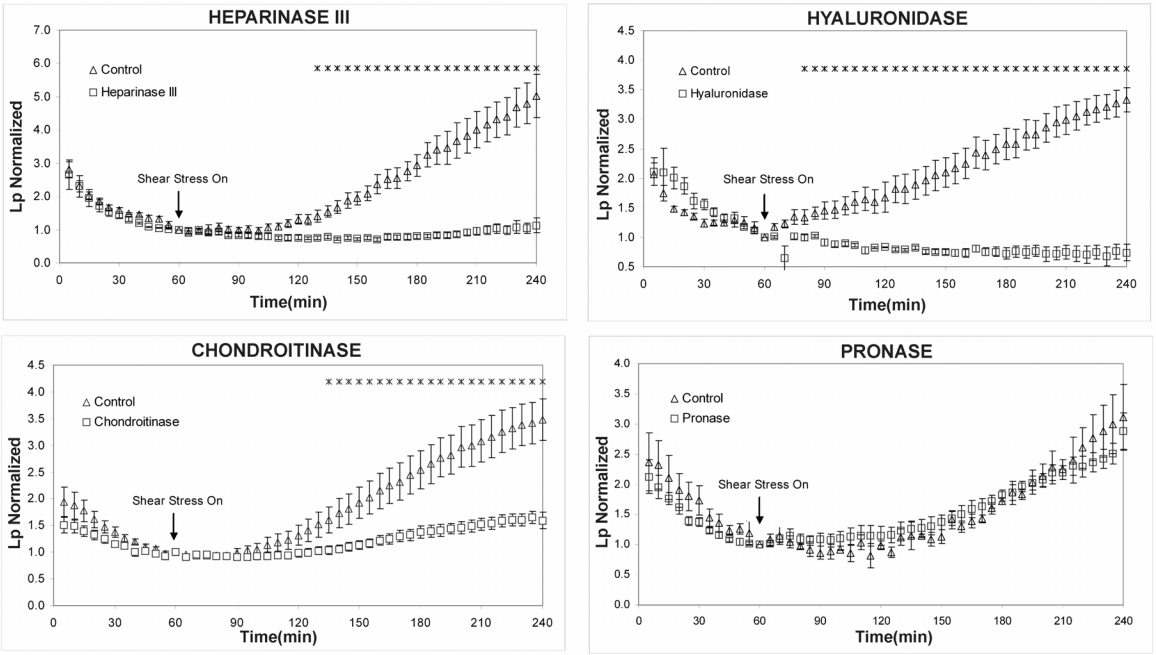

Fig. 16. Effect of different enzyme treatments on BAEC Lp response to shear stress. At time 0 min a hydrostatic pressure differential of 10 cm H2O was applied to the monolayers to drive water flow across them, and a baseline level was established after one hour. The Lp values were normalized to the baseline level for each monolayer. At time 60 min, shear stress of 20 dyn/cm2 was applied and Lp recorded for three hours. The monolayers that were treated with heparinase III (n=5), hyaluronidase (n=4), and chondroitinase (n=16) displayed a significant attenuation of the shear stress effect on Lp,,whereas the pronase-treated monolayers (n=6) did not. Inhibition of the shear response by chondroitinase was not as great as by heparinase or hyaluronidase. The asterisk denotes a significant difference between treated and control monolayers ($p<0.05$).

The Lp values are normalized by the control values provided in Table 7 so that the normalized Lp value is 1.0 at 60 min for all cases. All of the experiments showed the

characteristic “sealing” behavior in which Lp decreased continuously to its baseline value during the first 60 minutes of exposure to the pressure differential. This behavior has been observed in all previous experiments with BAECs [189] and in other cell types in vitro [207] as well as in vivo [194]. The sealing effect was not affected significantly by any of the enzyme pre-treatments as the control and treatment curves cannot be distinguished during the first 60 min.

The most important results displayed in figure 16 are the observations that pre-treatments with heparinase III and hyaluronidase completely blocked the shear-induced increase in Lp whereas chondroitinase pre-treatment significantly inhibited the shear-Lp response but pronase had no significant effect on the response. These observations indicate that the glycocalyx mediates shear-induced changes in endothelial Lp, and suggest that the mechanism involves shear-induced NO production since it was shown previously that heparinase and hyaluronidase block shear-induced NO production in BAECs [68]. The mechanism is subtle because heparinase blocks shear-induced Lp while having no significant influence on baseline Lp and pronase, which has a significant effect on baseline Lp, does not affect shear-induced Lp.

To explore these nuances further, NO production was measured in response to shear stress in media lacking protein (BSA-free MEM), because several previous studies have shown that protein-free media leads to large increases in Lp – up to 10-fold [217, 218].

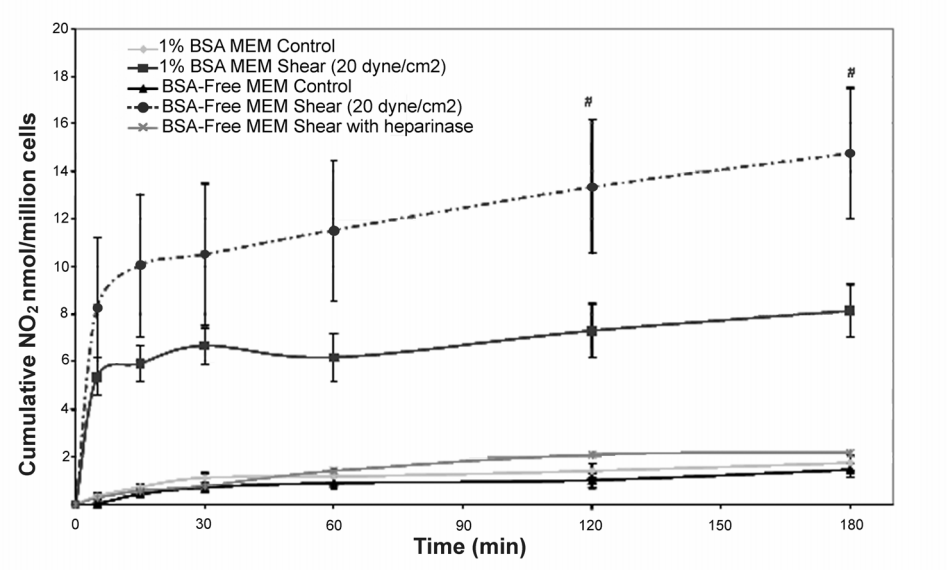

Fig. 17. Cumulative NO concentration versus time for BAECs under static and shear conditions for 1% BSA media, BSA-free media and heparinase-treated monolayers in BSA-free media. Shear was applied at time 0. n=9; # symbolizes significant difference ($p<0.05$ vs. 1% BSA shear).

Figure 17 shows the characteristic NO response to shear stress in 1% BSA MEM media as has been described previously [211]. Also shown is the surprising enhancement of NO production in response to shear stress in BSA-free MEM media and the complete suppression of the shear response in this media when the monolayer was pre-treated with heparinase. Earlier studies by us showed that in media containing 1% BSA MEM, heparinase completely blocked the shear response as well.

4.4 Discussion

Shear-induced alterations in endothelial Lp appear to be a fundamental physiological response to acute changes in flow that have been observed in many endothelial cell types

in vitro [19, 189, 207] and in several preparations either in vivo or in intact vessels [209, 215, 216]. Several studies have shown that this response is mediated by shear-induced NO release [207, 219, 220] and recent investigations have indicated that shear-NO induction is mediated by the glycocalyx [68]. The present study provides evidence that it is indeed the glycocalyx that mediates the mechanotransduction events relating the mechanical force of shear stress to the physiological response of hydraulic conductivity. The glycocalyx has also been implicated in cell alignment and proliferation [221] and in maintaining the integrity of arteries [222].

The rotating disk device employed in these experiments induces a radial gradient in shear stress across the endothelial monolayer, and an earlier study using the same apparatus showed that BAEC Lp has a threshold of sensitivity to (maximum) shear stress of 1 dyn/cm^2 and an increasing response up to 20 dyn/ cm^2. This implies that there could be a radial gradient in Lp across the monolayer and that an "average" response over the entire surface is being sampled.

The enzyme treatments for heparinase, hyaluronidase and chondroitinase employed in this study, including the concentrations and times of exposure, were identical to those previously described by Florian et al [211] and Pahakis et al [68]. Those studies showed that about 43% of the fluorescence associated with an antibody (heparan sulfate) or a specific lectin (chondroitin sulfate) was removed by the treatment. The hyaluronic acid removal, determined by ELISA quantification of the hyaluronic acid released into the media, was 62%. Pahakis et al [68] also showed that no enzyme removed more than 5%

of a non-target component, indicating the specificity of the enzymes. Furthermore they demonstrated that none of the enzyme treatments affected agonist-induced NO release (histamine or bradykinin) indicating that the NO production apparatus of the cells was not impaired by the enzyme treatments.

The effects of enzyme treatments on endothelial Lp have been investigated in only a few previous studies. Parameswaran et al [223] applied hyaluronidase to rabbit mesentery and found that Lp increased by 72%. This is of the same order as the 97% increase that we observed (Table 1). Dull et al [224] used a heparinase III treatment on lung microvascular endothelial cells in vitro, and observed a 144% increase in Lp. These changes after heparinase treatment are much higher than the 25% increase in Lp observed in the present study (Table 7). However, Dull et al. used 15 mU/mL in International Units (personal communication, R. O. Dull) and we used 15 mU/mL in Sigma Units.Therefore their concentration was much higher since one International Unit equals 600 Sigma units. Chondroitinase, which increased Lp by 81% (Table 1) has not been investigated for its effect on Lp in any previous studies. The general proteolytic enzyme, pronase, at a concentration of 0.1 mg/ml, induced a 91% increase in baseline Lp. This was somewhat lower than the range observed by Williams [216] (160%) and Adamson [225] (145%), both using 0.1 mg/ml pronase in frog mesenteric capillaries. It therefore appears that our baseline data on enzyme influences on Lp are consistent with the limited data available in the literature. Even higher increases in baseline Lp (up to 900%) have been observed in preparations using protein-free media, but without any enzyme treatment in BAEC [217] and frog mesentery [218].

It was somewhat surprising to observe that heparinase, which removed as much antibody-associated fluorescence as chondroitinase, had a much smaller effect on baseline Lp than chondroitinase (Table 7). The change in fluorescence intensity, however, is not equivalent to the change in mass because of possible differences in the binding affinities of the antibodies, and it may be that more CS was removed than HS. CS also resides closer to the plasma membrane than HS [226] and this may be significant. But not enough is know about the detailed structure of the glycocalyx to explain the contributions of individual components to the overall hydraulic resistance.

It is worth noticing in figure 16 that none of the enzymes affected the transient behavior of Lp during the initial 60 minute "sealing" period. This was also observed by Dull et al [224] using lung microvascular endothelial cells treated with heparinase III. These results imply that "sealing" is not mediated by the glycocalyx. DeMaio et al [227] using BAECs, showed that "sealing" involves the recruitment along microtubules of the protein zonula occludens-1 (ZO-1) to the tight junction regions of the cell. When the BAEC monolayers were subjected to the same elevation in pressure (10 cm H_2O) without any differential pressure to drive transmural flow, the recruitment of ZO-1 to the junctions was blocked (DeMaio, unpublished data, 2004 – available upon request). This indicates that it is the flow through the intercellular junctions induced by the pressure differential and not the elevation of pressure per se that drives the "sealing" process. Tarbell et al. [226] estimated the fluid wall shear stress in the intercellular junctions associated with normal transmural flow to be on the order of 25-50 dyne/cm^2, the same magnitude as that

of flowing blood on the walls of endothelial cells [228]. Thus, it may be this intercellular junction shear stress acting in a region of the junction that is not covered by glycocalyx that drives the "sealing" phenomenon. It is generally believed that the glycocalyx extends into the entrance of the interendothelial junction, but does not line the entire junction [229].

The data in figure 16 for the control cases, show shear-induced increases in Lp after 3 hrs of exposure to a maximum of 20 dyne/cm^2 ranging between 3.5X and 5.0X the 60 min baseline value. Even though this range is consistent with the shear-induced responses observed in previous studies [189, 207] for the purpose of comparison in the present study, monolayers that had been cultured and platted from the same flask for each set of control and enzyme-treated cells were used. It is evident that pre-treatment with either heparinase III or hyaluronidase completely blocks the response while chondroitinase also inhibits the response significantly, but not completely. A previous study employing the same cell type, shear stress magnitude, and enzyme treatments, showed that the significant shear-induced increase in NO production over 3 hrs was blocked by heparinase III and hyaluronidase, but not chondroitinase. Earlier studies have shown that shear-induced increases in Lp are mediated by NO [194, 207, 220]. Taken together, these studies strongly suggest that shear-induced increase in endothelial Lp is mediated by the glycocalyx serving as a mechanotransducer for NO production.

This interpretation of the data is not, on the surface, supported by the observation that chondroitinase inhibits the shear-Lp response (Figure 16) while having no influence on the shear-NO response. This seeming contradiction could be the result of an effect of the

enzyme on a pathway downstream of NO or in parallel with NO that influences the hydraulic conductivity. For example, it is has been observed that reduction of chondroitin sulfate can up-regulate cAMP activity [230], and it is well known that elevation of cAMP reduces endothelial Lp. Chondroitin sulfate proteoglycans and CD44 that contains CS interact with cytoskeletal elements including microtubules [231] that are known to mediate movement of tight junction proteins away from intercellular junctions. Additional studies will be required to assess these possibilities.

Unlike the present observations with heparinase, hyaluronidase and chondroitinase, Williams [216], using pronase in frog mesenteric capillaries at a concentration (0.1 mg/ml) that greatly increased baseline Lp (160%), found that this treatment actually led to an increase in the sensitivity of Lp to step increases in shear stress. This suggests that there is something fundamentally different about the mechanotransduction process when the GCX is highly disrupted. To pursue this hypothesis, the cells were also treated with pronase at the same dose and exposure time as Williams [216], and although the baseline Lp was not altered as much as in that study (91% versus 160%), it was observed that the shear-Lp response was not attenuated as it was for all other enzymes (Figure 16). Unfortunately, it was not possible to increase the pronase dose because it had been shown by Adamson [225] and Chang [207] in frog mesenteric capillaries and BAEC, respectively, that at only a slightly higher dose (0.125 vs. 0.100 mg/ml) there was a complete breakdown of the endothelial transport barrier.

To examine further the behavior of endothelial mechanotransduction under conditions

where the GCX is highly disrupted, experiments in protein-free media were conducted. Shear-Lp experiments were not pursued in this media because of the extreme elevation of baseline Lp (900%). However, since it was found in BAEC that shear-induced NO production mediates the shear-Lp response, as discussed above, the NO response to shear under conditions where baseline Lp was most highly disturbed - in protein-free media were measured. Consistent with the observations of Williams [216] it was found that shear-induced NO (that mediates Lp increase) was significantly enhanced in protein-free media (Figure 17). But, when the cells were pre-treated with heparinase at the same concentration and time of exposure as in the experiments of figure 16 and then sheared in protein-free media, the shear-induced NO production was completely inhibited.

The basic observations presented in figures 16 and 17 support a mechanism involving shear-induced NO, mediated by the glycocalyx, that enhances Lp. It is noteworthy that glypicans which contain HS are linked to caveolae where endothelial nitric oxide synthase (eNOS) resides [19]. It is also important to realize that HA binds to its CD44 receptor that is localized in caveolae [19], thus providing a link between HA and shear-induced Lp (NO) that is blocked when HA is depleted. Several studies have implicated a role for PECAM-1 in shear stress induction of eNOS and NO (e.g., Dusserre et al. [232]). The relationship between the glycocalyx and PECAM-1 is not clearly established, but Tarbell and Pahakis [68] speculated that the glycocalyx may serve to sense fluid shear stress and then distribute the associated force to the intercellular junctions where PECAM-1 resides, using the cytoskeleton that is linked to both the glycocalyx and PECAM-1 to transmit the force.

The observation of Williams [216] that pronase treatment (which increased Lp by 160%) actually leads to an enhanced sensitivity of Lp to shear stress is consistent with our observation that the sensitivity of NO production to shear stress is enhanced when the glycocalyx is highly disrupted in protein-free media (Figure 17) and is not inconsistent with our observation that pronase treatment that was less disruptive to the GCX (increased Lp by 91%) did not suppress the shear-Lp response. Even though the glycocalyx is highly disrupted in protein-free media, as suggested by the highly elevated Lp (900%), it appears that HS still plays a central role in mechanotransduction of shear stress since shear-induced NO is completely blocked by heparinase in this media (Figure 17) like it is in 1% BSA media, as shown in an earlier study by our group [211]. This is still consistent with a glypican-caveolae-eNOS mechanism since these connections would be expected to remain intact even when the glycocalyx has been diminished by lack of protein interactions.

The final, and most difficult, observation to account for in terms of a glypican-caveolae-eNOS mechanism is the observation of Williams that pronase treatment led to an enhanced sensitivity of Lp to shear stress [216] and our observation that pronase treatment did not suppress the shear-Lp sensitivity. It may be that the short exposure to the enzyme (1 min) was not sufficient to degrade the glypicans that reside deep in the glycocalyx in caveolae and that fluid shear stress, not dissipated by a degraded glycocalyx, was able to penetrate to the level of the caveolae. Future studies will be required to resolve these issues.

CHAPTER 5

High glucose attenuates shear-induced changes in endothelial hydraulic conductivity

5.1 Introduction

Hyperglycemia is a characteristic feature of type 1 and type 2 diabetes and it has been long associated with both microvascular and macrovascular dysfunction [233]. Factors such as dyslipidemia, hyperinsulinemia, and hypertension together with endothelial dysfunction interact during the progression of the disease. Given the complex interaction between these factors the mechanism that leads to vascular complications is not completely understood. However, it has been suggested that an impaired endothelium is an early marker of diabetes induced vascular pathologies [234].

The interaction between blood and endothelium is not only a result of molecular interactions, but also includes the mechanosensing of shear forces which are exerted by the flowing of blood [70]. This sensing enables the endothelium to strictly and acutely monitor vasoregulation. Vasoregulation occurs due to the production of vasodilators such as endothelium derived hyperpolarization factor (EDHF), prostaglandins (PGI2/ PGE2) and nitric oxide (NO) [235]. And as demonstrated in the previous chapter, shear forces affect the endothelial transport barrier (specifically Lp) through the GCX.

The GCX, which covers the surface of the endothelial cells, consists of proteoglycans

linked either to the membrane (glypicans) or to the cytoskeleton (syndecans) with extracellular side chains (GAGs) covalently linked to the core proteins. The most abundant of these GAGs are heparan sulfate (HS), chondroitin sulfate (CS) and hyaluronic acid (HA) [19, 68]. The GCX not only constitutes a sieve to prevent transvascular leakage of macromolecules [29] but also moderates hydraulic conductivity (Lp). In the last few years, evidence has emerged that damage to the GCX plays a pivotal role in several vascular pathologies. It has been demonstrated in vivo and in vitro that enzymatic depletion of HA leads to a reduction in thickness of the GCX and an increase in endothelial hydraulic conductivity [29, 236]. The whole GCX may contribute as much as 60% of the hydraulic resistance of the capillary wall [225]. Loss of GCX leads to vascular abnormalities including increased permeability [66, 225], mononuclear and platelet adhesion and impaired NO bioavailability [182]. It has been demonstrated that even acute hyperglycemia can perturb the GCX [182] and that restoration is associated with reversal of abnormalities [236]. Therefore the GCX acts as a protective structure to ensure homeostasis of the vasculature.

Zuurbier et al., [183] showed that short-term hyperglycemia (2 to 4 weeks) caused a rapid decrease in the ability of the GCX to sieve 70-kDa dextran but not 40-kDa dextran and suggested that hyperglycemia mainly affects the hyaluronan component of the GCX. In-vitro models have shown that in the presence of high glucose there is a significant shedding of the HS and the HA components into the culture media [21], and reduced levels of HS caused by hyperglycemia have been related to impaired alignment of endothelial cells exposed to shear levels of 12 dyn/cm^2 [22].

The above studies present evidence to support the idea that hyperglycemia interferes with either the synthesis and or the shedding of at least two GAGs - HS and HA. However to our knowledge, there are no studies that address if hyperglycemia can go as far as to impair the shear-induced Lp response. Previously in our laboratory it had been observed that shear stress increases endothelial hydraulic conductivity and that this effect can be attenuated by an eNOS inhibitor [207], demostrating the relationship between endothelial Lp response and NO production. It was also shown by our group that several GAG components of the GCX affect the shear induced Lp response [66]. Therefore, in the present study, we examine whether hyperglycemia can alter endothelial shear-induced Lp and NO production.

5.2 Materials and Methods

5.2.1 Chemicals

The following chemicals were obtained from Sigma-Aldrich Chemical Company (St. Louis, MO): bovine serum albumin (BSA-30% solution), Minimum Essential Medium Eagle (MEM), phenol red-free MEM (PF), penicillin-streptomycin solution, L-glutamine, trypsin-EDTA solution, HEPES, sodium bicarbonate, heparin (sodium salt, grade I-A, 181 USP units/mg), fibronectin, and (6R)-5,6,7,8-Tetrahydrobiopterin (BH4). Fetal bovine serum (FBS) was purchased from Hyclone Laboratories (Logan, UT). Transwell polyester filters (12-mm diameter, 0.4-μm pore size) were purchased from Costar (Cambridge, MA). Primary Anti- Heparan Sulfate H1890 was purchased from US

Biological (Swamscott, MA). The secondary antibody IgM was purchased from Molecular probes (Carlsbad, CA). The Western blot kit, from Cayman (Ann Arbor, MI). The Phospho-eNOS (Ser1177) and β-actin antibody were obtained from Cell Signaling (Beverly, MA).

5.2.2 BAEC culture and insert preparation

As in the previous study on chapter 3, BAEC were purchased from VEC Technologies (Rensselaer, NY) and grown in T-75 flasks with 10% FBS-MEM. The flasks were kept at 37°C in 5% CO_2. In asimilar manner, the model for the endothelium was developed by plating BAECs at a density of 6 x 10^4 cells/cm^2 on 12 mm diameter Transwell polyester filters previously coated with fibronectin. The filters were incubated in the same conditions with either 5mM glucose or 25 mM glucose 10%FBS-MEM. Cells were used from passages 5 to 10.

5.2.3 Shear Stress Apparatus

In order to apply shear stress on monolayers seeded onto small (12 mm diameter) Transwell polyester filters, it was necessary to design and fabricate an accessory for our existing experimental apparatus. The accessory (Figure 18) consists of a cylindrical lid made out of aluminum that fastens into the chamber by means of a thread and holds the rotating shaft at a set distance above the endothelial cells monolayer. The rotational motion is facilitated by the utilization of bearings and the shafts are moved by the action

of a belt and a pulley connected to a stepper motor that was previously used in our laboratory.

The stepper motor was programmed to obtain the desire level of shear stress. This new accessory made it possible to apply shear stress to EC monolayers plated on 12 mm diameter inserts and at the same time monitor Lp behavior.

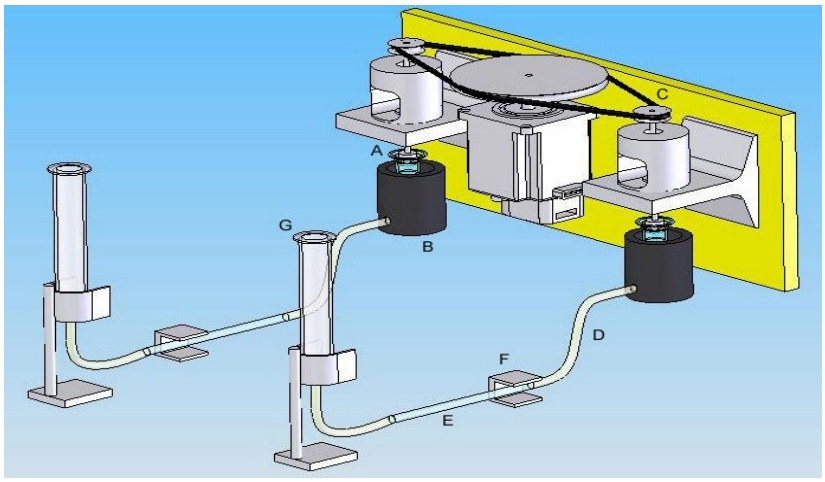

Fig. 18. Schematic of the accessory designed and fabricated in our laboratory in order to apply shear stress to EC monolayers. The components of the total apparatus include: A: Polyester filters B: Chamber C:Rotating rod D:Tygon Tube E: Borosilicate glass tubing F:Bubble Tracking apparatus G:Reservoir.

5.2.4 Determination of Shear Stress induced Lp response

The measurement of water flow across the endothelial monolayer was performed in the

same manner as described in the previous chapter, section 3.2.3. Basically when a 10 cm H2O differential pressure (ΔP) was applied, the volumetric flow rate (Jv) was measured by tracking the position of a bubble that was inserted into the calibrated borosilicate glass tube. A rotating disk imparted a maximum shear stress of 20 dyne/cm2. The hydraulic conductivity (Lp) was calculated from the relationship: Lp= (Jv/A)/ΔP. Where A is the cross sectional area of the filter. The shear-Lp experiments were run 6 days after plating, once the cells reached total confluency but were free from overgrowth. The experimental media consisted of 1%BSA-MEM enriched with BH4 (60μM), a cofactor for eNOS activity [212, 213].

5.2.5 Six well apparatus design and construction

In order to apply shear stress to cells for longer periods of time (more than 6 hours) and during culture, a six well apparatus was designed and built in the Mechanical Engineering shop as part of a small grant offered to Ph.D. students from the Graduate Center. The finalization of the design and the fabrication of the different parts were possible thanks to the generous help of Dr. Alexis Pierides, who kindly guided Ronny Amaya and myself through the process and lent us the necessary tools.

Briefly, to accomplish this task, biocompatible and durable materials were chosen so that they could be sterilized for repeated use. The general dimensions of the device were

picked so that it could hold in place a commercially available Corning TM 6 well tray with its inserts. The motor, the shear rods, bearings and the controller were chosen to deliver the revolutions per minute and the power required to apply the desired levels of shear stress, before machining, all components were drafted using the software SolidWorks (Figure 19).

A lathe was used to machine the shear rods and a mill coupled to the appropriate drills and cutting edges was used to machine the main body. Assembling the motor case and the cells compartment required stainless steel screws and acrylic glue. Bearings and collars were used to set the position of the shear stress rods. The motor was refrigerated through a cupper coil covered with a conductive paste to increase the heat exchange. A controller specified by the manufacturer (MS2-D from US Digital) was used to control the rotational speed of the motor, thus the shear stress.

Once the device was completed, it was tested by placing a well tray and its 6 inserts seeded with BAEC in the appropriate compartment. Next, the motor was positioned and the device was left inside an incubator at a controlled temperature of $37^{o}C$ and at a 5% CO_2 air mixture to maintain adequate living conditions for the cells.

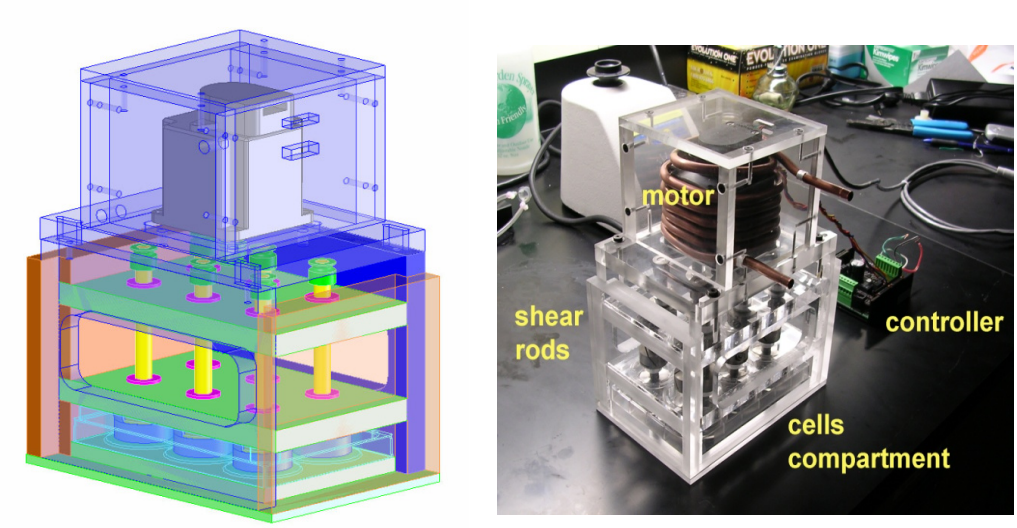

Fig. 19. Schematic (left) of the 6 well rotating shaft apparatus (right) designed and fabricated in order to apply shear stress to EC monolayers while in culture.

We gradually increased the level of shear stress during 4 days of continuous operation.

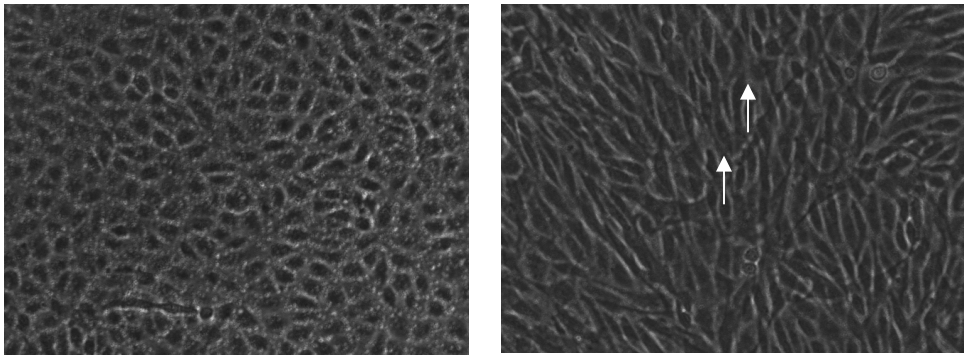

Fig. 20. Microscopic picture of a control monolayer (left) and a sheared monolayer (right). The control monolayer shows the typical cobblestone appearance of endothelial cells grown under static conditions. The sheared monolayer (24 hours - 20 dyn/cm2) shows elongation and alignment of the cells. The arrows indicated the direction of flow.

At the end of the 4th day the cells did not have any contamination, the media pH was maintained between 7 and 7.4 and the cells were elongated in the direction of the shear as compared to static controls (Figure. 20).

5.2.6 Heparan sulfate immunostaining

Monolayers grown in either normal (5mM) or high glucose (25mM) for six days were rinsed with cold PBS and fixed with 4% paraformaldehyde-PBS for 15 minutes. Then they were blocked with 4%BSA-PBS for 30 minutes, incubated with primary antybody: HepSS-1 diluted 1:200 in 4% BSA-PBS for 2 hours and washed gently with 1% BSA-PBS. The monolayers were incubated with secondary antibody: Alexa Fluor 594 conjugated with anti-mouse IgM diluted 1:500 for 1 hour. The monolayers then were washed gently 3 times and 6 random images where taken per condition with the Nikon Eclipse TE2000-E inverted microscope.

5.2.7 Determination of eNOS phosphorylation by Shear Stress

Once the viability of the experiment with the new shear apparatus was determined, BAEC monolayers grown for six days in either normal (5mM) or high glucose (25 mM) 10%FBS MEM media were placed in the compartment where they were sheared for 12 hours at a maximum level of 12 dyne/cm^2. Then the cells were collected for western blots to quantify eNOS phosphorylation.

5.2.8 Western Blotting

Once shear stress was applied for 12 hours, the monolayers where scraped from the filters in the presence of RIPA lysis buffer (NaCl 0.6M, NP-40 4%, Tris 0.2M, Brij 35 0.4% EDTA 4mM) supplemented with a protease and phosphatase inhibitor cocktail,

Na_3VO_4 and PMSF. Protein concentration was determined with the Cayman kit # 704002 (Ann Arbor, MI). Western blot was carried out by standard techniques, loading 20 μg of protein into the gel wells and incubating over night with antibodies to phospho-eNOS (Serine 1177), and regulatory protein β-actin both from Cell Signaling Technologies (Beverly, MA), followed by reaction with matched secondary anti-rabbit IgM antibody from Molecular probes (Carlsbad, CA). The blots were scanned with the Universal Hood II (BioRad) and visualized with the software Quantity One version 4.5 (BioRad).

5.2.9 Statistical Analysis

Lp values are presented as means ± SE. Tests for statistical significance were conducted using the 2 way ANOVA function (time and treatment) from Minitab software, and a post hoc analysis using the Tukey method with $P < 0.05$ considered significant. Western blots and immunostaining pictures were quantified and analyzed using the NIH image J software.

5.3 Results

5.3.1 Shear Stress induced Lp response

The baseline values for Lp 60 min after the application of a 10 cm H_2O pressure differential for normal ($3.82X10^{-7}$ ± 0.57 cm/s/cm H_2O) vs high glucose ($4.71X10^{-7}$ ± 0.65 cm/s/cm H_2O) were not significantly different from one another (p=0.34). Both values of the baseline Lp are within the normal ranges that have been reported for

BAECs in previous studies [44, 193, 194], including those reported in the previous chapter.

Figure 21 shows the shear stress responses of Lp for monolayers grown in high glucose media (25 mM) for six days compared to the companion control monolayers grown in normal glucose media. The Lp values were normalized by the Lp value at 60 min for both cases. Both experiments showed the characteristic "sealing effect" which has been observed numerous times before [189].

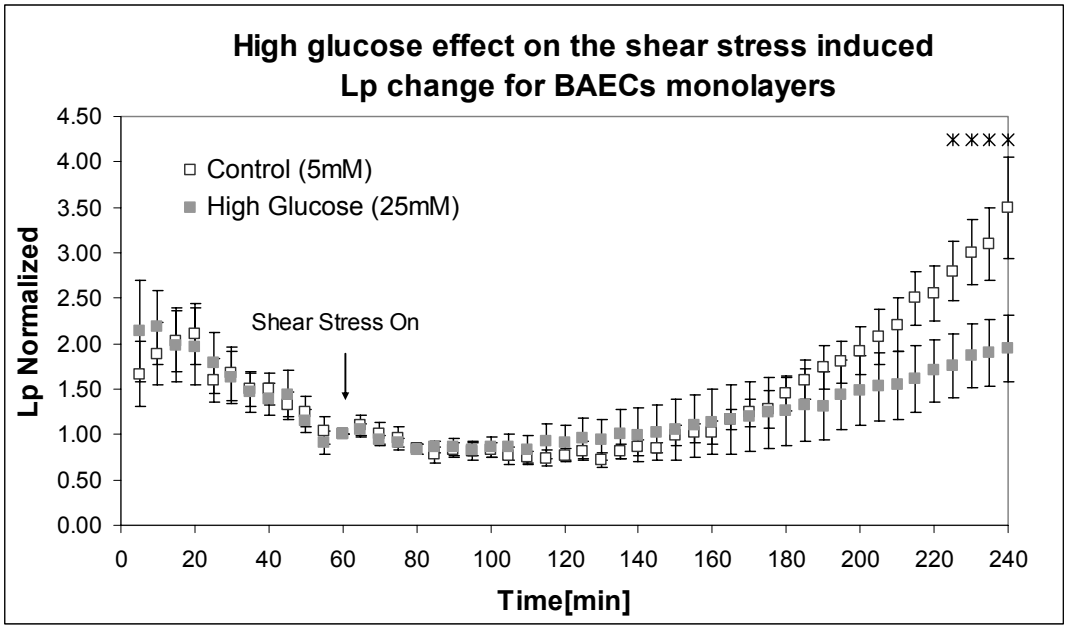

Fig. 21. Normalized shear induced Lp response of BAEC monolayers grown in normal glucose (5mM) vs high glucose (25 mM) for six days. At time 0 min a hydrostatic pressure differential of 10 cm H2O was applied to the monolayers to drive water flow across them, and a baseline level was established after one hour. The Lp values were normalized to the baseline level for each monolayer. At time 60 min, a shear stress of 20 dyn/cm2 was applied and Lp recorded for three more hours. The monolayers that were treated with high glucose displayed a significant attenuation of the shear stress effect on Lp compared to controls (n=6). The asterisk denotes a significant difference between high glucose and control monolayers ($p<0.05$).

High glucose did not affect this sealing but significantly attenuated the shear induced Lp response. A similar behavior was observed in the previous chapter for monolayers treated with heparinase (Figure 16), the enzyme that selectively removes the heparan sulfate component of the GCX. High glucose increased baseline Lp by 23% (not significant) similar to the 25% increase observed before when BAEC where incubated with the enzyme [66].

5.3.2 Heparan sulfate immunostaining

The visualization of the heparan sulfate component of the GCX was carefully performed as described in the methods. It was necessary to fix the cells to preserve structural integrity. As shown in figure 22, incubating the cells with high glucose media (25 mM) for six days significantly reduced (by 15 ±0.5 %) the presence of this GAG chain.

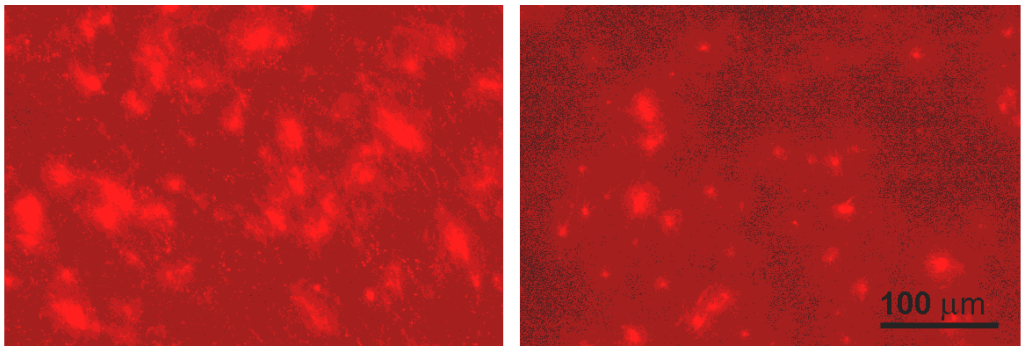

Fig. 22. Heparan sulfate staining of BAEC monolayers cultured in either NG (left panel) or HG (right panel) media for 6 days. After careful immunostaining of the HS component the monolayers were observed under the Nikon 2000 Eclipse inverted microscope for observation. Six random fields were chosen for each conditon. The HS fluorescence was significantly decreased by 15 ±0.5 % in HG ($p=0.04$).

5.3.3 eNOS phosphorylation

The phosphorylation of eNOS was observed after the monolayers cultured in either normal glucose (5mM) or high glucose (25 mM) media were subjected to a physiological level of shear stress (12 dyne/cm^2) for 12 hours while maintained in the incubator at 37ºC and pH of 7.4. The Western blots were performed as described in the methods and quantified with the software image J. The monolayers cultured in high glucose presented a lower phosphorylation ratio (sheared monolayers over static controls) than the monolayers cultured in normal glucose (1.36 ± 0.07 vs 1.59 ± 0.09, n=3) and this difference was significant (p=0.02).

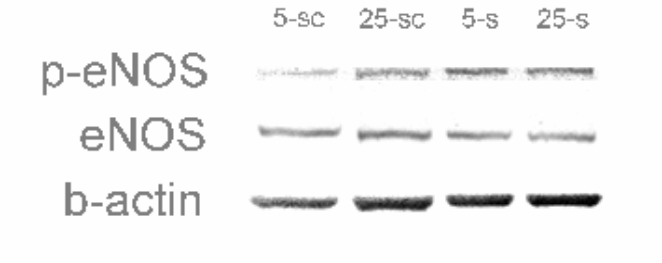

Fig. 23. Representative Western blots for p-eNOS, eNOS and β-actin. The phosphorylation ratios (sheared monolayers over static controls values) of eNOS was significantly decreased from 1.59 ± 0.09 to 1.36 ± 0.07, (n=3, p=0.02) when cells subjected to a shear stress of 12dyne/cm2 for 12 hours were incubated with high glucose compared to normal glucose. Baseline eNOS levels where not significantly changed (1.25 ± 0.03 vs 1.29 ± 0.11, p=0.76, n=3) when cells were cultured in high glucose. Labels are as follows: 5-sc: 5mM glucose static control, 25-sc: 25mM static control, 5-s: 5mM with shear stress, 25-s: 25 mM with shear stress.

Additionally, the blots were reprobed with an antibody for total eNOS to make certain that a difference in phosphorylation was not a result of a change in the total eNOS protein.

The amount of eNOS protein did not differ between monolayers cultured in normal vs high glucose (1.25 ± 0.03 vs 1.29 ± 0.11, p=0.76, n=3). The β-actin band served as a loading control and the values mentioned above were obtained after normalizing the levels of the proteins to the levels of the corresponding β -actin control. The representative results are shown in figure 23.

5.3 Discussion

The purpose of this study was to determine if high glucose can impair the endothelial response to shear stress. Shear stress has been shown to regulate endothelial hydraulic conductivity by a mechanism that involves the transduction of mechanical forces into the production of NO [194, 207, 220].

The observation that with diabetes, atherosclerosis is distributed more uniformly in arteries and not just limited to the typical atherogenic regions near bifurcations and curvatures [237] and that vasodilation is altered in patients with diabetes [238] suggests that there is something fundamentally different in the mechanosensing apparatus of the endothelium in this disease state. These observations have motivated our study of the effects of hyperglycemia on mechanosensing.

The molecules responsible for the transduction of mechanical forces into biochemical signals in the vasculature are a subject of growing interest; however many of the detailed interactions within proposed mechanisms are still not elucidated.

The main observations of the present study were that the normal Lp increase caused by steady shear stress was significantly attenuated by high glucose (Figure 21), coincident with decreased HS component (Figure 22) and decreased eNOS activation (Figure 23).

Previous studies have linked high glucose to dysfunction of the endothelium [11, 239], and one of the main roles for this organ is to procure homeostasis in response to different stimuli, one of them being the shear stress caused by circulating blood in the vasculature. The GCX, which has been extensively described before [19, 68, 69] protrudes into the lumen with its GAG elements that bind plasma proteins and other solutes and are connected to core proteins linked either to the cell membrane or to the cytoskeleton. Because of its structure, the GCX is a prominent mechanosensor/transducer.

The GCX has received a great deal of attention for its role in mechanotransduction in recent years. Florian [211] and Pahakis [68] showed that HS cleavage blocked shear induced NO production, providing direct evidence for the role of HS in sensing and transducing flow induced forces. The present data demonstrates that there is an impaired endothelial Lp response to shear in high glucose, which is coincident with lower content of HS and reduced shear stress induced activation of eNOS.

The downregulation of HS by hyperglycemia could be critical. Several atheroprotective properties have been attributed to HS proteoglycans based on their capacity to inhibit monocyte binding to the subendothelial region [240], to inhibit arterial smooth muscle

cell proliferation and to regulate fibroblast growth factor [241]. Our results in figure 21, which show decreased HS content in cells cultured in high glucose media are consistent with a previous study on BAEC and human endothelial cells, which showed that the HS proteoglycan perlecan is posttranslationally affected by high glucose allowing for less HS side chain binding [75]. The diminished HS content in high glucose media has also been explained by endothelial over-secretion of the heparanase molecule which specifically cleaves HS [242].

In human arteries, hyperlipidemia has been characterized by a decreased amount of HS [243] and diabetes has been shown to reduce the amount even more [244]. With respect to the mechanosensing and adaptation, a recent in-vitro study showed that endothelial monolayers cultured in high glucose had reduced HS and were not able to align normally after being exposed to shear stress [22].

In other tissues, like kidney [240] and retina [245], exposure to high glucose results in decreased synthesis of HS side chains and subsequent reduction of basement membrane anionic sites. Heparan sulfate therefore appears to play an important role in homeostasis of various tissues, and the studies discussed above suggest that high glucose may affect the synthesis and/or metabolism of HS proteoglycans and HS for various cell types. These data associate hyperglycemia induced modifications to GAGs and proteoglycans to atherosclerosis, kidney and retinal pathologies. Another GCX component, HA, has been reported to be higher in serum of patients with diabetes, due to increased levels of reactive oxygen species (ROS) able to stimulate hyaluronan degradation [246]. Overall,

shedding of the GCX is an important factor in atherosclerosis, because it exposes cell membrane adhesion molecules, such as vascular cell adhesion molecule-1 (VCAM-1) and intercellular adhesion molecule-1 (ICAM-1), which are required for the adhesion of leukocytes to the endothelial surface [181], therefore initiating an inflammatory response.

The shear induced Lp response which is mediated by the production of NO [220] has not been observed before in a hyperglycemic environment. In the present study, the attenuated response that coincides with lower activation of eNOS suggests that hyperglycemia could affect the mechanotransducers upstream of NO and in fact we present evidence that shows a reduced amount of the HS component in hyperglycemic media (Figure 22).

Other studies have shown that phosphorylation of eNOS by several serine/threonine kinases is a fundamental step in NO production by endothelial cells. Phosphorylation by AMP kinase, Akt, also called protein kinase A or protein kinase B on serine 1177, leads to increased activation of the enzyme and increased NO production in bovine cells [247]. Phosphorylation at serine 1177 is considered a marker of the activation state of eNOS in response to vascular endothelial growth factor (VEGF) and fluid shear stress. Certainly VEGF induced angiogenesis and hyperpermeability in vivo require eNOS derived NO [248]. The activation state of eNOS was examined with an antibody that recognizes serine 1177. As seen in figure 22, the activation of eNOS but not the total eNOS content was reduced when the cells were incubated in high glucose. This observation is consistent with a previous study by Du et al. [249] that showed that hyperglycemia did not change

the level of total eNOS, but reduced eNOS activation. Du and coworkers attributed this behavior to post translational modifications due to mitochondrial superoxide overproduction.

Another possibility for a reduced endothelial response is that once released, NO is quickly modified and its potency is reduced in a hyperglycemic environment due to the presence of advanced glycation end products which also modify eNOS [250]. NO is produced by endothelial cells from L-arginine in the presence of cofactors, the most common of them being tetrahydrobiopterin (BH4) [163]. In this respect, Cai et al. [251] reported that during hyperglycemia BH4 is oxidized by peroxynitrite, which is formed by the interaction of superoxide with NO, resulting in an increase in the monomeric form of eNOS and hence an uncoupling of the enzyme. However it should be noted that our experiments used BH4 enriched media to ensure bioavailability of the cofactor.

Most of the glucose in the body goes directly into cells where it is modified to produce the energy source ATP. However about 5 percent of all glucose is converted to another sugar moiety, beta-N-acetyl-glucosamine. O-Linked attachment of beta-N-acetyl-glucosamine (O-GlcNAc), on serine and threonine residues of nuclear and cytoplasmic proteins is a dynamic posttranslational modification that plays a key role in signal transduction pathways. In healthy mice blood vessel walls, Toste et al., [252] observed that increased activity by O-GlcNAc competed with protein phosphorylation to maintain balance. However, In hyperglycemia, excess O-GlcNAc impedes phosphorylation of eNOS and therefore reduces NO production.

Endothelial dysfunction (ED) explains an increased risk for cardiovascular disease in diabetic patients. Improved understanding of the mechanisms that lead to ED in this setting could provide new approaches for treatments. The mechanisms through which hyperglycemia causes ED are varied and may present complex interactions, however, the findings in this study point to the GCX as a possible target for early therapeutic intervention. A future approach for vascular disease may be based on the design and administration of copolymers [253] that are able to mimic the mechanosensing activity of an intact GCX, or the development of agents that can inhibit shedding of the GCX components [242] or that stimulate their synthesis in localized areas.

CHAPTER 6

Future Work

It is well established that endothelial dysfunction plays an important role in the development of cardiovascular disease both in the macro and microvasculature [16-18]. Continued effort should be placed on understanding the endothelial responses to different stimuli in the environment and the mechanisms that procure vascular homeostasis.

There are multiple steps and complex interactions between different factors along the pathways in diabetes. However, the results presented in this study suggest that VEGF plays a critical role in the development of diabetic retinopathy (DR). Elucidating the signaling pathways activated by VEGF which result in an increase of endothelium permeability is a mandatory step in this line of research. For instance, classic PKC isoforms have been implicated in the VEGF induced hyperpermeability via phosphorylation of TJ protein occludin [109] and selective inhibitors of the beta isoform of the protein kinase C enzyme (PKC-β) are effective in reducing VEGF induced retinal permeability and neovascularization [116]. Other PKC isoforms should be tested for their efficacy in blocking the VEGF induced hyperpermeability.

Another approach to future therapies for DR includes the understanding of the interaction between hyperglycemia and hypertension. Hypertension is an independent risk factor for

this disease; studies have shown that hypertension increases VEGF receptors in the retina [254]. Additionally, NO secreted by the endothelium functions as a negative feedback mechanism that downregulates VEGF expression [255]. Therefore, the upregulation of VGEF in the retina of diabetics and subsequent vascular leakage could be caused by lack of NO bioavailability. A condition that then is worsened by hypertension.

A decreased NO bioavailability is supported by the fact that capillary vasodilation is decreased in diabetics [179]. Therefore, future therapies should aim to reestablish normal vascular NO release.

Shear stress resulting from circulatory flow modulates EC functions by activating mechanosensors, signaling pathways, and gene and protein expressions. In previous studies, it was demonstrated that the shear induced NO production is mediated by different components of the GCX [68, 211], and in chapter 4 of this study, it was shown that shear induced Lp response is also mediated by this layer. Enzymatic cleavage of CS and HA attenuated the Lp response and increased Lp baseline values, while HS cleavage on the other hand, did not interfere with baseline Lp but attenuated the shear response as well. In chapter 5 it was observed that the shear induced Lp response obtained when the cells were grown in high glucose was very similar to the response obtained when the GCX was cleaved with heparinase. However in the high glucose condition, nitric oxide levels were not measured. A quantitative measurement of shear induced NO production should be performed on monolayers cultured in high glucose to see if it correlates to the attenuated shear induced Lp response.

The interactions between the GCX, linking proteins, adhesion molecules, circulating plasma proteins and cytoskeleton are not fully established.

The present study constitutes only one of the first steps to elucidate how hyperglycemia could alter the functional relationships between the different elements that are involved in endothelial mechanotransduction and permeability.

Bibliography

1. Singh, R., et al., *Diabetic retinopathy: an update.* Indian J Ophthalmol, 2008. **56**(3): p. 178-88.
2. Schmier, J.K., et al., *Medicare Expenditures Associated With Diabetes And Diabetic Retinopathy.* Retina, 2008.
3. Lee, L.J., et al., *Direct and indirect costs among employees with diabetic retinopathy in the United States.* Curr Med Res Opin, 2008. **24**(5): p. 1549-59.
4. Davidov, E., et al., *Diabetic retinopathy and health-related quality of life.* Graefes Arch Clin Exp Ophthalmol, 2008.
5. Fong, D.S., et al., *Diabetic retinopathy.* Diabetes Care, 2003. **26 Suppl 1**: p. S99-S102.
6. Porte, D., Jr. and M.W. Schwartz, *Diabetes complications: why is glucose potentially toxic?* Science, 1996. **272**(5262): p. 699-700.
7. Frank, R.N., *On the pathogenesis of diabetic retinopathy.* Ophthalmology, 1984. **91**(6): p. 626-34.
8. Frank, R.N., *Diabetic retinopathy.* N Engl J Med, 2004. **350**(1): p. 48-58.
9. Fujita, H., *[Vascular endothelial cell dysfunction in diabetes mellitus].* Nippon Rinsho, 1999. **57**(3): p. 573-7.
10. Brausewetter, F., et al., *Microvascular permeability is increased in both types of diabetes and correlates differentially with serum levels of insulin-like growth factor I (IGF-I) and vascular endothelial growth factor (VEGF).* Horm Metab Res, 2001. **33**(12): p. 713-20.
11. Ding, H. and C.R. Triggle, *Endothelial dysfunction in diabetes: multiple targets for treatment.* Pflugers Arch, 2010. **459**(6): p. 977-94.
12. King, G.L., et al., *Cellular and molecular abnormalities in the vascular endothelium of diabetes mellitus.* Annu Rev Med, 1994. **45**: p. 179-88.
13. Gardner, T.W., et al., *The molecular structure and function of the inner blood-retinal barrier. Penn State Retina Research Group.* Doc Ophthalmol, 1999. **97**(3-4): p. 229-37.
14. Engler, C.B., et al., *Probenecid inhibition of the outward transport of fluorescein across the human blood-retina barrier.* Acta Ophthalmol (Copenh), 1994. **72**(6): p. 663-7.
15. Antonetti, D.A., et al., *Diabetic retinopathy: seeing beyond glucose-induced microvascular disease.* Diabetes, 2006. **55**(9): p. 2401-11.
16. Hayashi, T. and A. Iguchi, *Possibility of the regression of atherosclerosis through the prevention of endothelial senescence by the regulation of nitric oxide and free radical scavengers.* Geriatr Gerontol Int, 2010. **10**(2): p. 115-30.
17. Lin, K.Y., et al., *Impaired nitric oxide synthase pathway in diabetes mellitus: role of asymmetric dimethylarginine and dimethylarginine dimethylaminohydrolase.* Circulation, 2002. **106**(8): p. 987-92.
18. Santilli, F., et al., *The role of nitric oxide in the development of diabetic*

angiopathy. Horm Metab Res, 2004. **36**(5): p. 319-35.
19. Tarbell, J.M. and M.Y. Pahakis, *Mechanotransduction and the glycocalyx.* J Intern Med, 2006. **259**(4): p. 339-50.
20. Tarbell, J.M. and E.E. Ebong, *The endothelial glycocalyx: a mechano-sensor and -transducer.* Sci Signal, 2008. **1**(40): p. pt8.
21. Wang, F., et al., *Glucose-induced endothelial heparanase secretion requires cortical and stress actin reorganization.* Cardiovasc Res, 2010. **87**(1): p. 127-36.
22. Brower, J.B., et al., *High glucose-mediated loss of cell surface heparan sulfate proteoglycan impairs the endothelial shear stress response.* Cytoskeleton (Hoboken), 2010. **67**(3): p. 135-41.
23. Lakshminarayanan, S., et al., *Effect of VEGF on retinal microvascular endothelial hydraulic conductivity: the role of NO.* Invest Ophthalmol Vis Sci, 2000. **41**(13): p. 4256-61.
24. Wilcox, J.N., et al., *Localization of tissue factor in the normal vessel wall and in the atherosclerotic plaque.* Proc Natl Acad Sci U S A, 1989. **86**(8): p. 2839-43.
25. Abukawa, H., et al., *Modulation of retinal capillary endothelial cells by Muller glial cell-derived factors.* Mol Vis, 2009. **15**: p. 451-7.
26. Persidsky, Y., et al., *Blood-brain barrier: structural components and function under physiologic and pathologic conditions.* J Neuroimmune Pharmacol, 2006. **1**(3): p. 223-36.
27. Deanfield, J.E., J.P. Halcox, and T.J. Rabelink, *Endothelial function and dysfunction: testing and clinical relevance.* Circulation, 2007. **115**(10): p. 1285-95.
28. Michel, C.C., *Microvascular permeability, ultrafiltration, and restricted diffusion.* Am J Physiol Heart Circ Physiol, 2004. **287**(5): p. H1887-8.
29. van Haaren, P.M., et al., *Localization of the permeability barrier to solutes in isolated arteries by confocal microscopy.* Am J Physiol Heart Circ Physiol, 2003. **285**(6): p. H2848-56.
30. Malek, A.M., S.L. Alper, and S. Izumo, *Hemodynamic shear stress and its role in atherosclerosis.* JAMA, 1999. **282**(21): p. 2035-42.
31. Libby, P., P.M. Ridker, and G.K. Hansson, *Inflammation in atherosclerosis: from pathophysiology to practice.* J Am Coll Cardiol, 2009. **54**(23): p. 2129-38.
32. Schwartz, C.J., et al., *The pathogenesis of atherosclerosis: an overview.* Clin Cardiol, 1991. **14**(2 Suppl 1): p. I1-16.
33. Ward, B.J., K.F. Bauman, and J.A. Firth, *Interendothelial junctions of cardiac capillaries in rats: their structure and permeability properties.* Cell Tissue Res, 1988. **252**(1): p. 57-66.
34. Wittchen, E.S., J. Haskins, and B.R. Stevenson, *Protein interactions at the tight junction. Actin has multiple binding partners, and ZO-1 forms independent complexes with ZO-2 and ZO-3.* J Biol Chem, 1999. **274**(49): p. 35179-85.
35. Michel, C.C. and F.E. Curry, *Microvascular permeability.* Physiol Rev, 1999. **79**(3): p. 703-61.
36. Furuse, M., et al., *Occludin: a novel integral membrane protein localizing at tight junctions.* J Cell Biol, 1993. **123**(6 Pt 2): p. 1777-88.
37. Heiskala, M., P.A. Peterson, and Y. Yang, *The roles of claudin superfamily proteins in paracellular transport.* Traffic, 2001. **2**(2): p. 93-8.

38. Fanning, A.S., et al., *The tight junction protein ZO-1 establishes a link between the transmembrane protein occludin and the actin cytoskeleton.* J Biol Chem, 1998. **273**(45): p. 29745-53.
39. Fanning, A.S., T.Y. Ma, and J.M. Anderson, *Isolation and functional characterization of the actin binding region in the tight junction protein ZO-1.* Faseb J, 2002. **16**(13): p. 1835-7.
40. Furuse, M., et al., *Direct association of occludin with ZO-1 and its possible involvement in the localization of occludin at tight junctions.* J Cell Biol, 1994. **127**(6 Pt 1): p. 1617-26.
41. Itoh, M., et al., *Direct binding of three tight junction-associated MAGUKs, ZO-1, ZO-2, and ZO-3, with the COOH termini of claudins.* J Cell Biol, 1999. **147**(6): p. 1351-63.
42. Ebnet, K., et al., *The cell polarity protein ASIP/PAR-3 directly associates with junctional adhesion molecule (JAM).* Embo J, 2001. **20**(14): p. 3738-48.
43. Russ, P.K., et al., *Partial characterization of the human retinal endothelial cell tight and adherens junction complexes.* Invest Ophthalmol Vis Sci, 1998. **39**(12): p. 2479-85.
44. Adamson, R.H. and C.C. Michel, *Pathways through the intercellular clefts of frog mesenteric capillaries.* J Physiol, 1993. **466**: p. 303-27.
45. Nollet, F., P. Kools, and F. van Roy, *Phylogenetic analysis of the cadherin superfamily allows identification of six major subfamilies besides several solitary members.* J Mol Biol, 2000. **299**(3): p. 551-72.
46. Navarro, P., et al., *Catenin-dependent and -independent functions of vascular endothelial cadherin.* J Biol Chem, 1995. **270**(52): p. 30965-72.
47. Itoh, M., et al., *Involvement of ZO-1 in cadherin-based cell adhesion through its direct binding to alpha catenin and actin filaments.* J Cell Biol, 1997. **138**(1): p. 181-92.
48. Vittet, D., et al., *Targeted null-mutation in the vascular endothelial-cadherin gene impairs the organization of vascular-like structures in embryoid bodies.* Proc Natl Acad Sci U S A, 1997. **94**(12): p. 6273-8.
49. Walker, D.C., A. MacKenzie, and S. Hosford, *The structure of the tricellular region of endothelial tight junctions of pulmonary capillaries analyzed by freeze-fracture.* Microvasc Res, 1994. **48**(3): p. 259-81.
50. Barry, P.A., et al., *The spatial organization of corneal endothelial cytoskeletal proteins and their relationship to the apical junctional complex.* Invest Ophthalmol Vis Sci, 1995. **36**(6): p. 1115-24.
51. Weinbaum, S., et al., *Effect of cell turnover and leaky junctions on arterial macromolecular transport.* Am J Physiol, 1985. **248**(6 Pt 2): p. H945-60.
52. Chen, Y.L., et al., *Ultrastructural studies on macromolecular permeability in relation to endothelial cell turnover.* Atherosclerosis, 1995. **118**(1): p. 89-104.
53. Behl, Y., et al., *Diabetes-enhanced tumor necrosis factor-alpha production promotes apoptosis and the loss of retinal microvascular cells in type 1 and type 2 models of diabetic retinopathy.* Am J Pathol, 2008. **172**(5): p. 1411-8.
54. Kowluru, R.A. and S.N. Abbas, *Diabetes-induced mitochondrial dysfunction in the retina.* Invest Ophthalmol Vis Sci, 2003. **44**(12): p. 5327-34.
55. Wu, M., et al., *Intraretinal leakage and oxidation of LDL in diabetic retinopathy.*

Invest Ophthalmol Vis Sci, 2008. **49**(6): p. 2679-85.
56. Nagase, K., et al., *Functional and molecular characterization of adenosine transport at the rat inner blood-retinal barrier.* Biochim Biophys Acta, 2006. **1758**(1): p. 13-9.
57. Tornquist, P., A. Alm, and A. Bill, *Permeability of ocular vessels and transport across the blood-retinal-barrier.* Eye, 1990. **4 (Pt 2)**: p. 303-9.
58. Mandarino, L.J., J. Finlayson, and J.R. Hassell, *High glucose downregulates glucose transport activity in retinal capillary pericytes but not endothelial cells.* Invest Ophthalmol Vis Sci, 1994. **35**(3): p. 964-72.
59. Busik, J.V., et al., *Glucose-induced activation of glucose uptake in cells from the inner and outer blood-retinal barrier.* Invest Ophthalmol Vis Sci, 2002. **43**(7): p. 2356-63.
60. Minshall, R.D. and A.B. Malik, *Transport across the endothelium: regulation of endothelial permeability.* Handb Exp Pharmacol, 2006(176 Pt 1): p. 107-44.
61. Lin, W.L. and E. Essner, *Luminal vesicles in endothelial cells of retinal and iridial vessels of the rat.* Curr Eye Res, 1987. **6**(6): p. 785-92.
62. Lawrenson, J.G., M.C. Glyn, and B.J. Ward, *Ultrastructural and morphometric comparison of retinal and myocardial capillaries following acute ischaemia.* Microvasc Res, 2002. **64**(1): p. 65-74.
63. Sagaties, M.J., et al., *The structural basis of the inner blood-retina barrier in the eye of Macaca mulatta.* Invest Ophthalmol Vis Sci, 1987. **28**(12): p. 2000-14.
64. Michel, C.C., *Capillaries, caveolae, calcium and cyclic nucleotides: a new look at microvascular permeability.* J Mol Cell Cardiol, 1998. **30**(12): p. 2541-6.
65. Luft, J.H., *Ruthenium red and violet. II. Fine structural localization in animal tissues.* Anat Rec, 1971. **171**(3): p. 369-415.
66. Lopez-Quintero, S.V., et al., *The endothelial glycocalyx mediates shear-induced changes in hydraulic conductivity.* Am J Physiol Heart Circ Physiol, 2009. **296**(5): p. H1451-6.
67. Megens, R.T., et al., *Two-photon microscopy of vital murine elastic and muscular arteries. Combined structural and functional imaging with subcellular resolution.* J Vasc Res, 2007. **44**(2): p. 87-98.
68. Pahakis, M.Y., et al., *The role of endothelial glycocalyx components in mechanotransduction of fluid shear stress.* Biochem Biophys Res Commun, 2007. **355**(1): p. 228-33.
69. Reitsma, S., et al., *The endothelial glycocalyx: composition, functions, and visualization.* Pflugers Arch, 2007. **454**(3): p. 345-59.
70. Weinbaum, S., et al., *Mechanotransduction and flow across the endothelial glycocalyx.* Proc Natl Acad Sci U S A, 2003. **100**(13): p. 7988-95.
71. Rapraeger, A., *Transforming growth factor (type beta) promotes the addition of chondroitin sulfate chains to the cell surface proteoglycan (syndecan) of mouse mammary epithelia.* J Cell Biol, 1989. **109**(5): p. 2509-18.
72. Rapraeger, A., et al., *The cell surface proteoglycan from mouse mammary epithelial cells bears chondroitin sulfate and heparan sulfate glycosaminoglycans.* J Biol Chem, 1985. **260**(20): p. 11046-52.
73. Tarbell, J.M., *Shear stress and the endothelial transport barrier.* Cardiovasc Res, 2010. **87**(2): p. 320-30.

74. Ballinger, M.L., et al., *Regulation of glycosaminoglycan structure and atherogenesis.* Cell Mol Life Sci, 2004. **61**(11): p. 1296-306.
75. Vogl-Willis, C.A. and I.J. Edwards, *High-glucose-induced structural changes in the heparan sulfate proteoglycan, perlecan, of cultured human aortic endothelial cells.* Biochim Biophys Acta, 2004. **1672**(1): p. 36-45.
76. Ihrcke, N.S. and J.L. Platt, *Shedding of heparan sulfate proteoglycan by stimulated endothelial cells: evidence for proteolysis of cell-surface molecules.* J Cell Physiol, 1996. **168**(3): p. 625-37.
77. Vink, H., A.A. Constantinescu, and J.A. Spaan, *Oxidized lipoproteins degrade the endothelial surface layer : implications for platelet-endothelial cell adhesion.* Circulation, 2000. **101**(13): p. 1500-2.
78. Constantinescu, A.A., H. Vink, and J.A. Spaan, *Endothelial cell glycocalyx modulates immobilization of leukocytes at the endothelial surface.* Arterioscler Thromb Vasc Biol, 2003. **23**(9): p. 1541-7.
79. Sperandio, M., *Selectins and glycosyltransferases in leukocyte rolling in vivo.* FEBS J, 2006. **273**(19): p. 4377-89.
80. Ruegg, C. and A. Mariotti, *Vascular integrins: pleiotropic adhesion and signaling molecules in vascular homeostasis and angiogenesis.* Cell Mol Life Sci, 2003. **60**(6): p. 1135-57.
81. Huxley, V.H. and F.E. Curry, *Differential actions of albumin and plasma on capillary solute permeability.* Am J Physiol, 1991. **260**(5 Pt 2): p. H1645-54.
82. Agre, P., et al., *Aquaporin CHIP: the archetypal molecular water channel.* Am J Physiol, 1993. **265**(4 Pt 2): p. F463-76.
83. Preston, G.M., et al., *Appearance of water channels in Xenopus oocytes expressing red cell CHIP28 protein.* Science, 1992. **256**(5055): p. 385-7.
84. Gonen, T. and T. Walz, *The structure of aquaporins.* Q Rev Biophys, 2006. **39**(4): p. 361-96.
85. Nielsen, S., et al., *Distribution of the aquaporin CHIP in secretory and resorptive epithelia and capillary endothelia.* Proc Natl Acad Sci U S A, 1993. **90**(15): p. 7275-9.
86. King, L.S., S. Nielsen, and P. Agre, *Aquaporin-1 water channel protein in lung: ontogeny, steroid-induced expression, and distribution in rat.* J Clin Invest, 1996. **97**(10): p. 2183-91.
87. King, L.S. and P. Agre, *Pathophysiology of the aquaporin water channels.* Annu Rev Physiol, 1996. **58**: p. 619-48.
88. Rippe, B. and B. Haraldsson, *Transport of macromolecules across microvascular walls: the two-pore theory.* Physiol Rev, 1994. **74**(1): p. 163-219.
89. Curry, F.E., C.C. Michel, and J.C. Mason, *Osmotic reflextion coefficients of capillary walls to low molecular weight hydrophilic solutes measured in single perfused capillaries of the frog mesentery.* J Physiol, 1976. **261**(2): p. 319-36.
90. Rippe, B. and G. Stelin, *Simulations of peritoneal solute transport during CAPD. Application of two-pore formalism.* Kidney Int, 1989. **35**(5): p. 1234-44.
91. Motulsky, E., et al., *Aquaporin expression in blood-retinal barrier cells during experimental autoimmune uveitis.* Mol Vis, 2010. **16**: p. 602-10.
92. Iandiev, I., et al., *Diabetes alters the localization of glial aquaporins in rat retina.* Neurosci Lett, 2007. **421**(2): p. 132-6.

93. Verkman, A.S., J. Ruiz-Ederra, and M.H. Levin, *Functions of aquaporins in the eye.* Prog Retin Eye Res, 2008. **27**(4): p. 420-33.
94. Cunha-Vaz, J., J.R. Faria de Abreu, and A.J. Campos, *Early breakdown of the blood-retinal barrier in diabetes.* Br J Ophthalmol, 1975. **59**(11): p. 649-56.
95. Boyd, R.B., et al., *Significance of capillary basement membrane changes in diabetes mellitus.* J Am Podiatr Med Assoc, 1990. **80**(6): p. 307-13.
96. Nguyen, T.T., J.J. Wang, and T.Y. Wong, *Retinal vascular changes in pre-diabetes and prehypertension: new findings and their research and clinical implications.* Diabetes Care, 2007. **30**(10): p. 2708-15.
97. Yeh, P.T., et al., *Macular Hole In Proliferative Diabetic Retinopathy With Fibrovascular Proliferation.* Retina, 2008.
98. Hornof, M., E. Toropainen, and A. Urtti, *Cell culture models of the ocular barriers.* Eur J Pharm Biopharm, 2005. **60**(2): p. 207-25.
99. Funk, R.H., *Blood supply of the retina.* Ophthalmic Res, 1997. **29**(5): p. 320-5.
100. Ramirez, J.M., et al., *Structural specializations of human retinal glial cells.* Vision Res, 1996. **36**(14): p. 2029-36.
101. Bill, A., *Some aspects of the ocular circulation. Friedenwald lecture.* Invest Ophthalmol Vis Sci, 1985. **26**(4): p. 410-24.
102. Cunha-Vaz, J.G., *The blood-retinal barriers.* Doc Ophthalmol, 1976. **41**(2): p. 287-327.
103. Frank, R.N., *The galactosemic dog. A valid model for both early and late stages of diabetic retinopathy.* Arch Ophthalmol, 1995. **113**(3): p. 275-6.
104. Antonetti, D.A., et al., *Vascular permeability in experimental diabetes is associated with reduced endothelial occludin content: vascular endothelial growth factor decreases occludin in retinal endothelial cells. Penn State Retina Research Group.* Diabetes, 1998. **47**(12): p. 1953-9.
105. Amin, R.H., et al., *Vascular endothelial growth factor is present in glial cells of the retina and optic nerve of human subjects with nonproliferative diabetic retinopathy.* Invest Ophthalmol Vis Sci, 1997. **38**(1): p. 36-47.
106. Kuiper, E.J., et al., *The angio-fibrotic switch of VEGF and CTGF in proliferative diabetic retinopathy.* PLoS ONE, 2008. **3**(7): p. e2675.
107. Khalfaoui, T., et al., *Immunohistochemical analysis of cellular adhesion molecules (ICAM-1, VCAM-1) and VEGF in fibrovascular membranes of patients with proliferative diabetic retinopathy: Preliminary study.* Pathol Biol (Paris), 2008.
108. Engerman, R.L., *Pathogenesis of diabetic retinopathy.* Diabetes, 1989. **38**(10): p. 1203-6.
109. Harhaj, N.S., et al., *VEGF activation of protein kinase C stimulates occludin phosphorylation and contributes to endothelial permeability.* Invest Ophthalmol Vis Sci, 2006. **47**(11): p. 5106-15.
110. Haselton, F.R., E.J. Dworska, and L.H. Hoffman, *Glucose-induced increase in paracellular permeability and disruption of beta-receptor signaling in retinal endothelium.* Invest Ophthalmol Vis Sci, 1998. **39**(9): p. 1676-84.
111. Gillies, M.C., T. Su, and D. Naidoo, *Electrical resistance and macromolecular permeability of retinal capillary endothelial cells in vitro.* Curr Eye Res, 1995. **14**(6): p. 435-42.

112. Lum, H. and A.B. Malik, *Regulation of vascular endothelial barrier function.* Am J Physiol, 1994. **267**(3 Pt 1): p. L223-41.
113. Lynch, J.J., et al., *Increased endothelial albumin permeability mediated by protein kinase C activation.* J Clin Invest, 1990. **85**(6): p. 1991-8.
114. Stasek, J.E., Jr., C.E. Patterson, and J.G. Garcia, *Protein kinase C phosphorylates caldesmon77 and vimentin and enhances albumin permeability across cultured bovine pulmonary artery endothelial cell monolayers.* J Cell Physiol, 1992. **153**(1): p. 62-75.
115. Yokota, T., et al., *Role of protein kinase C on the expression of platelet-derived growth factor and endothelin-1 in the retina of diabetic rats and cultured retinal capillary pericytes.* Diabetes, 2003. **52**(3): p. 838-45.
116. Aiello, L.P., et al., *Vascular endothelial growth factor-induced retinal permeability is mediated by protein kinase C in vivo and suppressed by an orally effective beta-isoform-selective inhibitor.* Diabetes, 1997. **46**(9): p. 1473-80.
117. Moseley, R., R.J. Waddington, and G. Embery, *Degradation of glycosaminoglycans by reactive oxygen species derived from stimulated polymorphonuclear leukocytes.* Biochim Biophys Acta, 1997. **1362**(2-3): p. 221-31.
118. Mulivor, A.W. and H.H. Lipowsky, *Role of glycocalyx in leukocyte-endothelial cell adhesion.* Am J Physiol Heart Circ Physiol, 2002. **283**(4): p. H1282-91.
119. Mamputu, J.C. and G. Renier, *Advanced glycation end products increase, through a protein kinase C-dependent pathway, vascular endothelial growth factor expression in retinal endothelial cells. Inhibitory effect of gliclazide.* J Diabetes Complications, 2002. **16**(4): p. 284-93.
120. Pfister, F., et al., *Pericyte migration: a novel mechanism of pericyte loss in experimental diabetic retinopathy.* Diabetes, 2008. **57**(9): p. 2495-502.
121. Yamashita, T., et al., *Increased transendothelial permeation of albumin by high glucose concentration.* Metabolism, 1995. **44**(6): p. 739-44.
122. Leto, G., et al., *Increased retinal endothelial cell monolayer permeability induced by the diabetic milieu: role of advanced non-enzymatic glycation and polyol pathway activation.* Diabetes Metab Res Rev, 2001. **17**(6): p. 448-58.
123. Barber, A.J., D.A. Antonetti, and T.W. Gardner, *Altered expression of retinal occludin and glial fibrillary acidic protein in experimental diabetes. The Penn State Retina Research Group.* Invest Ophthalmol Vis Sci, 2000. **41**(11): p. 3561-8.
124. Rincon-Choles, H., et al., *ZO-1 expression and phosphorylation in diabetic nephropathy.* Diabetes, 2006. **55**(4): p. 894-900.
125. Grammas, P. and M. Riden, *Retinal endothelial cells are more susceptible to oxidative stress and increased permeability than brain-derived endothelial cells.* Microvasc Res, 2003. **65**(1): p. 18-23.
126. Bogatcheva, N.V. and A.D. Verin, *The role of cytoskeleton in the regulation of vascular endothelial barrier function.* Microvasc Res, 2008. **76**(3): p. 202-7.
127. Lee, H.Z., F.T. Yeh, and C.H. Wu, *The effect of elevated extracellular glucose on adherens junction proteins in cultured rat heart endothelial cells.* Life Sci, 2004. **74**(17): p. 2085-96.
128. Ning, A., et al., *Expression of integrins in human proliferative diabetic retinopathy membranes.* Can J Ophthalmol, 2008. **43**(6): p. 683-688.

129. Li, Y.J., et al., *Up-regulation of integrin-linked kinase in the streptozotocin-induced diabetic rat retina.* Graefes Arch Clin Exp Ophthalmol, 2007. **245**(10): p. 1523-32.
130. Mondal, L.K., et al., *Alteration of timing of secretion of vascular endothelial growth factors is responsible for progression of diabetic retinopathy.* J Indian Med Assoc, 2008. **106**(8): p. 508, 510, 515.
131. Chen, L., et al., *[Vitreous levels of stromal cell-derived factor-1 and vascular endothelial growth factor in diabetic retinopathy].* Yan Ke Xue Bao, 2008. **24**(1): p. 6-8.
132. Petrovic, M.G., et al., *Local and genetic determinants of vascular endothelial growth factor expression in advanced proliferative diabetic retinopathy.* Mol Vis, 2008. **14**: p. 1382-7.
133. Qaum, T., et al., *VEGF-initiated blood-retinal barrier breakdown in early diabetes.* Invest Ophthalmol Vis Sci, 2001. **42**(10): p. 2408-13.
134. Simorre-Pinatel, V., et al., *Vasculotropin-VEGF stimulates retinal capillary endothelial cells through an autocrine pathway.* Invest Ophthalmol Vis Sci, 1994. **35**(9): p. 3393-400.
135. Nomura, M., et al., *Possible participation of autocrine and paracrine vascular endothelial growth factors in hypoxia-induced proliferation of endothelial cells and pericytes.* J Biol Chem, 1995. **270**(47): p. 28316-24.
136. Adamis, A.P., et al., *Synthesis and secretion of vascular permeability factor/vascular endothelial growth factor by human retinal pigment epithelial cells.* Biochem Biophys Res Commun, 1993. **193**(2): p. 631-8.
137. Millauer, B., et al., *High affinity VEGF binding and developmental expression suggest Flk-1 as a major regulator of vasculogenesis and angiogenesis.* Cell, 1993. **72**(6): p. 835-46.
138. Dimmeler, S., et al., *Activation of nitric oxide synthase in endothelial cells by Akt-dependent phosphorylation.* Nature, 1999. **399**(6736): p. 601-5.
139. Rajah, T.T. and P. Grammas, *VEGF and VEGF receptor levels in retinal and brain-derived endothelial cells.* Biochem Biophys Res Commun, 2002. **293**(2): p. 710-3.
140. Brock, T.A., H.F. Dvorak, and D.R. Senger, *Tumor-secreted vascular permeability factor increases cytosolic Ca2+ and von Willebrand factor release in human endothelial cells.* Am J Pathol, 1991. **138**(1): p. 213-21.
141. Franke, T.F., et al., *Direct regulation of the Akt proto-oncogene product by phosphatidylinositol-3,4-bisphosphate.* Science, 1997. **275**(5300): p. 665-8.
142. Fulton, D., et al., *Regulation of endothelium-derived nitric oxide production by the protein kinase Akt.* Nature, 1999. **399**(6736): p. 597-601.
143. Huang, Q. and Y. Yuan, *Interaction of PKC and NOS in signal transduction of microvascular hyperpermeability.* Am J Physiol, 1997. **273**(5 Pt 2): p. H2442-51.
144. Mayhan, W.G., *VEGF increases permeability of the blood-brain barrier via a nitric oxide synthase/cGMP-dependent pathway.* Am J Physiol, 1999. **276**(5 Pt 1): p. C1148-53.
145. Ramirez, M.M., D.D. Kim, and W.N. Duran, *Protein kinase C modulates microvascular permeability through nitric oxide synthase.* Am J Physiol, 1996. **271**(4 Pt 2): p. H1702-5.

146. Dvorak, H.F., et al., *Vascular permeability factor, fibrin, and the pathogenesis of tumor stroma formation.* Ann N Y Acad Sci, 1992. **667**: p. 101-11.
147. Peters, S., et al., *Angiopoietin modulation of vascular endothelial growth factor: Effects on retinal endothelial cell permeability.* Cytokine, 2007. **40**(2): p. 144-50.
148. Antonetti, D.A., et al., *Vascular endothelial growth factor induces rapid phosphorylation of tight junction proteins occludin and zonula occluden 1. A potential mechanism for vascular permeability in diabetic retinopathy and tumors.* J Biol Chem, 1999. **274**(33): p. 23463-7.
149. Miyamoto, K., et al., *Vascular endothelial growth factor (VEGF)-induced retinal vascular permeability is mediated by intercellular adhesion molecule-1 (ICAM-1).* Am J Pathol, 2000. **156**(5): p. 1733-9.
150. Fu, B.M. and S. Shen, *Acute VEGF effect on solute permeability of mammalian microvessels in vivo.* Microvasc Res, 2004. **68**(1): p. 51-62.
151. Esser, S., et al., *Vascular endothelial growth factor induces VE-cadherin tyrosine phosphorylation in endothelial cells.* J Cell Sci, 1998. **111 (Pt 13)**: p. 1853-65.
152. Angelini, D.J., et al., *TNF-alpha increases tyrosine phosphorylation of vascular endothelial cadherin and opens the paracellular pathway through fyn activation in human lung endothelia.* Am J Physiol Lung Cell Mol Physiol, 2006. **291**(6): p. L1232-45.
153. Andriopoulou, P., et al., *Histamine induces tyrosine phosphorylation of endothelial cell-to-cell adherens junctions.* Arterioscler Thromb Vasc Biol, 1999. **19**(10): p. 2286-97.
154. Enaida, H., et al., *Effect of growth factors on expression of integrin subtypes in microvascular endothelial cells isolated from bovine retinas.* Fukushima J Med Sci, 1998. **44**(1): p. 43-52.
155. Garcia, C., et al., *Vasoinhibins prevent retinal vasopermeability associated with diabetic retinopathy in rats via protein phosphatase 2A-dependent eNOS inactivation.* J Clin Invest, 2008. **118**(6): p. 2291-300.
156. Nievelstein, P.F., et al., *Lipid accumulation in rabbit aortic intima 2 hours after bolus infusion of low density lipoprotein. A deep-etch and immunolocalization study of ultrarapidly frozen tissue.* Arterioscler Thromb, 1991. **11**(6): p. 1795-805.
157. Navab, M., et al., *Monocyte transmigration induced by modification of low density lipoprotein in cocultures of human aortic wall cells is due to induction of monocyte chemotactic protein 1 synthesis and is abolished by high density lipoprotein.* J Clin Invest, 1991. **88**(6): p. 2039-46.
158. Hessler, J.R., A.L. Robertson, Jr., and G.M. Chisolm, 3rd, *LDL-induced cytotoxicity and its inhibition by HDL in human vascular smooth muscle and endothelial cells in culture.* Atherosclerosis, 1979. **32**(3): p. 213-29.
159. Fogelman, A.M., et al., *Malondialdehyde alteration of low density lipoproteins leads to cholesteryl ester accumulation in human monocyte-macrophages.* Proc Natl Acad Sci U S A, 1980. **77**(4): p. 2214-8.
160. Cui, X., et al., *Macrophage foam cell formation is augmented in serum from patients with diabetic angiopathy.* Diabetes Res Clin Pract, 2010. **87**(1): p. 57-63.
161. Stout, R.W., *Diabetes and atherosclerosis.* Biomed Pharmacother, 1993. **47**(1): p. 1-2.
162. Baron, A.D., *Insulin and the vasculature--old actors, new roles.* J Investig Med,

1996. **44**(8): p. 406-12.
163. McMackin, C.J. and J.A. Vita, *Update on nitric oxide-dependent vasodilation in human subjects.* Methods Enzymol, 2005. **396**: p. 541-53.
164. Moncada, S., R.M. Palmer, and E.A. Higgs, *Nitric oxide: physiology, pathophysiology, and pharmacology.* Pharmacol Rev, 1991. **43**(2): p. 109-42.
165. Kawabata, A., *Evidence that endogenous nitric oxide modulates plasma fibrinogen levels in the rat.* Br J Pharmacol, 1996. **117**(2): p. 236-7.
166. Sekiguchi, N., et al., *Immunohistochemical study of prostacyclin-stimulating factor (PSF) in the diabetic and atherosclerotic human coronary artery.* Diabetes, 1997. **46**(10): p. 1627-32.
167. Umeda, F., et al., *Difference in serum-induced prostacyclin production by cultured aortic and capillary endothelial cells.* Prostaglandins Leukot Essent Fatty Acids, 1997. **56**(1): p. 51-5.
168. Cosentino, F., et al., *High glucose causes upregulation of cyclooxygenase-2 and alters prostanoid profile in human endothelial cells: role of protein kinase C and reactive oxygen species.* Circulation, 2003. **107**(7): p. 1017-23.
169. Briner, V.A., P. Tsai, and R.W. Schrier, *Bradykinin: potential for vascular constriction in the presence of endothelial injury.* Am J Physiol, 1993. **264**(2 Pt 2): p. F322-7.
170. Christopher, J., et al., *Regulation of B(2)-kinin receptors by glucose in vascular smooth muscle cells.* Am J Physiol Heart Circ Physiol, 2001. **280**(4): p. H1537-46.
171. Otsuki, M., et al., *Circulating vascular cell adhesion molecule-1 (VCAM-1) in atherosclerotic NIDDM patients.* Diabetes, 1997. **46**(12): p. 2096-101.
172. Vlassara, H., et al., *Identification of galectin-3 as a high-affinity binding protein for advanced glycation end products (AGE): a new member of the AGE-receptor complex.* Mol Med, 1995. **1**(6): p. 634-46.
173. Klein, R.L., M. Laimins, and M.F. Lopes-Virella, *Isolation, characterization, and metabolism of the glycated and nonglycated subfractions of low-density lipoproteins isolated from type I diabetic patients and nondiabetic subjects.* Diabetes, 1995. **44**(9): p. 1093-8.
174. Chiu, J.J., S. Usami, and S. Chien, *Vascular endothelial responses to altered shear stress: pathologic implications for atherosclerosis.* Ann Med, 2009. **41**(1): p. 19-28.
175. Keen, H. and R.J. Jarrett, *The WHO multinational study of vascular disease in diabetes: 2. Macrovascular disease prevalence.* Diabetes Care, 1979. **2**(2): p. 187-95.
176. Woo, C.H., et al., *Extracellular signal-regulated kinase 5 SUMOylation antagonizes shear stress-induced antiinflammatory response and endothelial nitric oxide synthase expression in endothelial cells.* Circ Res, 2008. **102**(5): p. 538-45.
177. Tzima, E., et al., *A mechanosensory complex that mediates the endothelial cell response to fluid shear stress.* Nature, 2005. **437**(7057): p. 426-31.
178. Widlansky, M.E., et al., *The clinical implications of endothelial dysfunction.* J Am Coll Cardiol, 2003. **42**(7): p. 1149-60.
179. Johnstone, M.T., et al., *Impaired endothelium-dependent vasodilation in patients with insulin-dependent diabetes mellitus.* Circulation, 1993. **88**(6): p. 2510-6.

180. McVeigh, G.E., et al., *Impaired endothelium-dependent and independent vasodilation in patients with type 2 (non-insulin-dependent) diabetes mellitus.* Diabetologia, 1992. **35**(8): p. 771-6.
181. Libby, P., *Inflammation in atherosclerosis.* Nature, 2002. **420**(6917): p. 868-74.
182. Nieuwdorp, M., et al., *Loss of endothelial glycocalyx during acute hyperglycemia coincides with endothelial dysfunction and coagulation activation in vivo.* Diabetes, 2006. **55**(2): p. 480-6.
183. Zuurbier, C.J., et al., *Short-term hyperglycemia increases endothelial glycocalyx permeability and acutely decreases lineal density of capillaries with flowing red blood cells.* J Appl Physiol, 2005. **99**(4): p. 1471-6.
184. Sapieha, P., et al., *Proliferative retinopathies: angiogenesis that blinds.* Int J Biochem Cell Biol, 2010. **42**(1): p. 5-12.
185. Antonetti, D.A., et al., *Molecular mechanisms of vascular permeability in diabetic retinopathy.* Semin Ophthalmol, 1999. **14**(4): p. 240-8.
186. Curry, F.E. and C.C. Michel, *A fiber matrix model of capillary permeability.* Microvasc Res, 1980. **20**(1): p. 96-9.
187. Busik, J.V., S. Mohr, and M.B. Grant, *Hyperglycemia-induced reactive oxygen species toxicity to endothelial cells is dependent on paracrine mediators.* Diabetes, 2008. **57**(7): p. 1952-65.
188. Antonetti, D.A. and E.B. Wolpert, *Isolation and characterization of retinal endothelial cells.* Methods Mol Med, 2003. **89**: p. 365-74.
189. Sill, H.W., et al., *Shear stress increases hydraulic conductivity of cultured endothelial monolayers.* Am J Physiol, 1995. **268**(2 Pt 2): p. H535-43.
190. Cancel, L.M., A. Fitting, and J.M. Tarbell, *In vitro study of LDL transport under pressurized (convective) conditions.* Am J Physiol Heart Circ Physiol, 2007. **293**(1): p. H126-32.
191. Curry, F.E., *Mechanics and thermodynamics of transcapillary*
exchange. , vol. IV, Microcirculation, part 1. Handbook of Physiology, section 2, The Cardiovascular
System, 1984. **IV**: p. 309-374.
192. Fu, B.M., et al., *A junction-orifice-fiber entrance layer model for capillary permeability: application to frog mesenteric capillaries.* J Biomech Eng, 1994. **116**(4): p. 502-13.
193. DeMaio, L., et al., *A transmural pressure gradient induces mechanical and biological adaptive responses in endothelial cells.* Am J Physiol Heart Circ Physiol, 2004. **286**(2): p. H731-41.
194. Kim, M.H., N.R. Harris, and J.M. Tarbell, *Regulation of capillary hydraulic conductivity in response to an acute change in shear.* Am J Physiol Heart Circ Physiol, 2005. **289**(5): p. H2126-35.
195. Rutledge, J.C., et al., *Solvent drag of LDL across mammalian endothelial barriers with increased permeability.* Am J Physiol, 1995. **268**(5 Pt 2): p. H1982-91.
196. Nitta, T., et al., *Size-selective loosening of the blood-brain barrier in claudin-5-deficient mice.* J Cell Biol, 2003. **161**(3): p. 653-60.
197. Barber, A.J. and D.A. Antonetti, *Mapping the blood vessels with paracellular permeability in the retinas of diabetic rats.* Invest Ophthalmol Vis Sci, 2003. **44**(12): p. 5410-6.

198. Wiklund, O., T.E. Carew, and D. Steinberg, *Role of the low density lipoprotein receptor in penetration of low density lipoprotein into rabbit aortic wall.* Arteriosclerosis, 1985. **5**(2): p. 135-41.
199. Shivers, R.R., *The effect of hyperglycemia on brain capillary permeability in the lizard, Anolis carolinensis. A freeze-fracture analysis of blood-brain barrier pathology.* Brain Res, 1979. **170**(3): p. 509-22.
200. Vorbrodt, A.W., et al., *Immunogold study of altered expression of some interendothelial junctional molecules in the brain blood microvessels of diabetic scrapie-infected mice.* J Mol Histol, 2006. **37**(1-2): p. 27-35.
201. Villarroel, M., et al., *High glucose concentration leads to differential expression of tight junction proteins in human retinal pigment epithelial cells.* Endocrinol Nutr, 2009. **56**(2): p. 53-8.
202. Natarajan, R., et al., *Effects of high glucose on vascular endothelial growth factor expression in vascular smooth muscle cells.* Am J Physiol, 1997. **273**(5 Pt 2): p. H2224-31.
203. Mathews, M.K., et al., *Vascular endothelial growth factor and vascular permeability changes in human diabetic retinopathy.* Invest Ophthalmol Vis Sci, 1997. **38**(13): p. 2729-41.
204. Gilbert, R.E., et al., *Vascular endothelial growth factor and its receptors in control and diabetic rat eyes.* Lab Invest, 1998. **78**(8): p. 1017-27.
205. Williams, B., et al., *Glucose-induced protein kinase C activation regulates vascular permeability factor mRNA expression and peptide production by human vascular smooth muscle cells in vitro.* Diabetes, 1997. **46**(9): p. 1497-503.
206. Murakami, T., E.A. Felinski, and D.A. Antonetti, *Occludin phosphorylation and ubiquitination regulate tight junction trafficking and vascular endothelial growth factor-induced permeability.* J Biol Chem, 2009. **284**(31): p. 21036-46.
207. Chang, Y.S., et al., *Shear-induced increase in hydraulic conductivity in endothelial cells is mediated by a nitric oxide-dependent mechanism.* Arterioscler Thromb Vasc Biol, 2000. **20**(1): p. 35-42.
208. Lever, M.J., J.M. Tarbell, and C.G. Caro, *The effect of luminal flow in rabbit carotid artery on transmural fluid transport.* Exp Physiol, 1992. **77**(4): p. 553-63.
209. Williams, D.A., *Network assessment of capillary hydraulic conductivity after abrupt changes in fluid shear stress.* Microvasc Res, 1999. **57**(2): p. 107-17.
210. Mochizuki, S., et al., *Role of hyaluronic acid glycosaminoglycans in shear-induced endothelium-derived nitric oxide release.* Am J Physiol Heart Circ Physiol, 2003. **285**(2): p. H722-6.
211. Florian, J.A., et al., *Heparan sulfate proteoglycan is a mechanosensor on endothelial cells.* Circ Res, 2003. **93**(10): p. e136-42.
212. Schulz, E., et al., *Nitric oxide, tetrahydrobiopterin, oxidative stress, and endothelial dysfunction in hypertension.* Antioxid Redox Signal, 2008. **10**(6): p. 1115-26.
213. Schmidt, T.S. and N.J. Alp, *Mechanisms for the role of tetrahydrobiopterin in endothelial function and vascular disease.* Clin Sci (Lond), 2007. **113**(2): p. 47-63.
214. Misko, T.P., et al., *A fluorometric assay for the measurement of nitrite in biological samples.* Anal Biochem, 1993. **214**(1): p. 11-6.
215. Williams, D.A., *Intact capillaries sensitive to rate, magnitude, and pattern of*

shear stress stimuli as assessed by hydraulic conductivity (Lp). Microvasc Res, 2003. **66**(2): p. 147-58.
216. Williams, D.A., *Change in shear stress (Deltatau)/hydraulic conductivity (Lp) relationship after pronase treatment of individual capillaries in situ.* Microvasc Res, 2007. **73**(1): p. 48-57.
217. Dull, R.O., et al., *The effect of varying albumin concentration and hydrostatic pressure on hydraulic conductivity and albumin permeability of cultured endothelial monolayers.* Microvasc Res, 1991. **41**(3): p. 390-407.
218. Huxley, V.H. and F.E. Curry, *Albumin modulation of capillary permeability: test of an adsorption mechanism.* Am J Physiol, 1985. **248**(2 Pt 2): p. H264-73.
219. Hillsley, M.V. and J.M. Tarbell, *Oscillatory shear alters endothelial hydraulic conductivity and nitric oxide levels.* Biochem Biophys Res Commun, 2002. **293**(5): p. 1466-71.
220. Lakshminarayanan, S., T.W. Gardner, and J.M. Tarbell, *Effect of shear stress on the hydraulic conductivity of cultured bovine retinal microvascular endothelial cell monolayers.* Curr Eye Res, 2000. **21**(6): p. 944-51.
221. Yao, Y., A. Rabodzey, and C.F. Dewey, Jr., *Glycocalyx modulates the motility and proliferative response of vascular endothelium to fluid shear stress.* Am J Physiol Heart Circ Physiol, 2007. **293**(2): p. H1023-30.
222. van den Berg, B.M., H. Vink, and J.A. Spaan, *The endothelial glycocalyx protects against myocardial edema.* Circ Res, 2003. **92**(6): p. 592-4.
223. Parameswaran, S., et al., *Effect of concentration and hyaluronidase on albumin diffusion across rabbit mesentery.* Microcirculation, 1999. **6**(2): p. 117-26.
224. Dull, R.O., I. Mecham, and S. McJames, *Heparan sulfates mediate pressure-induced increase in lung endothelial hydraulic conductivity via nitric oxide/reactive oxygen species.* Am J Physiol Lung Cell Mol Physiol, 2007. **292**(6): p. L1452-8.
225. Adamson, R.H., *Permeability of frog mesenteric capillaries after partial pronase digestion of the endothelial glycocalyx.* J Physiol, 1990. **428**: p. 1-13.
226. Tarbell, J.M., L. Demaio, and M.M. Zaw, *Effect of pressure on hydraulic conductivity of endothelial monolayers: role of endothelial cleft shear stress.* J Appl Physiol, 1999. **87**(1): p. 261-8.
227. DeMaio, L., et al., *Shear stress regulates occludin content and phosphorylation.* Am J Physiol Heart Circ Physiol, 2001. **281**(1): p. H105-13.
228. Lipowsky, H.H., *Microvascular rheology and hemodynamics.* Microcirculation, 2005. **12**(1): p. 5-15.
229. Zhang, X., et al., *A 1-D model to explore the effects of tissue loading and tissue concentration gradients in the revised Starling principle.* Am J Physiol Heart Circ Physiol, 2006. **291**(6): p. H2950-64.
230. Dittmann, J., C. Krischek, and G. Harisch, *Modulation of cAMP-dependent protein kinase by derivatives of chondroitin sulfate.* Life Sci, 1997. **60**(12): p. PL 201-6.
231. Lin, X.H., K. Dahlin-Huppe, and W.B. Stallcup, *Interaction of the NG2 proteoglycan with the actin cytoskeleton.* J Cell Biochem, 1996. **63**(4): p. 463-77.
232. Dusserre, N., et al., *PECAM-1 interacts with nitric oxide synthase in human endothelial cells: implication for flow-induced nitric oxide synthase activation.*

Arterioscler Thromb Vasc Biol, 2004. **24**(10): p. 1796-802.
233. Pirart, J., *[Diabetes mellitus and its degenerative complications: a prospective study of 4,400 patients observed between 1947 and 1973 (3rd and last part) (author's transl)].* Diabete Metab, 1977. **3**(4): p. 245-56.
234. Bakker, W., et al., *Endothelial dysfunction and diabetes: roles of hyperglycemia, impaired insulin signaling and obesity.* Cell Tissue Res, 2009. **335**(1): p. 165-89.
235. Shimokawa, H., R. Nakaike, and A. Takeshita, *Significance of defective endothelial signal transduction in impaired endothelium-dependent relaxation in atherosclerosis.* Gerontology, 1995. **41 Suppl 1**: p. 28-33.
236. Henry, C.B. and B.R. Duling, *Permeation of the luminal capillary glycocalyx is determined by hyaluronan.* Am J Physiol, 1999. **277**(2 Pt 2): p. H508-14.
237. Danese, C., et al., *Do hypertension and diabetes mellitus influence the site of atherosclerotic plaques?* Clin Ter, 2006. **157**(1): p. 9-13.
238. Reyes-Soffer, G., et al., *Endothelial function in individuals with coronary artery disease with and without type 2 diabetes mellitus.* Metabolism, 2010.
239. Tabit, C.E., et al., *Endothelial dysfunction in diabetes mellitus: molecular mechanisms and clinical implications.* Rev Endocr Metab Disord, 2010. **11**(1): p. 61-74.
240. Celie, J.W., et al., *Subendothelial heparan sulfate proteoglycans become major L-selectin and monocyte chemoattractant protein-1 ligands upon renal ischemia/reperfusion.* Am J Pathol, 2007. **170**(6): p. 1865-78.
241. Tran-Lundmark, K., et al., *Heparan sulfate in perlecan promotes mouse atherosclerosis: roles in lipid permeability, lipid retention, and smooth muscle cell proliferation.* Circ Res, 2008. **103**(1): p. 43-52.
242. Wang, J.Y., et al., *The effect of cilostazol on expression of thrombospondin-1 in diabetic retinopathy.* Fen Zi Xi Bao Sheng Wu Xue Bao, 2008. **41**(4): p. 301-8.
243. Hollmann, J., et al., *Relationship of sulfated glycosaminoglycans and cholesterol content in normal and arteriosclerotic human aorta.* Arteriosclerosis, 1989. **9**(2): p. 154-8.
244. Wasty, F., M.Z. Alavi, and S. Moore, *Distribution of glycosaminoglycans in the intima of human aortas: changes in atherosclerosis and diabetes mellitus.* Diabetologia, 1993. **36**(4): p. 316-22.
245. Bollineni, J.S., I. Alluru, and A.S. Reddi, *Heparan sulfate proteoglycan synthesis and its expression are decreased in the retina of diabetic rats.* Curr Eye Res, 1997. **16**(2): p. 127-30.
246. Mine, S., et al., *Serum hyaluronan concentration as a marker of angiopathy in patients with diabetes mellitus.* Endocr J, 2006. **53**(6): p. 761-6.
247. Michell, B.J., et al., *The Akt kinase signals directly to endothelial nitric oxide synthase.* Curr Biol, 1999. **9**(15): p. 845-8.
248. Fukumura, D., et al., *Predominant role of endothelial nitric oxide synthase in vascular endothelial growth factor-induced angiogenesis and vascular permeability.* Proc Natl Acad Sci U S A, 2001. **98**(5): p. 2604-9.
249. Du, X.L., et al., *Hyperglycemia inhibits endothelial nitric oxide synthase activity by posttranslational modification at the Akt site.* J Clin Invest, 2001. **108**(9): p. 1341-8.
250. Soro-Paavonen, A., et al., *Advanced glycation end-products induce vascular*

dysfunction via resistance to nitric oxide and suppression of endothelial nitric oxide synthase. J Hypertens, 2010. **28**(4): p. 780-8.
251. Cai, S., et al., *Endothelial nitric oxide synthase dysfunction in diabetic mice: importance of tetrahydrobiopterin in eNOS dimerisation.* Diabetologia, 2005. **48**(9): p. 1933-40.
252. Lima, V.V., et al., *O-GlcNAcylation: a novel post-translational mechanism to alter vascular cellular signaling in health and disease: focus on hypertension.* J Am Soc Hypertens, 2009. **3**(6): p. 374-87.
253. Giantsos, K.M., P. Kopeckova, and R.O. Dull, *The use of an endothelium-targeted cationic copolymer to enhance the barrier function of lung capillary endothelial monolayers.* Biomaterials, 2009. **30**(29): p. 5885-91.
254. Suzuma, I., et al., *Cyclic stretch and hypertension induce retinal expression of vascular endothelial growth factor and vascular endothelial growth factor receptor-2: potential mechanisms for exacerbation of diabetic retinopathy by hypertension.* Diabetes, 2001. **50**(2): p. 444-54.
255. Tsurumi, Y., et al., *Reciprocal relation between VEGF and NO in the regulation of endothelial integrity.* Nature Medicine, 1997. **3**(8): p. 879-886.